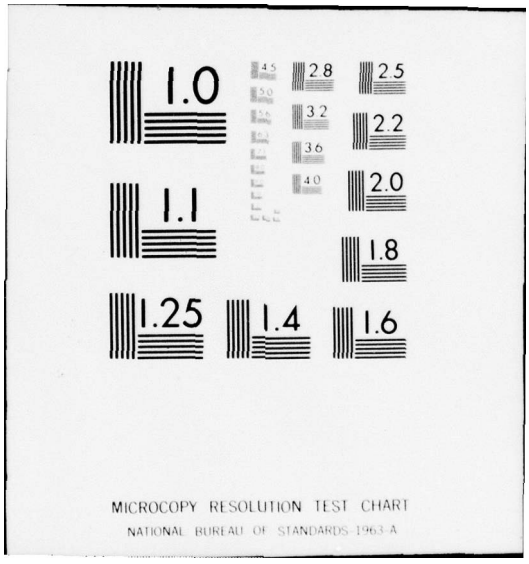
AD-A038 084 IBM THOMAS J WATSON RESEARCH CENTER YORKTOWN HEIGHTS N Y F/G 11/6
SPECTROSCOPIC STUDIES OF CHEMICAL ADSORPTION AND REACTIONS AT T--ETC(U)
MAR 77 J E DEMUTH, G W RUBLOFF N00014-75-C-0346
UNCLASSIFIED NL

1 OF 2
ADA038084




1.0
1.1
1.25
1.4
1.6
1.8
2.0
2.2
2.5
2.8
3.2
3.6
4.0
4.5
5.0
MICROCOPY RESOLUTION TEST CHART
NATIONAL BUREAU OF STANDARDS-1963-A

ADA038084

SPECTROSCOPIC STUDIES OF CHEMICAL ADSORPTION AND REACTIONS AT TRANSITION METAL SURFACES

J. E. Demuth and G. W. Rubloff

IBM Thomas J. Watson Research Center

P.O. Box 218, Yorktown Heights, New York 10598

March 15 1977

Final Report for period 1 January 1975 - 31 December 1976

Contract N00014-75-C-0346

Sponsored by Office of Naval Research

DDC
RECEIVED
MAR 31 1977
A

Approved for public release; distribution unlimited.

Reproduction in whole or part is permitted for any purpose of the United States Government.

SPECTROSCOPIC STUDIES OF CHEMICAL ADSORPTION AND REACTIONS AT TRANSITION METAL SURFACES

J. E. Demuth and G. W. Rubloff

IBM Thomas J. Watson Research Center

P.O. Box 218, Yorktown Heights, New York 10598

March 15 1977

Final Report for period 1 January 1975 - 31 December 1976

Contract N00014-75-C-0346

Sponsored by Office of Naval Research

Approved for public release; distribution unlimited.

Reproduction in whole or part is permitted for any purpose of the United States Government.

UNCLASSIFIED

SECURITY CLASSIFICATION OF THIS PAGE (When Data Entered)

REPORT DOCUMENTATION PAGE		READ INSTRUCTIONS BEFORE COMPLETING FORM
1. REPORT NUMBER (6)	2. GOVT ACCESSION NO.	3. RECIPIENT'S CATALOG NUMBER
4. TITLE (and Subtitle) SPECTROSCOPIC STUDIES OF CHEMICAL ADSORPTION AND REACTIONS AT TRANSITION METAL SURFACES, (9)		5. TYPE OF REPORT & PERIOD COVERED Final Report, 1 Jan [redacted] 75 — 31 Dec [redacted] 76
		6. PERFORMING ORG. REPORT NUMBER
7. AUTHOR(s) (10) J. E. DEMUTH [redacted] G.W. RUBLOFF		8. CONTRACT OR GRANT NUMBER(s) (15) N00014-75-C-0346 new
9. PERFORMING ORGANIZATION NAME AND ADDRESS IBM T. J. Watson Research Center P.O. Box 218, Yorktown Heights, NY 10598		10. PROGRAM ELEMENT, PROJECT, TASK AREA & WORK UNIT NUMBERS (12) 145 p.
11. CONTROLLING OFFICE NAME AND ADDRESS Office of Naval Research 800 N. Quincy Street Arlington, Virginia 22217 (11)		12. REPORT DATE 15 Mar [redacted] 77
		13. NUMBER OF PAGES
14. MONITORING AGENCY NAME & ADDRESS(if different from Controlling Office)		15. SECURITY CLASS. (of this report) UNCLASSIFIED
		15a. DECLASSIFICATION/DOWNGRADING SCHEDULE

16. DISTRIBUTION STATEMENT (of this Report)

Approved for public release;
distribution unlimited.

17. DISTRIBUTION STATEMENT (of the abstract entered in Block 20, if different from Report)

18. SUPPLEMENTARY NOTES

19. KEY WORDS (Continue on reverse side if necessary and identify by block number)

Surfaces, spectroscopy, electronic structure, energy levels, geometric structure, optical excitation, chemisorption, surface reactions, transition metals, hydrogen, carbon monoxide, methanol, hydrocarbons, single crystal metals, copper, nickel, (see over)

20. ABSTRACT (Continue on reverse side if necessary and identify by block number)

The accomplishments of the work ~~performed~~ under ~~the contract entitled~~ THE TITLE 'Spectroscopic Studies of Chemical Adsorption and Reactions at Transition Metal Surfaces' are summarized. Included are studies of flat and stepped surfaces, of surfaces with chemisorbed species and of reactions on these surfaces. Experimental techniques utilized include ultraviolet photoemission spectroscopy, optical reflectance spectroscopy, photoelectron yield spectroscopy and thermal desorption mass spectroscopy.

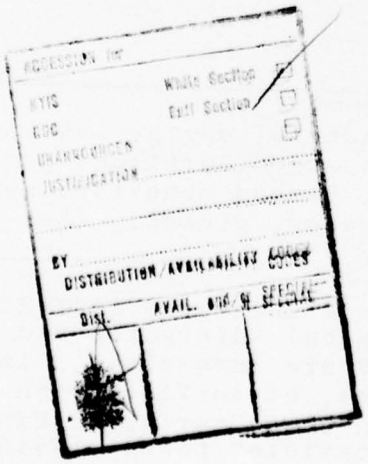
DD FORM 1 JAN 73 1473 EDITION OF 1 NOV 65 IS OBSOLETE

UNCLASSIFIED 249 250

SECURITY CLASSIFICATION OF THIS PAGE (When Data Entered)

(19)

palladium, platinum, nickel oxide, carbides, surface intermediates, surface radicals, hydrocarbon hybridization, chemically modified surfaces, stepped surfaces.



I. Initial Proposal

IBM proposed a one year best efforts experimental study of the electronic structure of transition metal surfaces with and without adsorbed atoms and molecules. The experimental methods proposed include in situ ultra-high vacuum measurements using primarily ultraviolet photoemission spectroscopy (PES) and surface reflectance spectroscopy (SRS), as well as low energy electron diffraction, Auger electron spectroscopy and mass spectroscopy. By using these techniques (which were to be combined into a single system) to study several related atoms and molecules adsorbed on the surface, we proposed to investigate the use of PES and SRS measurements to obtain fundamental information about the adsorbate-surface interaction and the properties of these adsorbed species. In addition, direct correlation of PES and SRS measurements were to be made in an effort to better understand and further develop both techniques for surface studies.

In an extension to this initial one year proposal IBM proposed a continuation of this and additional related work for a second year which included (1) surface reflectance spectroscopy (SRS) and electron energy loss spectroscopy (ELS) to deduce characteristic excitation energies and possible empty electronic states associated with the adsorbate and substrate surface electronic structure, (2) applying static and modulated molecular beam in conjunction with UPS and SRS and with mass spectroscopy to determine both static and transient reaction products on the surface and in the gas phase and (3) theoretical calculations for isolated molecules not directly observed in the gas phase and/or whose geometry may be significantly altered by adsorption.

II. Accomplishments under the Project

A significant portion of the completed work has been published or is available in preprint form, and several studies remain to be written and published. In the following we briefly summarize the accomplishments of this research. Where possible we refer to the published

work; other items are summarized with additional information provided in an Appendix. These accomplishments are:

(1) The determination of the state of hybridization of acetylene, ethylene, propylene and benzene chemisorbed on Ni(111) from comparisons of UPS results to Hartree-Fock calculations. This is an important question which has proven elusive in many previous investigations (Ref. 1).

(2) The observation of a different mode of bonding of CO to Cu, Ag and Au surfaces than on Ni, Pd or Pt as well as two phases of CO on a Cu(100) single crystal surface. Such results reflect differences in the role of s- and d-electrons in bonding in noble metals from that on transition metals (Refs. 2 and 3).

(3) UPS results show that the ethylene decomposition path ($C_2H_4 \rightarrow C_2H_2+H_2$) on a clean Ni(111) surface is altered on a stepped Ni(111) surface. On the stepped surface carbon is formed, preventing dehydrogenation to acetylene, so that ethylene is directly desorbed from the surface. (Ref. 2).

(4) Identification of a new bonding mode of acetylene on Pd and Pt by UPS and temperature programmed mass spectroscopy. Below T ~ 180K acetylene bonds but above these temperatures rehybridizes to form an olefinic "di-σ" like species - postulated to be of importance in catalytic reactions. (Ref. 4)

(5) Isolation and direct observation of a surface intermediate during methanol decomposition to H_2 + CO on Ni(111) by combined use of UPS and temperature programmed mass spectroscopy. This molecular intermediate contains C, O, and H and is probably a radical stabilized by its presence on the surface. (Ref. 5)

(6) A survey of UPS results for a wide variety of organic molecules chemisorbed on transition metal, noble metal, and semiconductor surfaces demonstrates that

uniform extramolecular relaxation/polarization shifts are a general phenomenon. This result significantly enhances the value of UPS as a tool for studies of chemisorbed molecular species. Deviations from the general pattern can be understood on the basis of simple molecular orbital calculations and have led to a resolution of controversy over the ordering of orbitals in H_2CO. (Ref. 6)

(7) UPS results show that the chemisorption of some aldehydes (H_2CO, $H(CH_3)CO$), ketones ($(CH_3)_2CO$), alcohols (CH_3OH), and ethers (CH_3OCH_3) on polycrystalline Pd affects primarily the oxygen lone-pair orbitals. These species undergo thermally-activated decomposition to yield chemisorbed CO. The particular orbital symmetries of some of these classes of oxygen-containing organics (aldehydes and ketones) permits an analysis of the reaction energetics using a Mulliken/Grimley approach. (Appendix, item 1)

(8) UPS determination of the differences in the bonding interactions of chemisorbed hydrogen with Ni(111) from that with Pd(111) and Pt(111) surfaces. Here we find that chemisorbed hydrogen interacts more strongly with the s-electrons of Ni than with those of Pd and Pt whereas strong d-electron interactions occur only for chemisorbed hydrogen on Pd and Pt. These results provide insight into the relative nature of hydrogen chemisorption bonding on these metals as well as a physical basis for understanding differences in, for example, hydrogenation reactions on these surfaces. (Appendix, item 2)

(9) Determination of the molecular geometry of acetylene and ethylene chemisorbed on Cu, Ni, Pd and Pt surfaces at T ~ 80K from their ionization levels and Hartree-Fock calculations. Trends in the geometric structures are found to be directly related to differences in the electronic structure of the substrate and adsorbate. (Appendix, item 3)

(10) Surface reflectance spectroscopy (SRS) studies in combination with UPS have been carried out in the range 1.5-40 eV for chemisorbed CO on Ni(111), chemisorbed C_6H_6 on Ni(111) and on polycrystalline Pd and Pt, condensed C_6H_6 on Ni(111), hydrogen and oxygen chemisorbed on Ni(111), and a thermally-grown oxide on Ni(111). These results have been complemented by total yield and constant-initial-state photoelectron spectroscopy studies as well. A preliminary analysis indicates the presence of optical structures related to valence and photoionizing excitations of the corresponding molecules in the vapor and/or solid phase. (Appendix, item 4)

(11) Direct UPS observation and identification of a CH radical on chemically modified Ni(111) surfaces or on the atomically "rough" Ni(110) surface via the use of Hartree-Fock calculations of radicals and surface complexes. Here the clean Ni(111) surface does not break the C-C bond of acetylene to form CH species as does the Ni(110) surface; however, chemical modification of the Ni(111) surface by (2x2) overlayers of π-bonded acetylene or oxygen does allow C-C bond scission. The radical also forms directly from acetylene on a NiO surface. (Appendix, item 5)

(12) UPS study of the atomically stepped Pt(755) and Pt(111) surface indicates small differences in the electronic structure of the stepped surface in contrast to the large changes in electronic structure previously found to occur after reconstruction of the Pt(100) surface. These small differences are consistant with small modifications in the local density of states of the atoms at steps. In particular, additional state density occurs on the stepped surface at the bottom of the d-bands - a region where adsorbate orbitals are located - which may enhance interactions with these molecules and facilitate chemical reactions. (Appendix, item 6)

(13) UPS and thermal desorption study of cyclic hydrocarbons, (C_6H_6, C_6H_8, C_6H_{10} and C_6H_{12}) on Ni(111), Pd(111), Pd(polycryst.), Pt(111) and Pt(755), indicate systematic differences in the bonding and reaction of these molecules to these surfaces. At room temperature all unsaturated cyclics decompose to benzene on Ni(111), Pd(111) and Pt(755) while on Pt(111) C_6H_{10} is stable. For room temperature exposure of C_6H_{12} to Pt(111), Pt(755), Pd(111) and polycrystalline Pd benzene forms. Also large exposures of Pt(111) to benzene indicate a new phase of benzene which is different from that obtained at low exposures (to be published).

REFERENCES

1. J. E. Demuth and D. E. Eastman, Phys. Rev. B **13**, 1523 (1976).

2. J. E. Demuth and D. E. Eastman, J. Vac. Sci. Technol. **13** 283 (1976).

3. J. E. Demuth and D. E. Eastman, Solid State Comm. **18**, 1497 (1976).

4. J. E. Demuth, Chemical Phys. Letters **45**, 12 (1977).

5. G. W. Rubloff and J. E. Demuth, J. Vac. Sci. Technol. **14**, 419 (1977).

6. G. W. Rubloff, W. D. Grobman, and H. Lüth, Phys. Rev. B **14**, 1450 (1976).

III. Personnel involved in contract work

J. E. Demuth - principal co-investigator.

G. W. Rubloff - principal co-investigator.

D. E. Eastman.

J. L. Freeouf.

J. J. Donelon.

A. Marx.

IV. APPENDIX

Item 1. preprint, "Chemisorption and Decomposition Reactions Of oxygen-containing Organic Molecules on Clean Pd Surfaces Studied by UV Photoemission", H. Lüth, G. W. Rubloff and W. D. Grobman, to be published in Surface Science.

Item 2. preprint, "Ultraviolet Photoemission Studies of Hydrogen Chemisorption Bonding to Ni, Pd and Pt Surfaces", J. E. Demuth.

Item 3. preprint, "Molecular Geometries of Acetylene and Ethylene Chemisorbed on Cu, Ni, Pd and Pt Surfaces", J. E. Demuth.

Item 4. Summary, "Surface Reflectance Spectroscopy and Related Studies of Surface Optical Excitations", G. W. Rubloff and J. Freeouf.

Item 5. preprint, "The Interaction of Acetylene with Ni(111), Chemisorbed Oxygen on Ni(111) and NiO(111): The Formation of CH Species on Chemically Modified Ni(111) Surfaces, J. E. Demuth.

item 6. Figure showing difference in UPS Spectra for Stepped and Flat Surfaces of Pt, J. E. Demuth, to be published.

APPENDIX

Item 1

CHEMISORPTION AND DECOMPOSITION REACTIONS OF OXYGEN-CONTAINING ORGANIC MOLECULES ON CLEAN PD SURFACES STUDIED BY UV PHOTOEMISSION*

H. Lüth,† G. W. Rubloff and W. D. Grobman
IBM Thomas J. Watson Research Center
Yorktown Heights, New York 10598

ABSTRACT: We have used uv photoemission (primarily at a photon energy $h\nu$ = 40.8 eV) to study chemisorption and decomposition reactions of small oxygen-containing organic molecules on clean polycrystalline Pd surfaces at 120 and 300 K. These molecules include methanol (CH_3OH), dimethyl ether (CH_3OCH_3) formaldehyde (H_2CO), acetaldehyde [$H(CH_3)CO$], and acetone [$(CH_3)_2CO$]. Chemisorption bonding of these molecules to the Pd surface occurs primarily through the lone-pair orbitals associated with the oxygen atoms, as evidenced by chemical bonding shifts of these orbitals toward larger electron binding energy relative to the other adsorbate valence orbitals. At 300 K all the molecules studied decompose on the surface, resulting in chemisorbed CO. Since chemisorbed (as well as condensed) phases of some of these molecules (CH_3OH and $H(CH_3)CO$) are observed at low temperature, the decomposition to CO is a thermally-activated reaction. The observed orbital shifts associated with chemisorption bonding are used to make rough estimates of interaction strengths and chemisorption bond energies (within the framework of Mulliken's theory of electron donor-acceptor complexes as applied to chemisorption by Grimley). The resulting heats of chemisorption are consistent with the observed surface reactions.

* Supported in part by ONR Contract #N00014-75-C-0346.

† Permanent address: 2 Physikalisches Institut der Rheinish-Westfälischen Technischen Hochschule Aachen, 5100 - Aachen, F. R. Germany.

I. INTRODUCTION

Ultraviolet photoemission spectroscopy (UPS) has recently become a powerful tool for surface chemistry because it has a high surface-sensitivity and because it directly reveals both the valence orbitals of adsorbed molecules and the surface electronic structure of the substrate, which together reflect the electronic properties of chemical bonding and reactions at surfaces. In particular, UPS can be used: (i) to determine the chemical identity of absorbed species (of which the valence orbitals represent a kind of "fingerprint")[1-5]; (ii) to reveal orbital bonding mechanisms responsible for chemisorption[1-4]; and (iii) in some special cases to estimate chemisorption interaction strengths in order to understand the energetics of surface reactions[1].

We have used UPS (primarily at $h\nu = 40.8$ eV) to study chemisorption bonding and surface reactions of several small oxygen-containing organic molecules on clean polycrystalline Pd surfaces at 120 and 300 K. These molecules include methanol (CH_3OH), dimethyl ether (CH_3OCH_3), formaldehyde (H_2CO), acetaldehyde [$H(CH_3)CO$] and acetone [$(CH_3)_2CO$]. These molecules are prototypes which represent the simplest members of several classes of organic molecules (alcohols, ethers, aldehydes and ketones) which contain oxygen. Their behavior on Pd surfaces has additional interest because of its possible relation to catalytic reactions of practical significance. The group VIII transition metals Ni, Pd and Pt are all catalytically active. Catalytic cracking of alcohols on metals at high temperatures has long been recognized[6], and considerable attention has been given to these reactions

since alcohol-type intermediates are believed[7] to be important in Fischer-Tropsch synthesis. Furthermore, the adsorption behavior of H_2CO and $H(CH_3)CO$ is of interest because aldehydes are thought to be intermediates in the decomposition of alcohols[8-10]. Perhaps an understanding of simple chemisorption and decomposition properties of such simple organic molecules on transition metals obtained from UPS studies will be of value in understanding the mechanisms for the corresponding reactions in heterogeneous catalysis at higher temperatures and pressures.

Our results show that chemisorption bonding of these oxygen-containing organic molecules to the Pd surface involves primarily the interaction between the Pd d-electrons and the lone-pair orbitals associated with the oxygen atoms. At 300 K all of these molecules decompose on the surface, resulting in chemisorbed CO. This decomposition reaction appears to be thermally activated: CO is not observed in significant concentration at 120 K. Estimates of interaction strengths and heats of chemisorption made from observed orbital bonding shifts are consistent with the observed decomposition reactions.

II. EXPERIMENTAL TECHNIQUES

Clean polycrystalline Pd surfaces were prepared by evaporation of Pd films from 0.25mm dia. Pd filaments (99.999% purity) in ultra high vacuum (operating pressure $\leq 10^{-10}$ torr). The usual substrate for the Pd film was the nonpolar $(1\bar{1}00)$ face of a ZnO single crystal, which could be heated electrically by resistive heating and cooled to $\sim$ 120 K. For the study of acetone at 300 K, the substrate for the Pd evaporation was a

polished, non-oriented Si surface. Before each new evaporation the old Pd film was cleaned of possible CO contamination by annealing to $\sim 250°$ C[11] in order to avoid any diffusion of CO already present to the surface of the fresh film. During Pd evaporation the substrate was at room temperature and the total pressure did not exceed $\sim 5 \times 10^{-9}$ torr.

Partial pressures of residual and input gases were monitored with a quadrupole mass spectrometer. Adsorbate gases of CH_3OH, CH_3OCH_3, $H(CH_3)CO$ and $(CH_3)_2CO$ were obtained from the equilibrium vapor pressure of reagent grade liquids. H_2CO gas was prepared and monitored with the mass spectrometer as described by Yates et. al[12]; paraformaldehyde crystals were heated to 350 K in a baked gas handling system to produce H_2CO vapor, which was distilled out at 77 K and then purified by multiple freeze-thaw-vaporize cycles. H_2CO vapor released at 195 K was then admitted into the UHV system during gas exposure. In all cases, we attempted to minimize exchange (displacement) reactions of adsorbate gases with residual gases on the walls of the UHV system during exposures; this was done by predosing the system with the adsorbate gas of interest before producing a clean fresh film to be studied and by using the mass spectrometer to monitor gases in the system during the exposures. Predosing the UHV system also served to minimize work function changes of the electron energy analyzer during measurement.

The incident photon beam consisted of He I and He II radiation (photon energies $h\nu$ = 21.2 and 40.8 eV respectively) from a differentially pumped He resonance lamp. The light beam intercepted the surface at $\sim 45°$ angle of incidence. Kinetic energy distributions of the resulting photoelectrons were measured using a double-pass cylindrical mirror

analyzer at an energy resolution $\sim$ 0.35 - 0.4 eV, in conjunction with electron counting techniques. The axis of the analyzer was $\sim$ 45° from the normal to the sample surface and $\sim$ 45° from the plane of incidence of the light beam, so that the photoelectron intensity was averaged over a range of angles from near-normal to near-grazing emission. Gas phase photoelectron spectra of the adsorbate molecules were measured with a similar apparatus in order to make a direct comparison to the adsorbate spectra at the same photon energies and with similar resolution and geometry. In these gas phase measurements, the gas inlet was made by a jet which produced a high gas concentration near the image point of the analyzer, and the emission lines of Xe were used as a reference for the ionization potential scale.[13]

III. RESULTS

The UPS spectrum at $h\nu$ = 40.8 eV for a clean evaporated Pd film at 300 K is shown by the dashed line in Fig. 1a. This spectrum is in complete agreement with that measured previously[11] on similar surfaces and shows the Pd d-band extending from the Fermi energy E_F to $\sim$ 4.5 eV electron binding energy (BE) (measured relative to a BE zero at E_F). The sharp increase in emission for BE > 16 eV (left side of Fig. 1a) is the onset of the spectrum produced by the 21.2 eV He I light from the resonance lamp. The work function ϕ of the clean evaporated Pd films varied between 5.5 and 5.7 eV as determined from the width ($h\nu$-ϕ) of the measured kinetic energy distribution; these values are in agreement with the value 5.55 $\pm$ 0.1 eV reported previously[14].

A. Methanol and Dimethyl Ether

The UPS spectrum at $h\nu = 40.8$ eV resulting from a 2.5 L exposure (1 L $\equiv 10^{-6}$ torr sec) of the clean Pd surface at 120 K to CH_3OH (methanol) is shown by the solid line in Fig. 1a. In addition to the work function decrease of $\Delta\phi = -0.5$ eV, new spectral features are observed between 3 and 16 eV BE. These adsorbate emission structures are more clearly seen in the difference curve in Fig. 1b, which is obtained by subtraction of the clean surface spectrum (attenuated by a constant factor to account for the overall reduction in Pd emission) from the exposed surface spectrum in Fig. 1a. New adsorbate emission peaks are observed at $\sim$ 4.9, 6.2, 8.8, 11.0 and 15.9 eV BE, and the top of the Pd d-band, i.e., just below the E_F, is preferentially attenuated compared to the rest of the band. Further exposure of this CH_3OH covered surface to a CH_3OH ambient of 5×10^{-8} torr strongly suppresses the Pd d-emission, reduces ϕ slightly (by $\sim$ 0.2 eV), and shifts the deeper-lying emission bands uniformly downwards (toward larger BE) by $\sim$ 0.3 eV. Only the highest lying orbital, the oxygen lone-pair, does not participate in this uniform shift; instead it is shifted to smaller BE by 0.3 eV. This behavior is seen in the difference curve in Fig. 1c, which is obtained by subtracting the 2.5 L spectrum of Fig. 1a (properly renormalized to account for the attenuation of substrate emission) from the spectrum measured in the ambient.

The UPS spectrum of gas phase CH_3OH at $h\nu = 40.8$ eV is shown in Fig. 1d. The spectral features of the adsorbate in Fig. 1c are

essentially identical to those of gas phase CH_3OH, except that the BE of orbitals in this adsorbed phase have been shifted uniformly to lower values from their corresponding gas phase ionization potentials (IP's). (Note that BE's for the adsorbed phase, referenced to the vacuum level (E_{vac}) for comparison to vapor phase IP's, are given by the relation $BE(E_{vac} = 0) = BE(E_F = 0) + \phi + \Delta\phi$.) This similarity in the spectra indicates that the adsorbed phase of CH_3OH in Fig. 1c has little chemical interaction with the surface. We therefore identify it as a condensed layer with adsorbate orbitals shifted to smaller BE (compared to gas phase values) by a uniform extramolecular relaxation/polarization shift[1,15,16] $\Delta E_R \tilde{=} 1.4$ eV.

The lower-lying (larger BE) adsorbate orbitals in Fig. 1b are very similar to those of CH_3OH in Figs. 1c and 1d, but they appear further shifted upwards (toward smaller BE) compared to the condensed phase spectrum. In contrast, the highest-lying, oxygen lone-pair orbital is shifted in a different way, toward larger BE relative to the condensed phase (and relative to the other orbitals of the phase in Fig. 1b). This distortion of the spectrum indicates a significant chemical interaction with the surface, and we identify the lower-coverage adsorbate phase in Fig. 1b as CH_3OH chemisorbed via the (highest-lying) oxygen lone-pair orbital, which is primarily an O(2p) atomic orbital perpendicular to the COH plane of the molecule. A uniform relaxation/polarization shift $\Delta E_R \tilde{=} 1.6$ eV (from gas phase I.P.'s) is observed for all the other valence orbitals. The total shift of the oxygen lone-pair, which involves bonding effects in addition, can be considered (at least for simplicity)

to contain a downward shift $\Delta E_B \tilde{=} 0.6$ eV (toward larger BE) associated with the chemisorption bonding in addition to the upward ΔE_R seen for the other orbitals.

Exposing the clean Pd surface at 300 K to 60 L CH_3OH produces a UPS spectrum with two characteristic new features (compared with clean Pd) at 7.9 and 10.9 eV BE and a marked distortion of the shape of the Pd d-band emission. The corresponding difference curve (exposed minus clean) is shown by the solid line in Fig. 1e. An essentially identical spectrum is obtained by exposing the clean Pd surface at 300 K to 80 L CH_3OCH_3 (Fig. 1e, dot-dash curve). The dashed difference spectrum in Fig. 1e is obtained by exposure of the clean Pd surface at 300 K to 10 L CO. Since all three curves in Fig. 1e are the same, it is clear that at room temperature both CH_3OH and CH_3OCH_3 are decomposed on the Pd surface, resulting in chemisorbed CO. The UPS spectra indicate no other reaction products on the surface, although the presence of adsorbed H cannot be ruled out since hydrogen adsorption gave no significant changes in the UPS spectra other than d-band distortions typical of most adsorbates. The two new emission peaks and the work function increase are very characteristic of CO chemisorbed on transition metals[11].

B. Acetaldehyde and Formaldehyde

Figures 2a, 2c, and 2e show results for the adsorption of the simple aldehydehydes H_2CO and $H(CH_3)CO$ on clean polycrystalline Pd surfaces measured at $h\nu$ = 40.8 eV. Room temperature exposures of H_2CO and $H(CH_3)CO$ (Fig. 2e) result in the same photoemission spectrum (that of adsorbed CO)

as was obtained with CH_3OH and CH_3OCH_3 at 300 K. Thus H_2CO and $H(CH_3)CO$ are spontaneously decomposed on clean Pd at 300 K to form chemisorbed CO.

The difference curve corresponding to a 68 L exposure of $H(CH_3)CO$ to the clean Pd surface at 120 K is shown in Fig. 2a. The work function change is negative ($\Delta\phi$ = -0.8 eV). This adsorbed species can be identified as undecomposed $H(CH_3)CO$ by comparison with the corresponding gas phase spectrum at $h\nu$ = 40.8 eV shown in Fig. 2b: by shifting the orbitals of the gas phase spectrum upward by $\Delta E_R \tilde{=}$ 1.6 eV to account for extramolecular relaxation/polarization effects, a spectrum very similar to that for the adsorbed phase is obtained. However, an additional shift $\Delta E_B \tilde{=}$ 0.4 eV downward (to larger BE) of the highest-lying gas phase orbital (the oxygen lone-pair) is required to match the adsorbed spectrum (Fig. 2a). This shift ΔE_B is attributed to chemical (chemisorption) bonding of the $H(CH_3)CO$ molecule to the surface via its oxygen lone-pair orbital, which is essentially an O(2p) atomic orbital perpendicular to the C = O axis and in the H-(C=O)-C plane of the molecule.

Measurement in a $H(CH_3)CO$ ambient ($p \sim 10^{-7}$ torr) at 120 K produces the same result as for a 68 L exposure. Considerably smaller exposures (5 - 20 L) show very weak CO structures which correspond to very small CO coverages produced at 120 K (estimated to be < 1/10 the saturation coverage of chemisorbed $H(CH_3)CO$). Since most of the adsorbed $H(CH_3)CO$ remains undecomposed at low temperature, the decomposition of $H(CH_3)CO$ to CO which occurs efficiently at higher temperature represents a thermally-activated process.

C. Acetone

The adsorption behavior of $(CH_3)_2CO$ (acetone), a ketone, is similar to that of the aldehydes. At 300 K, $(CH_3)_2CO$ decomposes to leave chemisorbed CO on the surface (Fig. 2e). However, this decomposition is accompanied by a work function decrease ($\Delta\phi$ = -0.3 eV), in contrast to the usual work function increase ($\Delta\phi$ = +0.3 to +0.7 eV) observed for chemisorbed CO, whether produced by CO exposure or by decomposition from CH_3OH, CH_3OCH_3, H_2CO, or $H(CH_3)CO$. The negative sign of $\Delta\phi$ for the case of acetone exposure suggests that in this case there may be an additional species adsorbed along with CO. However, the UPS spectra show no emission features other than those of chemisorbed CO, and the origin of the negative $\Delta\phi$ is not understood at present.

Cooling the sample to 120 K in a 1×10^{-7} torr $(CH_3)_2CO$ ambient causes a work function decrease of $\Delta\phi$ = -1.2 eV relative to the clean surface. Comparing Fig. 2c to the gas phase spectrum in Fig. 2d, we see that this additional adsorbed species is undecomposed $(CH_3)_2CO$. The gas phase orbitals are shifted uniformly upward (to smaller BE) by the relaxation/polarization shift $\Delta E_R \tilde{=} 1.8$ eV, while the oxygen lone-pair orbital undergoes an additional chemical bonding shift downward by $\Delta E_B \tilde{=} 0.5$ eV. The additional adsorbate present at 120 K therefore seems to be chemisorbed via the oxygen lone-pair orbital rather than simply condensed.

IV. DISCUSSION

The UPS spectra presented here for undissociated phases of adsorbed CH_3OH, $H(CH_3)CO$, and $(CH_3)_2CO$ are consistent with the original observation by Demuth and Eastman[1] that adsorption of an organic molecule in a particular surface phase shifts those molecular orbitals of the molecule not directly involved in forming the chemisorption bond toward smaller BE, by the same amount (to within 0.1 - 0.2 eV)[17]. This uniformity of the extramolecular relaxation/polarization shifts of nonbonding orbitals has since been documented in a wide range of organic adsorbate/substrate systems and constitutes a general rule of significant value for UPS studies of surface chemistry[16]. Such behavior makes it possible in many cases to determine orbital bonding mechanisms from the considerably different BE shifts of those orbitals which form the chemisorption bond.

The chemisorbed phases of CH_3OH, $H(CH_3)CO$, and $(CH_3)_2CO$ observed here (Figs. 1b, 2a, and 2c) suggest strongly that (as far as filled molecular orbitals are concerned) such molecules (alcohols, aldehydes, and ketones) are chemisorbed on this polycrystalline transition metal surface primarily via the oxygen lone-pair orbital. This orbital is the highest-lying one (smallest BE) in each case. The π orbital associated with the $C = O$ group in the aldehydes and ketones seems to play a considerably less important (if any) role in chemisorption on Pd. This may represent a general tendency for oxygen lone-pair orbitals, when present, to be more chemically active than π and σ orbitals in bonding to

transition metal surfaces. In unsaturated hydrocarbons, which contain no oxygen, the π orbitals account for chemisorption bonding to transition metals[1].

It is interesting to note that, although oxygen lone-pair orbitals are present in all the adsorbates studied here and are active in chemisorption bonding, their geometrical relation to the framework of the molecule differs. In CH_3OH and CH_3OCH_3, the highest-lying lone-pair orbital is perpendicular to the central molecular plane (COH or COC), while in H_2CO, $H(CH_3)CO$, and $(CH_3)_2CO$ the lone-pair orbital is in the central molecular plane and perpendicular to the C = O double bond. One would expect the methyl groups in these molecules to cause steric hindrance of a bonding geometry in which the central plane of the molecule lies flat on the surface. Such a configuration in general would leave the oxygen lone-pair with different orientations to the surface - perpendicular to the surface for chemisorbed CH_3OH, but parallel to it for chemisorbed $H(CH_3)CO$ and $(CH_3)_2CO$. Perhaps the most reasonable guess is that all these molecules are bonded end-on to the surface via the oxygen atom through its lone-pair orbital, so that the lone-pair would then lie parallel to the surface in all cases.

In the cases of chemisorption observed here, the Pd d-band shape is distorted by the adsorbate and shows preferential attenuation of the top of the d-band. This effect, noted previously for chemisorption of unsaturated hydrocarbons on Ni (111)[1], is indicative of strong participation of the Pd d-bands in bonding[1]. Thus the primary chemisorption bond formed via the oxygen lone-pair orbitals for the simple organic molecules studied here appears to involve a strong interaction with the Pd d-bands.

The decomposition to chemisorbed CO observed for CH_3OH, CH_3OCH_3, H_2CO, $H(CH_3)CO$, and $(CH_3)_2CO$ may represent a general tendency toward catalytic decomposition to CO for alchohols, ethers, aldehydes and ketones on Pd and perhaps on other transition metals.

V. ESTIMATES OF INTERACTION STRENGTHS, CHEMISORPTION BOND ENERGIES, AND HEATS OF REACTION

We now use the observed bonding shifts ΔE_B^n for the oxygen lone-pair orbitals of the undecomposed species to make rough estimates of interaction strengths and bond energies for chemisorption in relation to the observed reactions. We treat only the cases of chemisorbed $H(CH_3)CO$ and $(CH_3)_2CO$, omitting that of CH_3OH for reasons explained later. We follow the general approach of Demuth and Eastman[1] in using Mulliken's theory of electron donor-acceptor complexes[18] as applied to weak chemisorption by Grimley[19]. Caution must be used in interpreting chemisorption bond energies and heats of reaction using this model, since such an analysis involves a number of ad hoc assumptions whose accuracy is difficult to estimate.

Since the essential nature of the molecular orbital spectrum is preserved upon chemisorption, and since orbital bonding shifts are small compared to bond energies within the molecule, within this model an approximate wave function of the system is obtained in perturbation theory by mixing charge-transfer states into the "no bond" (neutral, isolated molecule) state. These charge-transfer states involve electron transfer (i) from the highest filled molecular orbital (the chemically active oxygen lone-pair) to the empty Pd d-band, and (ii) from the filled Pd d-band into the lowest-lying

empty molecular orbital (affinity level) of the adsorbate (the π^* orbital for $H(CH_3)CO$, and $(CH_3)_2CO$). When applied to this case, Grimley's result for the chemisorption energy ΔE^c (heat of adsorption) becomes[1]

$$-\Delta E^c = V^2_{\pi^* d} \frac{N_{\pi^*} N_d}{|E_d - E_{\pi^*}|} + V^2_{nd} \frac{N_n (1-N_d)}{|E_n - E_F|} \tag{1}$$

where N_n and N_{π^*} are the number of states in the lone-pair (n) and π^* orbitals (i.e., 2), and N_d is the fractional occupation of the Pd d-band (0.97). $|E_n - E_F|$ represents the energy separation between the filled lone-pair orbital and the empty d-states, which lie in a narrow band just above the Fermi energy E_F, while $|E_d - E_{\pi^*}|$ is the separation between the center of the filled d-bands ($\sim$ 6eV below the vacuum level) and the empty π^* electron affinity level (taken to be at the vacuum level). The interaction strengths V^2_{nd} and $V^2_{\pi^* d}$ are related to adsorbate orbital bonding shifts ΔE_B by[1]

$$V^2_{nd} \tilde{=} \Delta E^n_B |E_n - E_F| \tag{2a}$$

$$V^2_{\pi^* d} \tilde{=} \Delta E^{\pi^*}_B |E_d - E_{\pi^*}| \tag{2b}$$

The observed energy shift of the oxygen lone-pair orbital involves both extramolecular relaxation/polarization shifts ΔE_R, present for all adsorbate orbitals, and also a chemical bonding shift ΔE^n_B associated directly with chemisorption. For simplicity and because of the uniformity of ΔE_R observed for the other orbitals (and for the lone-pair in the

condensed phase), we assume ΔE_R^n for the oxygen lone-pair in the chemisorbed phase is the same as ΔE_R for the other orbitals. This allows us to make an estimate of the bonding contribution ΔE_B^n to the total shift. Values for ΔE_R, ΔE_B^n, $\Delta\phi$, E_n, and V_{nd} (obtained from ΔE_B^n by Eq. (2a)) are listed in Table I.

Although ΔE_B^n can be estimated in this way from spectroscopic photoemission data, the behavior of the empty states (such as the π^* orbital) is not observed in these experiments. Therefore, an estimate of $\Delta E_B^{\pi^*}$, the chemisorption-induced shift of the empty π^* orbital, must be made on theoretical grounds in order to calculate the heat of chemisorption ΔE_c. In the case of unsaturated hydrocarbons on Ni (111)[1], $V_{\pi^*d} = V_{\pi d}$ could be assumed because of the direct symmetry between the π and π^* orbitals, which should therefore have very similar overlap and interaction with the substrate.

If we assume an end-on bonding geometry for chemisorbed $H(CH_3)CO$ and $(CH_3)_2CO$ as suggested earlier, the interaction strengths V_{π^*d} and V_{nd} can be related in a simple way. If we take the central plane of the molecule as the XZ plane with the C=O bond along Z, then the oxygen lone-pair (n) orbital is primarily an atomic $O(2p_x)$. The π^* is composed of roughly equal contributions from atomic $O(2p_y)$ and $C(2p_y)$ orbitals. The end-on geometry thus gives the normal to the surface in the Z-direction. Since the $C(2p_y)$ part of the π^* orbital is relatively far from the surface (in the end-on configuration) compared to the $O(2p_y)$ part, its effect in bonding to the surface will be relatively small. The dominant part of the π^* orbital in the chemisorption bond (the $O(2p_y)$) then bears the same symmetry with

respect to the surface as does the n orbital, but only about half as much charge density of the π^* orbital (the $O(2p_y)$ half) is involved in the bonding. We therefore estimate

$$V^2_{\pi^* d} \tilde{=} 0.5\ V^2_{nd} \qquad (3)$$

for the cases of $H(CH_3)CO$ and $(CH_3)_2CO$. Since the lowest-lying empty orbital of CH_3OH bears no correspondingly simple geometric relation to the oxygen lone-pair, we cannot estimate the relative interaction strengths in order to approximate a heat of chemisorption for CH_3OH.

Using the above approach, we estimate chemisorption bond energies $-\Delta E^c$ of 0.32 and 0.35 eV for the 120 K phases of $H(CH_3)CO$ and $(CH_3)_2CO$.[22] In comparison, the heat of chemisorption for CO (the decomposition product) on Pd is $\sim$ 1.21 eV/molecule[20], while that for H_2 on Pd is $\sim$ 0.9 eV/molecule[21].

The considerably smaller heats of chemisorption for $H(CH_3)CO$ and $(CH_3)_2CO$ compared to those for CO and H_2 suggest that the decomposition reaction is likely. However, to understand correctly why decomposition to CO in fact occurs on Pd at 300 K for $H(CH_3)CO$ and for $(CH_3)_2CO$, one must consider the total energy of the reaction, including the chemisorption energies of all adsorbed species. To favor decomposition, the total energy change ΔH^s on the surface must be negative (energy gained by decomposition):

$$\Delta H^s = \Delta H^g + [\Delta E^c\ (\text{decomp}) - \Delta E^c\ (\text{undecomp})] < 0 \qquad (4)$$

ΔH^g is the total energy required to decompose the molecule in the gas phase. The quantity ΔE^c (undecomp) is the chemisorption energy of the undecomposed molecule and ΔE^c (decomp) is the total chemisorption energy of

all adsorbed decomposition products. For the present we assume the simplest possible reaction products which include adsorbed CO:

$$H(CH_3)CO\ (ads) \xrightarrow{Pd} CO\ (ads) + CH_4\ (gas)\ , \qquad (5a)$$

$$(CH_3)_2CO\ (ads) \xrightarrow{Pd} CO\ (ads) + C_2H_6\ (gas)\ , \qquad (5b)$$

We estimate heats of reaction ΔH^g for decomposition reactions in the gas phase from the energies[23] required to break and reform chemical bonds of free molecules. These values are $\Delta H^g = +0.14$ and $+0.27$ eV/molecule for reactions 5a and 5b respectively (since $\Delta H^g > 0$, the reactions are not favored in the gas phase). In the reaction paths 5a and 5b, $-\Delta E^c$ (decomp) = 1.21 eV/molecule, simply the heat of chemisorption of CO on Pd[20]. Then from Eq. (4) the total heat of reaction on the surface $\Delta H^s = -0.75$ and -0.59 eV/molecule for the decompositions of $H(CH_3)CO$ (5a) and $(CH_3)_2CO$ (5b) respectively. Since $\Delta H^s < 0$, this predicts that the decomposition reactions are energetically favored on the surface, as observed (they are in fact thermally activated).

In the reaction paths (5a and 5b) above, it is assumed that the saturated hydrocarbons CH_4 and C_2H_6 are not chemisorbed ($-\Delta E^c \tilde{=} 0$). This assumption is consistent with the observation that they adsorb on Ni (111) only at low temperatures and form what appears to be a simple physisorbed layer (no chemical bonding shift)[24]. If reaction products other than CH_4 and C_2H_6 are considered in 5a and 5b (e.g., adsorbed carbon and hydrogen), then larger magnitudes of ΔH^s (<0) are obtained, so that decomposition to CO remains favorable for $H(CH_3)CO$ and for $(CH_3)_2CO$.

It is difficult to determine the accuracy of the above estimates of interaction strengths, bond energies and heats of reaction because several significant assumptions are required for the analysis. The predictions of this analysis, however, are very clear: the relatively large magnitudes of ΔH^s (cf. ΔH^g and ΔE^c (undecomp)) result primarily from the rather large heat of chemisorption of CO on Pd and imply that decomposition should occur. This prediction agrees with the experimental results. This consistency does not provide a stringent test of the validity of our analysis since ΔH^s is determined mainly by ΔE^c(CO); however, it is worth noting that in the cases analyzed here the Mulliken/Grimley model to relate measured orbital bonding shifts seen in UPS to chemisorption interaction strengths predicts results consistent with the observed surface reactions. The above discussion of this model for $H(CH_3)CO$ and $(CH_3)CO$ demonstrates further that its use for UPS studies is restricted to certain special classes of molecules in which the filled and empty molecular orbitals active in chemisorption bear a simple relation to each other, and this example also suggests that these classes include some organic molecules (e.g., aldehydes and ketones) other than the unsaturated hydrocarbons treated previously[1].

VI. CONCLUSIONS

The simple oxygen-containing organic molecules CH_3OH, CH_3OCH_3, H_2CO, $H(CH_3)CO$ and $(CH_3)_2CO$ have been observed to undergo a thermally-activated decomposition reaction at 300 K on clean polycrystalline Pd surfaces, resulting in a layer of chemisorbed CO. The chemisorption of all these molecules on the Pd surface is dominated by bonding via the oxygen

lone-pair orbital. Rough estimates of interaction strengths and heats of chemisorption made from orbital bonding shifts observed in the photoemission spectra are consistent with the reactions which occur.

VII. ACKNOWLEDGEMENTS

We are grateful for stimulating and useful discussions with D. E. Eastman and J. E. Demuth.

REFERENCES

1. J. E. Demuth and D. E. Eastman, Phys. Rev. Lett. 32, 1123 (1974); D. E. Eastman and J. E. Demuth, Japan J. Appl. Physics, Suppl. 2, Part 2, p. 827 (1974).

2. E. W. Plummer, B. J. Waclawski and T. V. Vorberger, Chem. Phys. Letters 28, 510 (1974).

3. P. R. Norton and P. J. Richards, Surface Sci. 49, 567 (1975).

4. H. Lüth, G. W. Rubloff and W. D. Grobman, to be published.

5. W. F. Egelhoff, Jr., D. L. Perry and J. W. Linnett, J. Electron Spectros. 5, 339 (1974).

6. P. Sabatier, Catalysis in Organic Chemistry (Van Nostrand, New York, 1922).

7. P. H. Emmett, ed., Catalysis, Vol. IV, (Reinhold, New York, 1956).

8. G. Blyholder and L. D. Neff, J. Catalysis 2, 138 (1963).

9. R. Paul, Bull. Soc. Chim. France 8, 507 (1941).

10. R. Paul, Compt. rend. 208, 1319 (1939).

11. J. Küppers, H. Conrad, G. Ertl, and E. E. Latta, Japan J. Appl. Phys. Suppl. 2, Part 2, p. 225 (1974).

12. J. T. Yates, Jr., T. E. Madey and M. J. Dresser, J. Catalysis 30, 260 (1973).

13. D. W. Turner et. al., Molecular Photoelectron Spectroscopy (John Wiley and Sons, N. Y., 1970).

14. D. E. Eastman, Phys. Rev. B 2, 1 (1970).

15. K. Y. Yu, J. E. McMenamin, and W. E. Spicer, J. Vac. Sci. Technol. 12, 286 (1975); also Surface Sci. 50, 149 (1975).

16. G. W. Rubloff, W. D. Grobman and H. Lüth, to be published in Phys. Rev. B15.

17. Two orbitals of $H(CH_3)CO$ exhibit deviations from this pattern (by $\sim$ 0.5 eV). These anomalies can be understood on the basis of the specific character of the molecular orbitals. See Ref. 16 for details.

18. R. S. Mulliken, J. Amer. Chem. Soc. 74, 811 (1952).

19. T. B. Grimley, in Molecular Processes on Solid Surfaces, edited by E. Dranglis (McGraw-Hill, New York, 1969), p. 299.

20. J. C. Tracy and P. W. Palmberg, Surface Sci. 14, 274 (1969).

21. H. Conrad, G. Ertl, and E. E. Latta, Surface Sci. 41, 435 (1974).

22. This value for the 120 K chemisorbed phase of $(CH_3)_2CO$ is meaningful only on the assumption that this phase is in contact with (and bonded to) the Pd surface rather than in a second layer.

23. T. L. Cottrell, The Strength of Chemical Bonds (Butterworths, London, 1958), and L. Pauling, The Nature of the Chemical Bond (Cornell University Press, Ithaca, N. Y., 1960).

24. J. E. Demuth and D. E. Eastman, to be published.

TABLE I

Summary of Chemisorption and Reaction Information for CH_3OH, $H(CH_3)CO$, and $(CH_3)_2CO$ on Pd (energies in eV). The energy positions E_n of the lone-pair orbitals are referred to a zero at the vacuum level.

	CH_3OH	$H(CH_3)CO$	$(CH_3)_2CO$
$\Delta\phi$	-0.5	-0.8	-1.2
ΔE_R	1.6	1.6	1.8
ΔE_B^n	0.4	0.4	0.5
E_n	11.0	10.2	9.6
V_{nd}	-	1.36	1.41
$-\Delta E^c$ (undecomp)	-	0.32	0.35
ΔH^g(eqs. 5)	-	+0.14	+0.27
ΔH^s(eqs. 5)	-	-0.75	-0.59

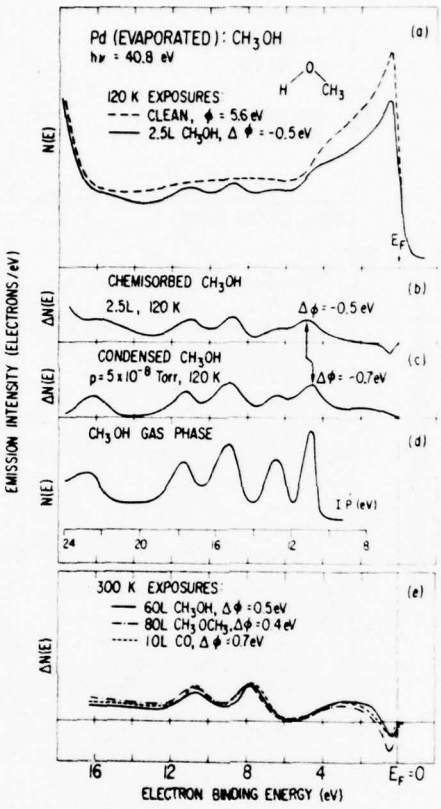


Fig. 1. UPS spectra at $h\nu = 40.8$ eV:

(a) spectra for the clean Pd surface (dashed curve) and after a 2.5 L exposure at 120 K to CH_3OH (solid curve);

(b) difference curve for chemisorbed CH_3OH (2.5 L) corresponding to (a);

(c) difference curve for condensed CH_3OH resulting from 5×10^{-8} torr CH_3OH ambient at 120 K;

(d) gas phase CH_3OH spectrum at $h\nu = 40.8$ eV;

(e) difference curves corresponding to exposures of the clean Pd surface at 300 K to 60 L of CH_3OH (solid curve), 80 L of CH_3OCH_3 (dot-dash curve), and 10 L of CO (dashed curve).

BEST AVAILABLE COPY

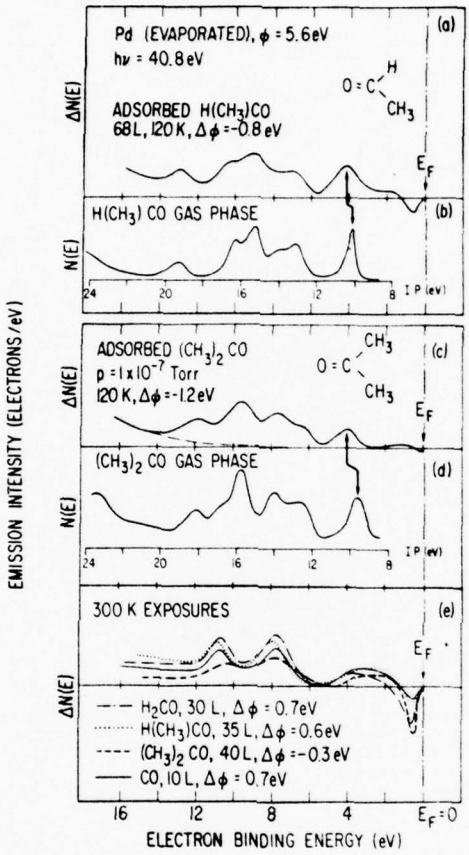


Fig. 2. UPS spectra at $h\nu$ = 40.8 eV:

(a) difference curve for chemisorbed $H(CH_3)CO$ (68 L) on Pd at 120 K;

(b) gas phase $H(CH_3)CO$ spectrum;

(c) difference curve for chemisorbed $(CH_3)_2CO$ on Pd at 120 K produced by exposure to an ambient $p = 1x10^{-7}$ torr);

(d) gas phase $(CH_3)_2CO$ spectrum;

(e) difference curves corresponding to exposures of the clean Pd surface at 300 K to 30 L of H_2CO (dot-dash curve), 35 L of $H(CH_3)CO$ (dotted curve), 40 L of $(CH_3)_2CO$ (dashed curve), and 10 L of CO (solid curve).

APPENDIX

Item 2

RC 6334 (#27209) 12/21/76
Surface Science 10 pages

ULTRAVIOLET PHOTOEMISSION STUDIES OF HYDROGEN CHEMISORPTION BONDING TO Ni, Pd AND Pt SURFACES*

J. E. Demuth

IBM Thomas J. Watson Research Center
Yorktown Heights, New York 10598

Typed by Marilyn Salvatore on CMC (JED.977)

ABSTRACT

Ultraviolet photoemission results for hydrogen chemisorbed on Ni(110), Ni(111), Pd(111) and Pt(111) surfaces indicate that while s- and d-electrons of the substrate are both involved in bonding, significant differences exist in the nature and relative strengths of these bonding components. The interaction of chemisorbed hydrogen with d-electrons of Ni differs from and is likely weaker than with the d-electrons of Pd or Pt while the interaction with the metallic s-band is the strongest for Ni. The implications of these results to surface reactions involving chemisorbed hydrogen are mentioned.

* Partially supported by ONR Contract N00014-75-C-0346.

ULTRAVIOLET PHOTOEMISSION STUDIES OF HYDROGEN CHEMISORPTION BONDING TO Ni, Pd AND Pt SURFACES*

The nature of the chemisorption bond of atomic hydrogen to transition metals is of interest for many reasons, one for example being that atomic hydrogen is directly involved in many chemical reactions at surfaces. Although the importance of d-electrons in transition metal chemistry and chemisorption is well recognized,[1] the role of s- and p-electrons is less understood but has been postulated to be of importance[2]. Recent calculations of hydrogen interacting with a single atom and diatom of Ni suggest that bonding occurs predominantly via s-electrons and that although d-electrons play an important role in molecular dissociation they play only a minor role in bonding[3-4]. We note that such conclusions for hydrogen bonded to 3d-transition metal atoms have recently been generalized to "transition metal" surfaces to suggest that d-electrons play only an indirect role in chemisorption and catalysis[5]. While one calculation for hydrogen chemisorbed to a Ni surface[6] supports such a viewpoint, other calculations on Ni surfaces[7] and clusters[8] conclude that d-electrons also play a major role in bonding. Thus, many questions exist regarding the nature of hydrogen bonding to Ni surfaces, the role of d-electrons in catalysis and, more importantly, whether Ni serves as a prototype transition metal for understanding bonding and catalysis on other transition metals surfaces.

Here, we present UV photoemission spectroscopy (UPS) results for hydrogen chemisorbed to Ni(111), Pd(111) and Pt(111) surfaces which show that the details of the bonding interactions for hydrogen on Ni are different from those on Pd or Pt surfaces. These results also provide insight as to the relative participation of s- versus d-electrons in hydrogen bonding to Ni, Pd and Pt surfaces, as well as to a possible cause for differences in, for example, hydrogenation reactions on these materials.

---

* Partially supported by ONR Contract N00014-75-C-0346.

Experimental Procedure: The present studies were performed in a turbomolecular pumped UHV system (base pressure $< 1 \times 10^{-10}$ torr) equipped with a He resonance lamp ($\sim 1 \times 10^{-10}$ total system pressure increase while in operation), electron energy analyzer, LEED optics, quadrupole mass spectrometer and auxiliary electron gun for Auger and energy loss spectroscopy. Single crystal samples of Ni(111), Ni(110), Pd(111) and Pt(111) were prepared by conventional techniques and mounted on a multiple sample holder which permitted the samples to be liquid nitrogen cooled to T ~ 78 K or independently resistivily heated to T ~ 1600 K as measured with a Chromel-Alumel thermocouple. The single crystals were cleaned by mild oxidation treatments, argon ion sputter-etching and subsequent annealing. Surface characterization was performed by LEED, Auger and photoemission analyses.

Energy analysis of the photoemitted electrons was performed with a double pass cylindrical mirror analyzer (CMA) operated in a fixed pass mode so as to have a minimum resolution of ~ .15 eV for He I, Ne I or Ne II UPS work and ~ .25 eV for He II UPS work. The samples could be rotated with their normal direction in the plane defined by the axis of the CMA and the photon beam. The photon beam lies 73° off the axis of the CMA, and we nominally chose the sample normal to be 20° from the axis of the CMA into the photon beam. Rotation of the sample between normal to the light beam and perpendicular to the analyzer axis allows examination of simple light polarization and angular emission effects. Work function changes were measured using the low-energy cutoffs of the photoemission energy distributions.

Experimental Results: In Figure 1 we summarize our photoemission spectra N(E) for the (111) surfaces of Ni, Pd and Pt (solid lines) and for saturation coverages of hydrogen (dashed lines), all for an incident photon energy of 21.2 eV. For hydrogen on Ni(111) at T ~ 300 K (Fig. 1a), or for slightly greater coverages at T ~ 80 K, we observe chemisorption-induced extra emission which extends from the Fermi level E_F to ~ 8 eV below. As seen more clearly in the difference spectra $\Delta N(E)$ in Fig. 2a – obtained by subtracting N(E) of the clean surface

from N(E) after chemisorption – this extra emission consists of a broad ~ 3 eV wide level peaked near 5.8 eV with enhanced emission extending throughout the d-bands. Hydrogen chemisorption on Ni(110) at T ~ 80 K also produces the same 3 eV wide level peaked at 5.8 eV as well as the d-band enhancement observed on Ni(111)[9].

The chemisorption-induced changes for hydrogen on Pd or Pt shown in Fig. 1b and c are qualitatively different from those observed for hydrogen on Ni. In contrast to hydrogen on Ni(111) or Ni(110), we find that hydrogen on Pd(111) or Pt(111) strongly redistributes emission in the d-band region and, in particular, preferentially attenuates d-band emission within ~ 1 eV of E_F. New levels ~ 1.5 eV wide are observed to form at 6.4 and 7.3 eV respectively. Warming to T $\gtrsim$ 400 K desorbs molecular hydrogen and restores the N(E) spectra identically to that of the initial clean surface for each substrate.

Our photoemission results for $h\nu$ = 16.8 and 26.9 eV show similar hydrogen-induced levels at 5.8, 6.4 and 7.3 eV for Ni, Pd and Pt(111) surfaces respectively, along with nearly uniform d-band enhancement for hydrogen on Ni and strong redistribution of d-band emission for hydrogen on Pd and Pt. In Fig. 2b-d we show the ΔN(E) spectra for saturation coverages of hydrogen on Ni, Pd and Pt, all for T ~ 80 K and $h\nu$ = 40.8 eV. These results for hydrogen on Pd and Pt are similar to those observed for $h\nu$ = 16.8, 21.2 (Fig. 1) and 26.9 eV while those for hydrogen on Ni show some features different than observed at lower photon energies. Namely, we observe additional, or spectrally modified, emission within the d-bands at 0.4 and 1.9 eV instead of the nearly uniform enhancement shown in Fig. 1a. Also the level at 5.8 eV is so weak and broad it is almost indecernable. This reduction in the adsorbate-induced level relative to the d-band emission for $h\nu$ = 40.8 eV, which is to a lesser degree also observed for hydrogen on Pd and Pt, is the result of differences in the photoionization cross sections of d- versus s-like wavefunctions[10] – the latter likely derived from the H(1s) state.

Finally, we note two points which we do not discuss here but which are relevant to the nature of the d-band enhancement observed for H on Ni. First, we find no dependence of the Ni(111) d-band enhancement at $h\nu = 21.2$ eV upon the orientation of the electric vector of the incident radiation, ie. pure s- or mixed s, p-polarization produce the same enhancement. Second, we find that the ratio of the maximum amplitude of the d-band enhancement found for hydrogen on Ni(111) (and similarly the d-band attenuation within 1 eV of E_F for hydrogen on Pd or Pt) is nearly a fixed fraction of the d-band intensity for each photon energy. Thus, the chemisorption-induced changes in the Ni d-band, although different from those observed on Pd or Pt, do reflect changes in substrate d-state density.

The Nature of Bonding: It has been established that hydrogen is dissociatively absorbed on the (111) surfaces of Ni, Pd and Pt and that both the isosteric heats of adsorption as well as the ratio of chemisorbed hydrogen atoms to substrate atoms are nearly the same on each surface[11]. In view of such similarities, we find striking differences in the manner that hydrogen chemisorption effects the d-bands of Ni from that of Pd or Pt. The lack of preferential d-band attenuation within ~ 1 eV of E_F for hydrogen on Ni is an exception to the generally observed attenuation and rearrangement of states within the d-band upon chemisorption. These latter d-band changes, which are found for hydrogen on Pd and Pt as well as for other atoms and molecules chemisorbed on most transition metals including Ni, have been interpreted as indicating d-electron participation in bonding[12-15]. Similar chemisorption-induced attenuation and rearrangement of state density within a band have been found for simplified chemisorption models[16] as well as in more detailed extended-Hückel calculations for H on paramagnetic Ni[7]. This latter calculation shows a 25% reduction of the d-state density ~ 1 eV within E_F for atoms in the first layer which is consistent with the observed d-band changes for hydrogen on Pd or Pt, assuming a 3-4 layer electron escape depth, but not with those observed for hydrogen on Ni(111) or Ni(110). Thus, from such calculations and previous observations we conclude that hydrogen chemisorption bonding to Pd and Pt directly

involves substrate d-electrons. If we assume, that each substrate has the same escape depth, the lack of preferential d-band attenuation within ~ 1 eV of E_F for hydrogen on Ni as well as the small non-uniformities in the Ni d-band enhancement would suggest smaller d-band interactions for hydrogen on Ni than on Pd or Pt.

The chemisorption-induced levels at 5.8 eV, 6.4 and 7.3 eV on Ni, Pd and Pt, respectively, which we associate with the H(1s) level, provide further information regarding the relative bonding interactions on these surfaces. The broad hydrogen-derived level on Ni is suggestive of a resonance of the H(1s) level with the Ni s-band[17,18]. The narrower width of the hydrogen-derived level on Pd and Pt relative to that on Ni, further suggests that s-band interactions of hydrogen with Pd and Pt are weaker than for Ni.

A larger s-band interaction and a smaller d-band interaction for hydrogen chemisorption on Ni, relative to that on Pd or Pt, are expected on the basis of several known factors. First, atomic 3d-wavefunctions do not contain radial nodes and are more localized relative to atomic 4s-wavefunctions than are the 4d or 5d wavefunctions, respectively[19]. Such trends in the localization of s- and d-wavefunctions are also reflected in the d-band widths of bulk band structure calculations[20], and as known from bulk hydrides, there is greater overlap and hybridization of hydrogen s-states with the wider, lower lying d-states of Pd than with the d-states of Ni[21]. Also, atomic 3d wavefunctions are less polarizable than 4d and 5d-wavefunctions which may thus limit interaction via distortions of the free atom or surface 3d-wavefunctions as may occur for 4d-or 5d-wavefunctions[22]. Finally, from energy band calculations of Ni, Pd and Pt as well as supporting saturation magnetization and Fermi surface measurements, it is known that Ni has the greatest number of s-electrons per atom in the valence band (~ 0.55-0.62) approximately 50-100% more than that for Pt and Pd (~ 0.42 and 0.31), respectively[20].

In view of this stronger interaction of hydrogen with Ni s-states, the Ni d-band changes observed upon hydrogen chemisorption, unlike the Pd or Pt d-band changes, may be a result of an indirect readjustment of d-states to this interaction – analogous to that proposed for hydrogen bonded to a Ni atom[3-4]. Unfortunately, we cannot uniquely identify such indirect d-electron interactions from our UPS results alone. Furthermore, magnetic effects related to a ferromagnetic substrate are largely unexplored and may be responsible for some of the differences in the d-band changes we observe between Ni and Pd or Pt.

Summary and Implication to Surface Reactions: We conclude that the interaction of hydrogen with the d-states of Ni is different and likely weaker than with the d-states of Pd or Pt where we find evidence that bonding directly involves d-electrons. Also a stronger interaction of the metallic s-slectrons with hydrogen occurs on Ni than on Pd or Pt which may in part be responsible for chemisorption-induced changes in the Ni d-band. Thus, our results support recent concepts for hydrogen chemisorption bonding to Ni surfaces proposed by Blyholder[6], Guse, Blint and Kunz[3] and Melius, Moskowitz, Baillie and Ratner[4,5] but not their extension to heavier transition metals such as Pd or Pt.

Although it is well established that the catalytic properties of Ni, Pd and Pt vary markedly, our results may be of significance for better understanding differences in surface reactions where chemisorbed atomic hydrogen plays a role as a starting specie, an intermediate specie, or as an end product. For such reactions the similarities in the heats of adsorption of hydrogen on Ni, Pd and Pt would not lead one to expect any significant differences in the reaction to be associated with hydrogen chemisorption bonding itself. However, the differences in the nature of the hydrogen bond to Ni from that on Pd and Pt give rise to differences in the wavefunctions of chemisorbed hydrogen which could modify reaction rates and products[23].

Acknowledgement: The author wishes to express his appreciation to D. E. Eastman, G. W. Rubloff, K. C. Pandey, N. D. Lang and A. R. Williams for useful discussions.

Notes Added: Recent UPS results at $h\nu$ = 21.2 eV by Yu, et. al.[24] for hydrogen chemisorbed to polycrystalline Fe show the same features as observed here for hydrogen chemisorption on Ni(111) or Ni(110), suggestive of a H-Fe interaction similar to that which occurs for hydrogen on Ni. Also, Conrad, Ertl and Latta[25] recently report UPS spectra for H on Ni(111) and Pd(111) in general agreement with our results. We are grateful to Professor Ertl for a preprint of their work prior to publication. Finally, recent Xα-multiple scattering calculations for H on Ni, Pd and Pt clusters[26] not only confirm our interpretation that the d-electrons of Pd and Pt are directly involved in bonding but also agree with previous results[3,4,6] for H on Ni.

REFERENCES

1. B. M. W. Trapnell, "Chemisorption" (Butterworths, London, 1955).

2. D. A. Dowdin, in "Chemisorption", edited by W. E. Gavner (Butterworths, London, 1958), pg. 3.

3. M. P. Guse, R. J. Blint and A. B. Kunz, Chem. Phys. Letters 36, 191 (1975): to be published.

4. C. F. Melius, J. W. Moskowitz, A. P. Mortola, M. B. Baillie, and M. A. Ratner, Surface Science 59, 279 (1976).

5. C. F. Melius, Chem. Phys. Letters 39, 287 (1976).

6. G. Blyholder, J. Chem. Phys. 62, 3193 (1975).

7. D. J. M. Fassaert, A. Van der Avoird, Surface Sci. 55, 291 (1976).

8. D. J. M. Fassaert, A. Van der Avoird, Surface Sci. 55, 313 (1976); D. J. Fassaert, H. Verbeek and A. Van der Avoird, Surface Sci. 29, 501 (1972).

9. A noteworthy point regarding Ni(110) is that for particular angular orientations of the sample where we collect emission normal to the surface we see strong attenuation of states ~ 0.2 eV below E_F for $h\nu = 21.2$ eV. This behavior is likely a final state effect as such attenuation was not observed under the same conditions for $h\nu = 40.8$ eV.

10. D. E. Eastman, in Proceedings of the IV International Conferences on Vacuum Ultraviolet Radiation Physics, (Pergamon, Vieweg, 1974), p. 28.

11. H. Conrad, G. Ertl and E. E. Latta, Surface Sci. 41, 435 (1974); K. Christmann, U. Schokev, G. Ertl and M. Neuman, S. Chem. Phys. 60, 4528 (1974); K. Christmann, G. Ertl and T. Pignet, Surface Sci. 54, 365 (1976).

12. J. E. Demuth and D. E. Eastman, Phys. Rev. Lett. 32, 1123 (1974); D. E. Eastman and J. E. Demuth, Jap. Journal of Applied Phys., Suppl. 2, 827 (1974).

13. E. W. Plummer, in Interactions on Metal Surfaces, Ed. R. Gomer, (Springer, New York, 1975).

14. P. R. Norton and P. J. Richards, Surface Sci. 49, 567 (1975).

15. P. J. Page and P. M. Williams, Faraday Disc. 58, 80 (1975).

16. T. Einstein, Surface Sci. 45, 713 (1975).

17. D. M. Newns and A. Bagchi, in The Physical Basis for Heterogeneous Catalysis, Ed. E. Drauglis and R. I. Jaffee, (Plenum Press, NY, 1975), p. 317.

18. N. D. Lang and A. R. Williams, Phys. Rev. Lett. 34 531 (1975).

19. F. Herman and S. Skillman, Atomic Structure Calculations, (Prentice Hall Inc., N. J., 1963); T. A. Carlson, C. C. Lu, T. C. Tucker, C. W. Nestor, Jr. and F. B. Malik, Oak Ridge National Labs., Report # 4614, 1970.

20. For Ni, J. Callaway and C. S. Wang, Phys. Rev. 7, 1096 (1973); for Pd, N. E. Christensen, Phys. Rev. B 12, (1976); for Pt, F. M. Mueller, J. W. Garland, M. H. Cohen and K. H. Bennemann, Annals of Physics 67, 19 (1971); O. K. Anderson, Phys. Rev. B 2, 883 (1970).

21. A. C. Switendick, Ber. Bunsenges. Phys. Chem. 76, 535 (1972).

22. R. P. Messmer, in The Physical Basis for Heterogeneous Catalysis, Ed. E. Drauglis and R. I. Jaffee, (Plenum Press, NY, 1975), p. 270.

23. See for example, R. B. Woodward and R. Hoffman, The Conservation of Orbital Symmetry (Weinheim, Verlag Chemie, 1970).

24. K. Y. Yu, W. E. Spicer, I. Lindau, P. Pianetta and S. F. Lin, Surface Sci. 57, 157 (1976).

25. H. Conrad, G. Ertl and E. E. Latta, Surface Sci. 58, 578 (1976).

26. K. M. Johnson, private communication.

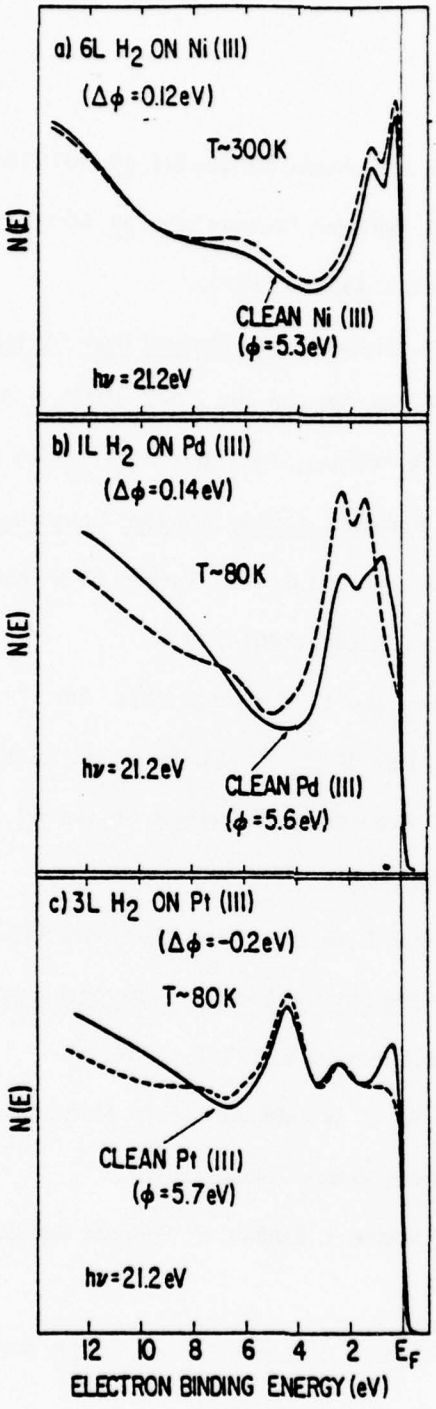


Fig. 1 **Photoemission energy distribution curves N(E) relative to the Fermi level E_F for both clean (solid line) and near saturation hydrogen coverages (dashed line) for (a) Ni(111), (b) Pd(111) and (c) Pt(111). The exposure in Langmuirs (L), sample temperature, clean surface work function ϕ and the corresponding change in workfunction $\Delta\phi$ are indicated. All spectra are for $h\nu$ = 21.2 eV.**

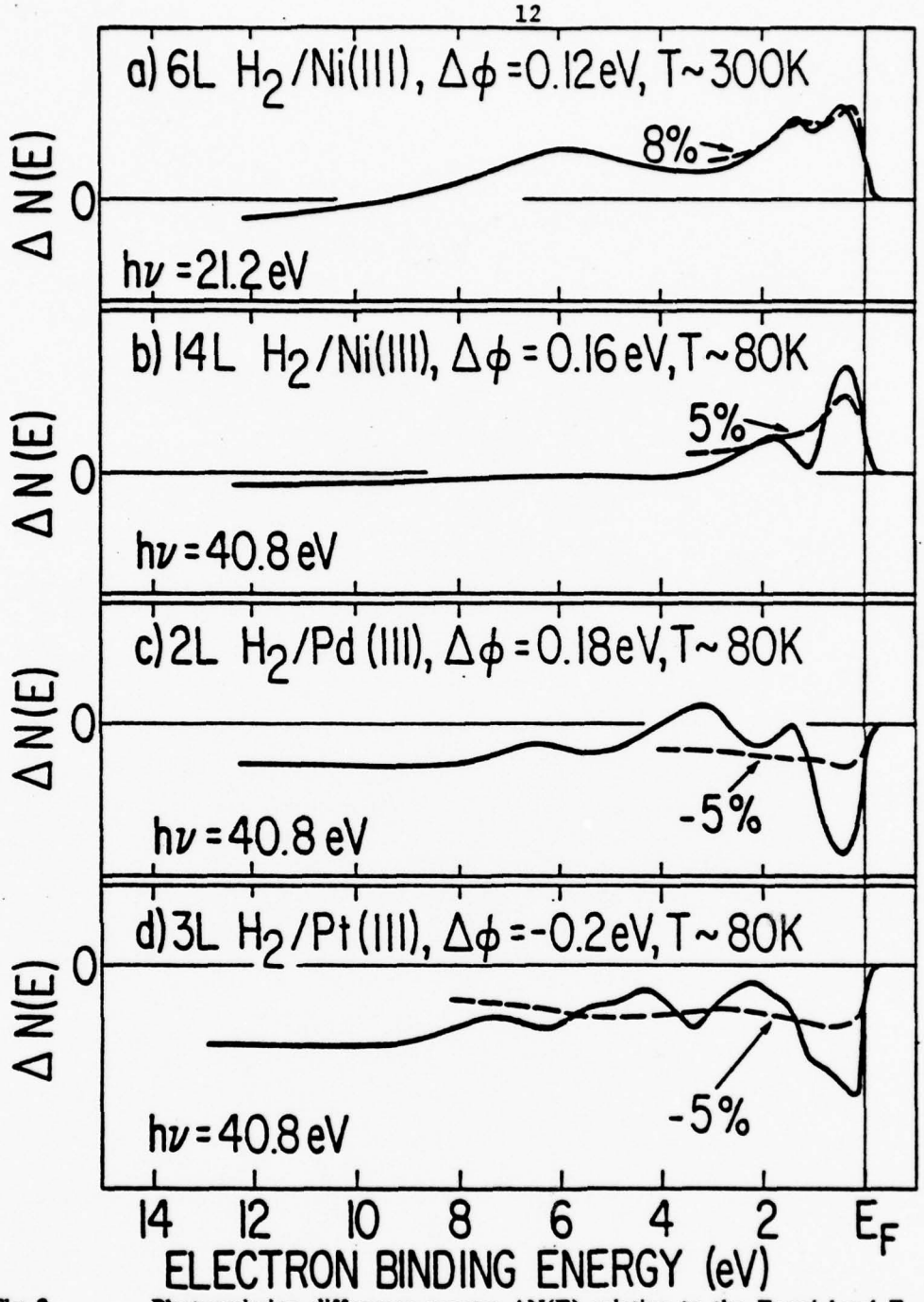


Fig. 2 **Photoemission difference spectra ΔN(E) relative to the Fermi level E_F for saturation hydrogen coverages on the clean surfaces of (a) Ni(111) at T ~ 300 K for hν = 21.2 eV, (b) Ni(111) at T ~ 80 K for hν = 40.8 eV and for (c) Pd(111) and (d) Pt(111) both at T ~ 80 K for hν = 40.8 eV. The dashed line near E_F indicates the d-band width as well as the shape of the d-band features if uniform enhancement (+) or attenuation (-) were to occur. (The indicated values are estimated so as to conserve state density within the d-band). The exposures in Langmuirs (L) and corresponding workfunction changes Δφ are indicated.**

APPENDIX

Item 3

MOLECULAR GEOMETRIES OF ACETYLENE AND ETHYLENE CHEMISORBED ON Cu, Ni, Pd and Pt SURFACES *

J. E. Demuth

IBM Thomas J. Watson Research Center

Yorktown Heights, New York 10598

ABSTRACT

The molecular geometries of acetylene chemisorbed on Cu(100), Ni(111), Pd(111) and Pt(111) and ethylene on Cu(111), Ni(111), Pd(111) and Pt(111) surfaces all at $T \sim 80K$ are determined from comparisons of the relative photoemission ionization energies of these species to Hartree-Fock ground state energies for distorted molecules calculated using a self-consistent-field linear-combination-of-atomic-orbitals method. We find two trends in the structure of these chemisorbed molecules on these surfaces: first, increasingly greater molecular distortions occur with increasing atomic number of the substrate atom, and secondly, greater molecular distortions occur for ethylene than acetylene on the same metal. These trends are consistent with a π-d bonding interaction and can be accounted for by the electronic structure of the substrate and of the molecule, respectively. With the exception of ethylene on Pd and Pt, we determine molecular geometries characteristic of small rehybridization. The molecular geometry of ethylene on Pd and Pt is characteristic of rehybridization to an sp^3 configuration.

* Partially supported by ONR Contract No. N00014-75-C-0346.

The determination of the geometry of adsorbed hydrocarbon molecules on transition metal surfaces is an important problem which, for example, may provide a greater understanding of fundamental processes in heterogeneous catalysis. That is, the geometric structure not only reflects the nature and/or strength of the electronic interaction but may also influence surface reactions. One can further divide the surface structure problem into two related aspects: the location of the molecule relative to the surface atoms and the geometry of the adsorbed molecule itself. This latter, molecular geometry reflects the state of hybridization of the carbon atoms in the hydrocarbon molecule and is important in understanding the chemisty of the adsorbed molecule.

Several approaches can be taken to obtain structural information about chemisorbed hydrocarbon species. Low energy electron diffraction (LEED) intensity analysis has proven to be a powerful technique for determining the locations of atoms on surfaces[1-4]. In particular, such an analysis for a phase of chemisorbed acetylene on Pt(111) has been used to determine the locations of the carbon atoms of this chemisorbed species relative to the Pt(111) substrate atoms[(5)]. Although this determination of bond site rules out several previously postulated bonding models, more detailed information about the adsorbed species can not be obtained since present LEED analyses lack the sensitivity to distinguish CC bond distances to within $\pm$ 0.1Å or to determine H atom locations[(5)]. Such limitations would appear to restrict the use of LEED as a method to obtain structural information relevant to the chemisty of absorbed hydrocarbon or other organic molecules on surfaces.

Another approach in determining molecular geometries is to perform theoretical calculations of the total energy for all possible geometries of the absorbed molecule on a transition metal surface so as to determine the geometry which provides the lowest total energy state of the system. Such an approach is not based upon an analysis of experimental observables and depends upon accurate, detailed theoretical models of fairly complex systems. To date no

rigorous ab-initio calculations have been performed for hydrocarbon molecules on any surface. However, Anderson[6] has used a modified extended Hückel approach in this manner to determine the geometries of acetylene and ethylene on a cluster of Ni atoms which simulate the Ni(111) surface.

In this work we shall use the electronic structure of chemisorbed acetylene and ethylene to obtain geometric information. This arises due to the interdependence of geometric and electronic structure. Such an approach has been used to obtain insight into the structure of amorphous semiconductors[7], the structure of silicon surfaces[8-9], and the structure of hydrogen surface compounds on Si[10] – where other conventional structural methods, such as X-ray diffraction or LEED intensity analyses, are either inapplicable or not yet tractable for these systems.

Here, we present UV photoemission results for the energy levels of the σ-orbital valence bonds of acetylene and ethylene chemisorbed on Cu, Ni, Pd and Pt single crystal surfaces at T ~ 80K which together with the eigenvalues of the σ-orbital valence bonds from molecular-orbital calculations for distorted molecules, we use to determine the molecular geometries of these particular chemisorbed species. We show that such use of ground state eigenvalues and distorted free molecule calculations - simplifications needed to render structural analysis tractable - do not introduce significant errors. Finally, we note that this work represents an extension of an earlier photoemission study of hydrocarbons on a Ni(111) surface where we used molecular orbital calculations to place a limit on the degree of rehybridization occurring for acetylene, ethylene, propylene and benzene chemisorbed on Ni(111)[11]. Previous UV photoemission studies of absorbed hydrocarbons have generally used ionization levels primarily to characterize the chemical nature of the absorbed hydrocarbon[12-15].

I. Experimental Procedure:

The present studies were performed in a turbomolecular pumped UHV system whose base pressure is less than 1×10^{-10} Torr. The system is equipped with a d.c. resonance lamp whose operation increased the total system pressure by 1×10^{-10} Torr, and a double pass cylindrical mirror electron energy analyser (CMA) for photoemission studies. The system also contains facilities for low-energy electron diffraction studies, a UTI quadrupole mass spectrometers for thermal disorption studies, and an auxiliary electron gun for Auger electron spectroscopy. Single crystal samples of Cu(111), Ni(111), Pd(111) and Pt(111) were prepared by conventional techniques[16] and mounted on a multiple sample holder which permitted the samples to be liquid nitrogen cooled to T ~ 80K or resistively heated to T ~ 1600K is measured with a Chromel-Alumel thermocouple spot welded to the back of the crystal. The Cu(111) sample was damaged in the course of this study and was replaced by a Cu(100) crystal. The Cu(100) crystal was prepared in an auxiliary system by vapor epitaxial growth on a chemically polished MgO(100) substrate held at T ~ 750K. (Polycrystalline Cu films were also formed in-situ by the evaporation of Cu onto a polycrystalline Ta substrate). The samples were cleaned by mild oxidation treatments, argon ion sputter-etching and subsequent annealing[16]. Surface characterization was performed by LEED, Auger and photoemission analyses. Research grade purity Matheson ethylene (99.98%) and purified Matheson acetylene (>99.6%) was used and examined for other impurities mass spectroscopically. In particular, the acetylene extraction procedures used to load our gas manifold provided essentially acetone-free acetylene. The ratio of mass 43 to mass 26, the principal mass numbers for acetone and acetylene, respectively, was 1/750 for ionizer voltages which produce 70V electrons and 15V ions.

Energy analysis of the photoemitted electrons was performed with a double pass cylindrical mirror analyzer (CMA) operated in a fixed pass mode so as to have a minimum resolution of ~ .15 eV for He I, and ~ .25 eV for He II UPS work. These two photon energies provide

wider energy windows than Ne I or II radiation and, therefore, were used almost exclusively. The sample could be rotated with their normal direction in the plane defined by the axis of the CMA and the photon beam. The photon beam lies 73° off the axis of the CMA, and we nominally chose the sample normal to be 20° from the axis of the CMA into the photon beam so as to collect electrons over a wide range of emission angles. Changes in the sample orientation did not change the observed adsorbate-derived ionization energies but in some instances could change the relative intensities of ionization features. Work functions and their changes were measured using the low-energy cutoffs of the photoemission energy distributions.

II. Experimental Results:

In Fig. 1 we show the changes in the energy distribution $\Delta N(E)$ of photoemitted electrons from the clean surfaces of Cu(100), Ni(111), Pd(111) and Pt(111) after exposure to acetylene at T ~ 80K for both $h\nu$ = 21.2 and 40.8 eV photon energies. These $\Delta N(E)$ spectra reflect both the emission from occupied valence orbitals of chemisorbed acetylene as well as the attenuation of the substrate emission associated with the presence of the overlayer and any alterations in the electronic structure of the surface atoms of the substrate. In order to show the location of the d-bands as well as any preferential d-band attenuation for each surface in Fig. 1, we indicate a uniform d-band attenuation for both $h\nu$ = 21.2 and 40.8 eV by the short dashed lines. The estimated change in secondary electron background is indicated by the longer dashed line.

The spectra shown in Fig. 1 are each representative of a saturation coverage of a single phase of acetylene that forms on the clean surface at T ~ 80K, before we observe any coverage-dependent changes characteristic of the onset of the formation of a second layer of "physically" absorbed acetylene. Here we concentrate on the initial phase of acetylene chemisorbed at T ~ 80K which appears to be very much the same on each surface as judged

from the similarities in the $\Delta N(E)$ spectra. In spite of these similarities, we note striking differences upon warming the samples. At higher temperatures on Cu(100) this phase of acetylene reversibly desorbs while on N(111) this phase is stable until T ~ 400K where it starts to decompose to carbon and hydrogen. In contrast, this initial phase of acetylene on Pd(111) or Pt(111) at T ~ 80K converts at T ~ 200K to form a new olefinic C_2H_2 species which starts to decompose to carbon and hydrogen at T ~ 460K [17].

The relative locations and intensities of the ionization features for this initial phase of chemisorbed acetylene which lie further than ~ 8 eV below E_F on each metal are similar to those occurring for gas phase acetylene. In Fig. 1a we show the ionization spectra for gas phase acetylene taken in a spectrometer of similar geometry and energy resolution as used for our studies[18]. We can readily relate the $2\sigma_g$, $2\sigma_u$ and $3\sigma_g$ molecular orbitals of gas phase acetylene to the ionization features we observe for chemisorbed acetylene. We derive average relaxation/screening shifts[19] of 4.1, 3.5, 3.7 and 3.5 eV, respectively, from the $2\sigma_u$ and $3\sigma_g$-derived ionization features.

The additional ionization features for this chemisorbed phase between ~ 3-7 eV can be related to the $1\pi^2$ orbitals of gaseous acetylene. As discussed previously for initially chemisorbed acetylene on Ni, Pd and Pt, the $1\pi^2$ orbitals of chemisorbed acetylene are shifted closer to the σ-orbitals relative to the gas phase by ~ 1.2, 1.9 and 2 eV respectively[17]. Such a shift is indicative of π-d bonding[12,20]. For acetylene on Cu(100) two well resolved ionization features at 4 and 5 eV below E_F are observed in the $\Delta N(E)$ spectra for both $h\nu$ = 21.2 and 40.8 eV which could be attributed to the $1\pi^2$ orbitals shifted 1.2 and 2.6 eV, i.e. a lifting of the degeneracy of the $1\pi^2$ orbitals by the surface. We also observe these same two features for acetylene on polycrystalline Cu as similarly found by Yu et al.[14] Although we find some suggestion of a splitting of the $1\pi^2$ derived levels for acetylene on Pd(111) or Pt(111), the strong redistribution of d-states at the bottom of the d-band characteristic of the π-d

interaction[21], places uncertainties in relating such features to only the π-orbitals of chemisorbed acetylene. We find no indication of a $1\pi^2$ orbital splitting for acetylene on Ni(111) or on Ni(110) at T ~ 80K.

In this work our interest lies in the relative positions of the higher lying σ-levels which reflect the chemical nature of the molecule. In Fig. 2 we summarize the σ-orbital derived vertical ionization potentials (I.P.) of gaseous acetylene and the corresponding ionization levels of chemisorbed acetylene as deduced from our results at both photon energies. We note that the location of the 2σ-derived ionization features indicated by the dashed lines in Fig. 2 are more uncertain than the other levels due to its low intensity and overlap with the onset of d-band emission from $h\nu$ = 23.7 eV radiation. Although it is clear that acetylene on these surfaces is chemically similar in each case to gaseous acetylene, we find a trend in the widening of the separation between the $2\sigma_u$ and $3\sigma_g$ derived ionization levels in going from Cu to Pt which we shall consider in detail later.

In Fig. 3 we show $\Delta N(E)$ spectra at $h\nu$ = 21.2 and 40.8 eV for ethylene chemisorbed at T ~ 80K onto clean Cu(111), Ni(111), Pd(111) and Pt(111) surfaces. As before, these spectra represent saturation coverages of an initial phase of ethylene which forms before multilayer adsorption. We note that ethylene chemisorbed on either Cu(100) or Cu(111) at T ~ 80K have the same relative ionization levels . For comparison we also show in Fig. 3a the ionization features for gas phase ethylene again obtained in a spectrometer of similar geometry and resolution as used in our studies. Comparison of these levels indicate that the $1b_{2u}$ orbital, the π-orbital, appears to be shifted toward the $1b_{2g}$ ionization level relative to the gas phase levels, indicative of π-d bonding[12,21]. We note that the exposure of ethylene to Ni, Pd and Pt at higher temperatures (T > 200K) or warming to T > 200K results in the chemical reaction of ethylene with the surface to form chemisorbed hydrogen and C_2H_2 species which we have discussed elsewhere[12,17]. Ethylene on Cu(111) reversibly desorbs upon warming.

We summarize in Fig. 4 the σ-orbital derived vertical I.P.'s of gaseous ethylene and the corresponding ionization levels of chemisorbed ethylene again determined from both $h\nu$ = 21.2 and 40.8 eV results. Here, we show that the relative σ-derived ionization levels for chemisorbed ethylene are more strongly modified from those in the gas phase than is the case for acetylene on these surfaces. The average relaxation/screening shifts[19] for ethylene on these surfaces are approximately 1.9 eV, 2.3, 2.0 and 2.9 eV respectively, as determined from the $1b_{3u}$, $3a_g$ and $1b_{2g}$-derived orbital ionization features.

III. The Structure of Initially Chemisorbed Acetylene and Ethylene

The similarities in the relative ionization levels of initially chemisorbed and gas phase acetylene and ethylene indicate that the surface species are chemically similar to their gas phase counterparts. However, some differences exist in these ionization energies relative to those in the gas phase which can be used to obtain geometric information. Fortunately, we find two approximations which simplify an analysis of these ionization levels and render the problem tractable without introducing significant errors. First we utilize calculations of distorted free molecules for all reasonable combinations of CC and CH bond distances and CCH and HCH bond angles to assess how geometric changes from the equilibrium gas phase geometry affect orbital energies. We then correlate the differences in ionization levels we observe experimentally between gaseous and chemisorbed molecules to the changes in energy levels found theoretically, to derive the geometry of the chemisorbed hydrocarbon.

A simple physical basis exists for the use of these approximations as well as the use of σ-orbital energies to obtain structural information regarding chemisorbed unsaturated hydrocarbons. Namely, the electrons in the hydrocarbon σ-valence orbitals are shielded by the π-electrons and separated in both space and energy from the substrate d-electrons so as to reduce any direct σ-d interaction. However, within the chemisorbed molecule the π- and σ-valence electrons are stilled largely coupled as they are in the free molecule so that any

distortions in the π-electron charge density caused by π-d bonding will directly influence the σ-electron charge density. Hence, the intermolecular interactions will directly affect the equilibrium positions of the atoms within the molecule and, subsequently, the eigenvalues of the σ-levels. Further, the possible shielding of the σ-electrons by the π-electrons as well as the similar delocalization of electrons in each of the σ-valence orbitals relative to the surface, would lead to similar final-state relaxation effects for each σ-valence orbital. Thus, to the extent that these conditions are valid, the observed differences in relative σ-orbital I.P.'s between these chemisorbed molecules and their gas phase counterparts will reflect changes in the molecular geometry that have occurred upon chemisorption.

More quantitative results indicate the validity of the forementioned qualitative arguments. First, free molecule calculations are supported by recent SCF X-α multiple-scattering calculations of ethylene interacting with one atom of Ni, Pd or Pt[21] or two atoms of Ni[20], extended Hückel calculations of gaseous and distorted acetylene on Ni clusters[6,22] as well as our own SCF LCAO calculations of gaseous and distorted acetylene and ethylene on Be and Li clusters. These calculations indicate that the presence of the metal atom or atoms alone does not significantly affect the relative ground state energies of the higher lying σ-valence orbitals. Further the changes in orbital energies which occur upon distortion of the molecule appear to be independent of whether metal atoms are present. Secondly, emphirical evidence shows that σ-orbital-dependent changes in final-state screening and relaxation effects associated with the presence of the surface are not significant for these chemisorbed species. We find that the valence orbital ionization levels for monolayer coverages of a variety of adsorbed saturated hydrocarbon molecules on Ni[11] or on Cu, Pd and Pt surfaces as well as for condensed unsaturated or saturated hydrocarbons on these surfaces are uniformly shifted from those of their gas phase counterparts. Possible errors introduced by these approximations will be discussed later.

For our free molecule calculations we utilize GAUSSIAN-70, an ab-initio SCF LCAO molecular orbital calculation[23], with a 4-31G basis set. These calculations require core storage of ~ 250 kilobytes and computation times of ~ 12 or 28 seconds per geometry for acetylene or ethylene, respectively, on an IBM 370-168 computer. In order to demonstrate that the relative ground state energy level positions of these molecular orbital calculations can be accurately related to vertical ionization potentials (I.P.'s) we show a comparison of our calculated eigenvalues and I.P.'s for acetylene[18,24], ethylene[18,24], ethane[18,25,26] and methane[25,26] in Fig. 5. Here, we have chosen the energy scales to allow visual comparison of relative level positions. Although some differences in the trends are observed, for example, in the relative locations of the C 2ss-derived levels, we observe rather good argeement between measured ionization levels and the relative ground state energy levels we calculate for free molecules. We expect these calculations to predict the relative changes in ionization levels for distorted free molecules with similar accuracy.

In our previous work to investigate possible rehybridization effects of unsaturated hydrocarbons on Ni[11], we had performed similar calculation on distorted molecules for specific geometries expected to be characteristic of a particular degree of rehybridization. Here we make no such assumptions and take combinations of many possible geometric distortions. For acetylene we have performed these calculations for all combinations of CC bond distances from 1.21Å to 1.46Å in .05Å increments with CCH bond angles from 180° to 108° in 12° increments. This represents 42 geometries each with a fixed CH bond length of 1.06Å. We have also examined CH bond lengths for acetylene of 1.08Å and 1.10Å for several selected geometries to establish how these CH bond length variations affect the eigenvalues. Similarly for ethylene we have calculated all combinations of geometries for CC bond lengths from 1.34 to 1.54Å in .05Å increments, CCH bond angles from 120.0 to 106.84° in 2.63° increments and HCH bond angles from 120° to 104.20° in 2.63° increments each with a fixed

CH bond distance of 1.10Å. This represents 245 geometries. Here the CH bond distance of 1.10Å was initially selected since this CH bond length is found in Zeise's salt[27], but we have also examined other CH bond lengths of 1.07 and 1.08Å to again determine how variations in CH bond length affect the eigenvalues. Finally, we note that from the dependence of these eigenvalues upon changes in CH or CC bond distances or CCH or HCH bond angles we could reliably extrapolate calculated eigenvalues to the next increment of each geometric parameter from the actual geometries considered. This represents a possible total of 216 geometries for acetylene and 1134 geometries for ethylene.

In Fig. 6 we illustrate how these geometric distortions typically modify the eigenvalues of acetylene for either a change in CC bond distance (Fig. 6a) or for a change in CCH bond angle from the equilibrium gas phase geometry of acetylene (Fig. 6c). Here we label the eigenvalues according to their bonding character. We also indicate by the dashed lines in Fig. 6b the eigenvalues for acetylene with a CH bond distance of 1.10Å. For all geometries we indicate the change in Hartree-Fock energy ΔE from the equilibrium acetylene geometry. Although the shifts in eigenvalues depend upon the particular change in geometry, similar trends exist, for example, in how variations in CCH bond angles change eigenvalues for other CC bond distance. Thus, for a CC bond distance of 1.41Å, a change in the CCH bond angle from 180° to 132° shifts the 2ss ($2\sigma_g$) eigenvalue downward and the 2ss* ($2\sigma_u$) and σ_{CC} ($3\sigma_g$) eigenvalues upward as indicated by the dashed levels in Fig. 6a. We also find that for some combinations of CC bond lengths and CCH bond angles the relative separation between 2ss ($2\sigma_g$) and 2ss* ($2\sigma_u$) eigenvalues can remain unchanged. This is also true for the 2ss* ($2\sigma_u$) and σ_{cc} ($3\sigma_g$) levels where the increased separation occuring for an increased CC bond length can be offset in some cases by a decrease in the CCH bond angle. Thus, the nature of the dependencies of these three σ-orbital eigenvalues upon certain geometric changes can lead in some cases to multiple geometries

The geometric dependence of the valence orbital eigenvalues of ethylene are shown in Fig. 7 for a fixed CH bond distance of 1.10Å. We again label these eigenvalues according to their bonding character. In Fig. 7b the eigenvalues for the gas phase geometry of ethylene, i.e. a CH bond distance of 1.08Å, are shown by the dotted lines; the solid lines indicate the eigenvalues for a CH bond distance of 1.10Å. Again we find that changes in the CH bond length for other geometries tend to shift the eigenvalues in the same manner. Unlike acetylene however, we find that for all distortions examined the shifts in eigenvalues are such that a duplication of eigenvalues does not occur, i.e., one unique set of eigenvalues appears to exist for each set of geometric parameters. For example, although an increase in the CH bond distance tends to produce a relative shift in the σ_{CC} ($3a_g$) level characteristic of an increased HCH bond angle, it also produces a shift in the $2ss^*$ ($2a_u$) level relative to the σ_{CH} ($1b_{3u}$ and $1b_{2g}$) levels which is not characteristic of an increased HCH bond angle.

In order to compare these calculated levels to the ionization levels which we observe experimentally we cannot directly compare absolute energies or differences as these are uncertain due to limitations and approximation in the calculation such as the treatment of exchange-correlation, basis set effects, etc., as well as the fact that we do not calculate ionization energies. In view of the apparent uniformity of final-state screening and relaxation effects for adsorbed hydrocarbons as mentioned earlier, as well as the close correspondence between eigenvalues and I.P.'s of gaseous molecules shown in Fig. 5, we believe that a scaling of the changes in relative energy level separations between gaseous and chemisorbed phases should be the most reliable and accurate procedure for comparing experiment to our calculations. Thus, for a given chemisorption system we adjust the calculated σ-level separations for the free molecule in proportion to the corresponding change in σ-level separation between the gaseous and chemisorbed phase ionization levels so as to determine a new set of energy levels. This scaled set of eigenvalues are then compared to all the calculated eigenvalues to determine the geometry which best reproduces these experimentally derived levels.

The molecular geometries determined in this manner for acetylene and ethylene on Cu, Ni, Pd and Pt are shown in Tables I and II, respectively. Indicated in each table is $d_\perp$, the separation between the plane containing the hydrogen atoms and the CC bond axis, as well as ΔE, the change in Hartree-Fock energy for each molecular geometry from the equilibrium gas phase geometry. In Table II we also indicate for comparison the molecular structure of ethylene in Zeise's salt as determined by a recent neutron diffraction study[27]. We note that in our analysis for chemisorbed acetylene we have initially neglected the $2\sigma_g$-derived ionization level due to uncertainties in its location, and in so doing we cannot determine CH bond distances or find unique geometries. That is, we find several acetylene geometries which match the observed $2\sigma_u$ - $3\sigma_g$ level separation: the structures with the larger CC bond distances and with CCH bond angles smaller than 144° arise from compensating effects in the geometric dependencies of the $3\sigma_g$ and $2\sigma_u$ eigenvalues as mentioned earlier. (In principle a continuous set of CC bond distances and CCH bond angles could be found over a certain range of these variables.) However, if we consider that the relative separation between the $2\sigma_g$ and $2\sigma_u$-derived ionization levels does not appear to change appreciably upon chemisorption, as suggested in Fig. 1 and 2, we can rule out all structures with CCH bond angles smaller than 132°.

To determine the overall accuracies of these results we must consider several sources of uncertainties. These are derived from the sensitivity of the calculated eigenvalues to molecular distortions, the ± 0.05 eV uncertainties in the relative ionization levels we observe[28], and the errors introduced by the approximations within our analysis. We can estimate the errors introduced in the scaling procedures used for relating the changes observed in I.P.'s to our calculated eigenvalues by considering how optimization of the scaling to match any pair of orbitals affects the determined geometry. This arises since the relative eigenvalues do not identically reproduce the I.P.'s in Fig. 5. We find that as a result of the sensitivity of the calculated eigenvalues to geometric distortions and the already close correspondence between

I.P.'s and eigenvalues, the determined geometry is almost independent of the scaling procedure. Namely, of the 9 ways to scale ethylene's I.P.'s, we find all give rise to the same molecular structure on Cu or Ni while on Pd and Pt one scaling procedure gives rise to a different structure which differ from the others by a CCH or HCH bond angle of 2.63°. Thus, uncertainties produced by our comparisons to ground state eigenvalues would appear to be small.

The neglect of substrate atoms in our calculations introduces small errors which we can also estimate. For example, screening of the molecule by the electrons of the substrate atoms may reduce the antibonding character of the C 2ss* ($1b_3u$) molecular orbital so as to shift it to lower energies. In one calculation[21] this shift is found to be substrate atom dependent – being the largest ~ 0.05 eV for Pt. Although we do not observe any noticeable change in separation between the corresponding C 2ss* - C 2ss levels for monolayer adsorption of ethane on Pt relative to gaseous ethane, the lack of consideration of such a 0.05 eV shift in the C 2ss* level of ethylene would primarily result in an overestimation of the CC bond expansion by ~ 0.025Å. Similar screening effects would be expected also for the $2\sigma_u$ orbital of acetylene.

Bearing in mind all such uncertainties we conservatively estimate that for small molecular distortions the overall accuracies of our geometries are about ± 0.025Å for CC bond lengths, ± 2.63° or ±6° for HCC bond angles for ethylene or acetylene, respectively, ± 2.63° for HCH bond angles and ± 0.02Å for CH bond distances for ethylene. For distortions which are characteristic of strong rehybridization of the carbon atoms in the adsorbed molecule, we expect these limits of accuracy to become larger due to the eventual breakdown of the approximations used.

IV. Discussion of Molecular Geometries

First, we can compare our detailed structural results for acetylene and ethylene on

Ni(111) to the extended Hückel results of Anderson[6,22] where the geometry of these molecules on small Ni clusters were selected on the basis of total energy optimization. Anderson's results indicate CC bond expansions of ~ 0.2Å as well as a decrease in the CCH bond angle by 45-55° from those of the free molecules – substantially greater than our findings. The energy levels for Anderson's determined geometries indicate energy level shifts from the undistorted molecule which are characteristic of those we find in our free molecule calculations when similar distortions occur. Thus, the small changes in ionization levels experimentally observed between gaseous or chemisorbed acetylene or ethylene on Ni are not consistent with Anderson's predicted geometries. The large molecular distortions predicted by Anderson may have resulted, for example, from his choice of parameters[30] which may cause small errors in total energies[30], from the use of small clusters, or from the lack of self-consistency in his calculations which may permit excessive charge transfer[31]. We do not compare our structural results for the low temperature phase of chemisorbed acetylene on Pt(111) to the structure of a room temperature phase of acetylene on Pt(111), deduced in a LEED intensity analysis by Kesmodel, et. al.[5], since these phases are not equivalent[17].

Since no other structural results exist for hydrocarbon molecules on surfaces, we now discuss the qualitative trends in the geometries of acetylene and ethylene on the different transition metals surfaces. The relative trends in these geometries are expected to be quite reliable regardless of the simplifications of our analysis. Further, we do not expect our consideration of acetylene on Cu(100) rather than on Cu(111) to affect such trends as little if any crystallographic dependencies were found for ethylene on Cu(100) and Cu(111). In summary, we find stronger distortions in the molecular geometries for the heavier substrate atoms, i.e. increasing distortions in going from Cu or Ni to Pt. Also the distortions for ethylene appear to correspond to a proportionally greater degree of rehybridization and increase in the change in Hartree-Fock energy than for acetylene on these surfaces. We find

that both these trends can be readily accounted for on the basis of the electronic structure of these surfaces and molecules as well as the occurrence of a π-d bonding interaction.

A π-d bonding interaction is commonly believed to occur for unsaturated hydrocarbons in organometallic transition metals compounds. Here bonding involves the admixture of occupied metallic d-states with unoccupied molecular π^*-states and occupied molecular π-states with occupied metallic d*-states, so as to produce both dative and retrodative (backbonding) bonding components, respectively[29]. The backbonding component not only provides the main contribution to the heat of adsorption[12], i.e. bonding energy, but is also though to be responsible for the distortions within the bonded molecule[32]. Here, we expect, a stronger π-d bonding interaction to occur with the Pd and Pt substrate atoms since their d-wavefunctions are more spatially extended and can more readily overlapp with π and π^* molecular orbitals[21]. Thus, the stronger distortions we observe for ethylene or acetylene on Pd and Pt surfaces versus the Cu or Ni surface can be attributed to the greater $d \rightarrow \pi^*$ "backbonding" component of a stronger π-d bonding interaction. This increased π-d interaction is also reflected in the increased π-orbital bonding shift for acetylene on these surfaces as previously discussed[17]. A similar increase in the π-orbital bonding shift for ethylene as a function of substrate likely occurs on these surfaces as well, but it is difficult to accurately separate ionization features of the $1b_{2u}$ (π orbital) from the $1b_{2g}$ derived orbitals.

In addition, we can associate the stronger distortions of chemisorbed ethylene relative to those of chemisorbed acetylene with the electronic structure of these molecules. In general, the π-π^* level separation should be larger in acetylene than in ethylene since the carbon atoms are closer together in acetylene. This is found to be true for the triplet $\pi \rightarrow \pi^*$ excitation of gas phase ethylene and acetylene where the transition energies are found to be 4.4[33] and 5.3 eV[34], respectively. Using the locations of the unperturbed π-levels for acetylene and ethylene on these surfaces, 3-4 eV versus 3.5-4.5 eV below E_F respectively, as well as the

$\pi \rightarrow \pi^*$ excitation energies for acetylene and ethylene, we can position the unperturbed π and π^* level of acetylene and ethylene relative to the substrate d-states. The unperturbed π^* level for acetylene should lie above the unperturbed π^* level for ethylene, ~ 1 1/2 eV further from the occupied d-bands. Thus, even though we expect a shift of both π^* levels associated with the π^*-d interaction, the separation between the initial π^* level and the highest lying occupied d-states is smaller for ethylene than for acetylene within this simple picture. This smaller d $\rightarrow \pi^*$ transition energy would permit a stronger π-d "backbonding" interaction for ethylene than for acetylene and thus account for the greater distortions of ethylene on these surfaces. A more detailed discussion is precluded by the lack of specific knowledge regarding ground state energies of the π orbitals as well as the $\pi \rightarrow \pi^*$ transition energies for these chemisorbed species, the geometric location of these molecules on these surfaces and the d-wavefunctions of the substrate atoms.

Another noteworthy distinction between the structures of acetylene and ethylene on these surfaces is the relatively strong distortion of ethylene on Pd and Pt. Namely, while the distortions for acetylene are relatively small and appear to vary uniformly from one surface to the next, the distortions for ethylene on Pd and Pt are markedly greater than on Cu or Ni. In particular, our analysis for ethylene on Pd and Pt shows that the hydrogen atoms are strongly bent away from the CC bond axis, even more than for pure sp^3 hybridization of the carbon atoms. However, while the hydrogen locations are characteristic of sp^3 hybridization, neither our determined CC bond distances nor the 3.6-4.0 eV splitting between the $2ss^*$ and higher lying σ-level derived ionization features is characteristic of complete sp^3 hybridization. (As shown in Fig. 5 this latter splitting strongly characterizes the nature of the CC bond and is ~ 5.2 eV for ethane.) The tendency to preserve the "olefinic" CC bond distance for ethylene on Pd and Pt may be necessary for optimal spatial overlap of d-and π-wavefunctions. Perhaps, this strongly distorted phase of ethylene on Pd and Pt may be related to the olefinic phase of acetylene on Pd and Pt which occur for $T \geq 200K$[17]. Clearly, we cannot answer such

questions at present and again caution that our geometric results become less certain for these large distortions.

Finally, the relative ionization intensities for ethylene on Pd and Pt also show an interesting difference from those observed for free ethylene or ethylene on Cu or Ni which may be related to the strong distortion of the hydrogen atoms locations in ethylene on Pd and Pt. Namely, we find that the σ_{CH} ($1b_{3u}$ and $1b_{2g}$) - derived ionization features of chemisorbed ethylene on Pd or Pt are more intense relative to the σ_{CC} ($3a_g$) -derived ionization feature than on Ni or Cu as shown in Fig. 3. Since our electron energy analyser preferentially collects photoemitted electrons over a range of angles between ~ 20° to 60° from the sample normal, the relative enhancement of CH orbitals on Pd and Pt may reflect additional emission due to a bending of these orbitals well out of the plane of the surface. Alternately, stronger rehybridization for ethylene on Pd or Pt may tend to mix the π-electrons into the σ_{CH} -orbitals as occurs for ethane (see Fig. 5b). Angle resolved and polarization dependent photoemission studies such as recently performed for CO on Ni[35-36] and Pt[36] will likely provide further insight into such questions.

V. Conclusions:

We have determined the molecular geometries of acetylene and ethylene chemisorbed on Cu, Ni, Pd and Pt surfaces at T ~ 80K via comparisons of the relative ionization levels of gaseous and chemisorbed species to eigenvalues obtained from SCF LCAO calculations of distorted free molecules. Despite the several approximations which are used to render such a structural analysis tractable, we argue that fairly accurate structural determinations can be made and that, in particular, the structural trends are reliable.

We conclude that at T ~ 80K acetylene adsorbs on all surfaces as a π-bonded species which is not strongly rehybridized. However, we observe increasing geometric distortions as the atomic number of the substrate atoms increases which can be related to an enhanced π-d

"backbonding" interaction associated with the greater spacial extent of the d-wavefunction of the heavier transition metal atoms. For chemisorbed ethylene at T ~ 80K we not only observe a similar dependence of the molecular geometry on the substrate but also greater molecular distortions than for acetylene. We relate these greater distortions to a stronger π-d "backbonding" interaction which may arise due to an expected smaller transition energy between occupied d-states of the metal and π^*-states of ethylene than for acetylene. Although the geometries of chemisorbed ethylene on Cu and Ni at T ~ 80K are characteristic of a weakly distorted, nearly planar molecule, ethylene on Pd and Pt at these same temperatures appears to be distorted into an sp^3 hybridization configuration with a CC bond distance less than expected for a CC single bond.

Acknowledgement:

The author wishes to acknowledge useful conversations with A. B. Anderson and R. P. Messmer regarding unpublished work as to how molecular orbital eigenvalues of distorted molecules are affected by the presence of transition metal atoms.

References

1. J. A. Strozier, Jr., D. W. Jepsen and F. Jona, in Surface Physics of Materials, Vol. 1, J. M. Blakely Ed., Academic Press, New York, 1975, pp. 1-77.
2. J. B. Pendry, Low Energy Electron Diffraction Theory, Academic Press, London 1974.
3. S. Y. Tong, Progress in Surface Science, Ed. S. G. Davison, Pergamon, Oxford, Vol. 7, part 2 (1975).
4. J. E. Demuth, Journal of Colloid and Interface Science, 58, 184 (1977).
5. L. L. Kesmodel, P. C. Stair, R. C. Baetzold and G. A. Somorjai, Phys. Rev. Lett. 36, 1316 (1976); to be published.
6. Alfred B. Anderson, J. Chem. Physics 65, 1729 (1976); 62, 1187 (1975).
7. J. D. Joannopoulos and M. L. Cohen, Phys. Rev. B 8, 2733 (1973).
8. J. A. Appelbaum and D. R. Hamann, Phys. Rev. Lett. 31, 106 (1973); 34, 806 (1974).
9. K. C. Pandey and J. C. Phillips, Phys. Rev. Lett. 34, 1450 (1975).
10. K. C. Pandey, T. Sakurai and H. D. Hagstrum, Phys. Rev. Lett. 35, 1728 (1975).
11. J. E. Demuth and D. E. Eastman, Phys. Rev. B 13, 1523 (1976).
12. J. E. Demuth and D. E. Eastman, Phys. Rev. Lett. 32, 1123 (1974); D. E. Eastman and J. E. Demuth, Jpn. J. Appl. Phys. Suppl. 2, 827 (1974).
13. E. W. Plummer, B. J. Waclawski and T. V. Vorburger, Chem. Phys. Lett. 28, 510 (1974).
14. K. Y. Yu, W. E. Spicer, I. Lindau, P. Pianetta and S. F. Lin, Surface Sci. 57, 157 (1976).
15. G. Broden and T. N. Rhodin, Chem. Phys. Letters 40, 247 (1976).
16. J. E. Demuth and T. N. Rhodin, Surface Sci. 42, 261 (1974).
17. J. E. Demuth, Chem. Phys. Letters 41, 12 (1977).
18. W. D. Grobman, private communication.

19. We define the average screening/relaxation shift ΔE^{SR} as

$$\Delta E^{SR} = \sum_{i=1}^{N} \frac{(\text{I.P.} - \text{B.E.})_i}{N} - (\phi_{clean} + \Delta\phi_{sat})$$

where I.P. is the gas phase ionization potential, B.E. the binding energy relative to E_F for the corresponding level, and $\phi_{clean} + \Delta\phi_{sat}$ represents the saturation coverage workfunction. The average of the difference between I.P. and B.E. is taken over the N valence orbitals observed. (We note that for physisorbed or condensed hydrocarbons I.P.-B.E. appears to be the same for each valence orbital.)

20. N. Rösch and T. N. Rhodin, Phys. Rev. Letters 32, 1189 (1974); private communications.

21. R. P. Messmer, in The Physical Basis for Heterogeneous Catalysis, Ed. E. Drauglis and R. I. Jaffee, Plenum Press, N. Y., 1975, p. 261.

22. Alfred B. Anderson, to be published.

23. R. Ditchfield, W. J. Hehre, and J. A. Pople, J. Chem. Phys. 54, 724 (1971).

24. D. G. Streets and A. W. Potts, J. Chem. Soc. Faraday Trans. II 70, 1505 (1974).

25. A. W. Potts and D. G. Streets, J. Chem. Soc. Faraday Trans. II 70, 875 (1974).

26. J. N. Murrell and W. Schmidt, J. Chem. Soc. Faraday Trans. II 68, 1709 (1972).

27. Richard A. Love, T. F. Koetzle, G. J. B. Williams, L. C. Andrews and R. Bau, Inorg. Chem. 14, 2653 (1975).

28. The uncertainties in relative ionization levels here is less than in previous studies (Ref. 12-15) due to our use of two photon energies and our ability to compare experimentally similar gas phase results.

29. R. B. King, Transition-Metal Organometallic Chemistry, Academic Press N. Y., 1969, p. 25.

30. R. P. Messmer, C. W. Tucker Jr. and K. H. Johnson, Chem. Phys. Lett. 36, 423 (1975).

31. L. L. Kesmodel, private communication.

32. See for example L. D. Pettit and D. S. Barnes, Fortschr der Chemie 28, 85 (1975), p. 121.

33. D. F. Dance and I. C. Walker, J. Chem. Soc. Faraday Soc. 1426 (1974).

34. E. H. Van Veen, Chem. Phys. Lett. 41, 540 (1976).

35. R. J. Smith, J. Anderson and G. J. Lapeyre, Phys. Rev. Lett. 37, 1081 (1976).

36. G. Apai, P. S. Wehner, R. S. Williams, J. Stohr and D. A. Shirley, Phys. Rev. Lett. 37, 1497 (1976).

Table I Molecular structure of acetylene on Cu(100), Ni(111), Pd(111) and Pt(111) surfaces at T ~ 80K as prescribed by bond distances d and bond angles θ. Also shown is $d_\perp$ the distance from the plane containing the hydrogen atoms to the CC bond axis as well as ΔE the change in Hartree-Fock energy for this distorted geometry. The CH bond distance cannot be determined (see text). The overall accuracies are discussed in the text.

		d_{CC}(Å)	θ_{CCH}	$d_\perp$(Å)	ΔE(eV)
/Cu(100)	†	1.21	180-169°	0-.22	.065
		1.26	114°	.98	—
/Ni(111)	†	1.235	180-168°	0-.22	.188
		1.26	117°	.95	—
/Pd(111)	†	1.235	168°	.22	.251
		1.26	120°	.93	—
		1.31	114°	.98	—
/Pt(111)	†	1.26	168°	.22	.374
	†	1.235	144°	.63	1.23
		1.26	126°	.86	—
		1.31	117°	.95	—

† preferred value based on general location of the $2\sigma_g$-derived ionization level of acetylene on these surfaces (see text).

Table II Molecular structure of ethylene on Cu(111), Ni(111), Pd(111) and Pt(111) surfaces at T ~ 80K as prescribed by bond distances d and bond angles θ. Also shown is $d_\perp$ the distance from the plane containing the hydrogen atoms to the CC bond axis as well as ΔE the change in Hartree-Fock energy for this distorted geometry. ($d_\perp$ for ethane = .52Å). The overall accuracies are discussed in the text.

	d_{CC}(Å)	d_{CH}(Å)	θ_{HCH}	θ_{CCH}	$d_\perp$(Å)	ΔE(eV)
/Cu(111)	1.34-1.39	1.07	120°	120-117.4°	.12Å	.133
/Ni(111)	1.39	1.10	117.4°	120°	.16Å	.347
/Pd(111)	1.44	1.10	106.8-109.5°	106.8-109.5°	.54Å	2.71
/Pt(111)	1.49	1.10	106.8°	106.8-109.5°	.56Å	2.96
Zeise's Salt†	1.375	1.10	114.9°	121.0°	.16Å	

† Ref. 27

FIGURE CAPTIONS

Fig. 1. Difference in emission $\Delta N(E)$ from clean surfaces of (a) Cu(100), (b) Ni(111), (c) Pd(111) and (d) Pt(111) for both $h\nu$ = 21.2 eV (He I) and $h\nu$ = 40.8 eV (He II) after saturation exposures of 3×10^{-6} Torr-sec. (3L) to acetylene or a 6×10^{-6} Torr-sec. (6L) exposure for Pt(111), all with the samples held at T ~ 80K. Indicated in each panel is the corresponding workfunction change as well as a uniform attenuation of the d-bands (short dashed lines) and estimated change in background emission (long dashed lines). All electron binding energies are referred to the Fermi level. In panel (a) for comparison we show the ionization levels ($h\nu$ = 40.8 eV) of gaseous acetylene which were obtained with a spectrometer of similar resolution and geometry (Ref. 18). The small vertical lines indicate the central position of each ionization feature, i.e. the vertical ionization levels, to which we compare.

Fig. 2. Summary of the σ-orbital derived vertical ionization potentials (I.P.) of gaseous acetylene (Ref. 18,24) relative to the corresponding ionization levels of chemisorbed acetylene which are shown in Fig. 1. The $3\sigma_g$-derived levels are aligned and we denote the separation in eV between pairs of levels. The $2\sigma_g$-derived levels for acetylene on Ni, Pd and Pt are less certain and are indicated as such by the dashed lines.

Fig. 3. Difference in emission from clean surfaces of (a) Cu(111), (b) Ni(111), (c) Pd(111) and (d) Pt(111) for $h\nu$ = 21.2 eV (He I) or $h\nu$ = 40.8 eV (He II) after saturation exposure of 6×10^{-6} Torr-sec. (6L) to ethylene with the samples held at T ~ 80K. Indicated in each panel is the corresponding workfunction change as well as a uniform attenuation of the d-bands (short dashed lines) and estimated change in background emission (long dashed lines). All electron binding energies are referred to the Fermi level. In panel (a) for

comparison we show the ionization levels of gaseous ethylene ($h\nu$ = 21.2 eV) which was obtained with a spectrometer of similar resolution and geometry (Ref. 18). The small vertical lines indicate the central positions of each ionization feature, i.e. the vertical ionization levels, to which we compare.

Fig. 4. Summary of the σ-orbital derived vertical ionization potentials (I.P.) of gaseous ethylene (Ref. 18,24) relative to the corresponding ionization levels of chemisorbed ethylene which are shown in Fig. 2. The $1b_{2g}$-derived levels are aligned and we denote the separation in eV between pairs of levels.

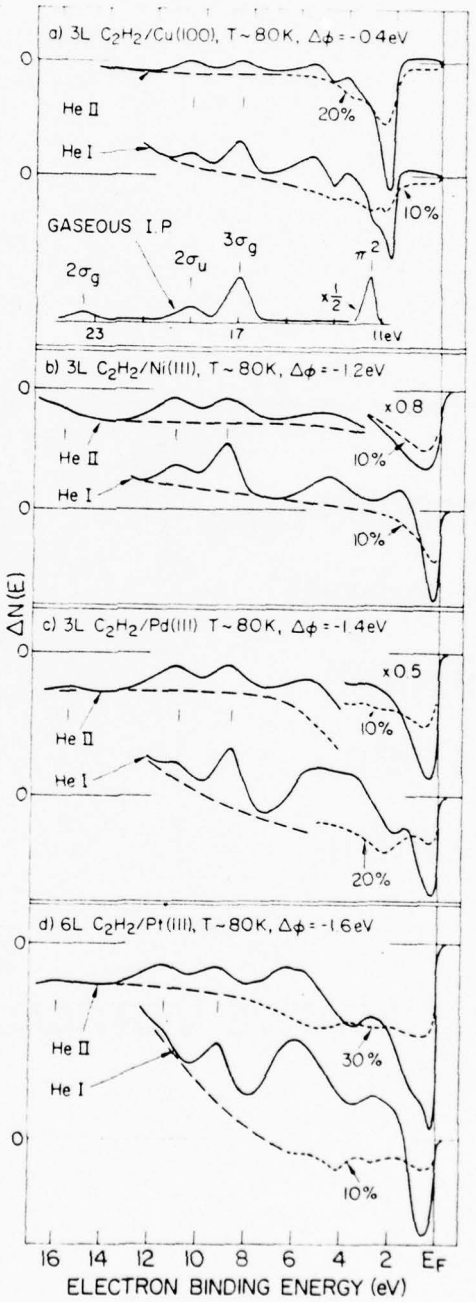
Fig. 5. Comparison of gas phase vertical ionization potentials in eV (top) (Ref. 18,24,25,26) to our calculated ground state energy levels in Hartrees (bottom) for gas phase acetylene, ethylene, ethane and methane. The ionization band from ~ 13-15 eV for methane is associated with Jahn-Teller distortions in the ion[26]. These ground state levels were calculated using an ab-initio SCF LCAO Hartree-Fock method (Ref. 23) with a 4-31G basis. The principal C 2p orbital components of the high lying valence molecular orbitals are shown where the x-direction lies along the CC bond direction. The bonding character of the various molecular orbitals for acetylene is indicated.

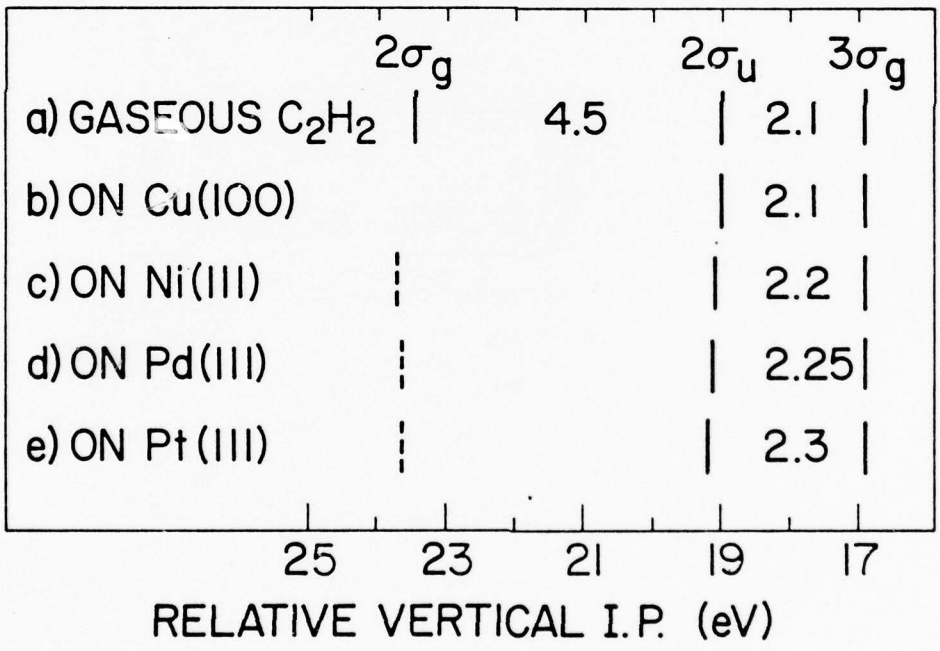
Fig. 6. The dependence of the calculated eigenvalues of acetylene upon geometric distortion. The equilibrium geometry is shown in panel (b) while panel (a) and (b) show the effect of either CC bond expansion or CCH bond angle reduction, respectively. ΔE represents the change in Hartree-Fock energy upon distortion from the gas phase geometry. The dashed lines in panel (b) are for CH bond distance of 1.10Å while those in panel (a) are for a CCH bond angle of 132° and a CC bond distance of 1.41Å. The bonding character of the 1π, $3\sigma_g$, $2\sigma_u$ and $2\sigma_g$ molecular orbitals is indicated.

Fig. 7. The dependence of the calculated eigenvalues of ethylene upon geometric distortion. The eigenvalues for gas phase ethylene is shown in panel (b) for CH bond distances of 1.10Å (solid lines) and 1.07Å (dashed lines). The effects of *CCH* bond angle reduction, *HCH* bond angle reduction and *CC* bond expansion are shown in panel (a), (c) and (d) respectively. The change in Hartree-Fock energy ΔE from nearly the gas phase geometry, i.e. a CH bond distance of 1.10Å, is indicated for each distortion. The bonding character of the $1b_{2g}$, $3a_g$, $1b_{3u}$, $2a_u$ and $2a_g$ molecular orbitals is indicated.

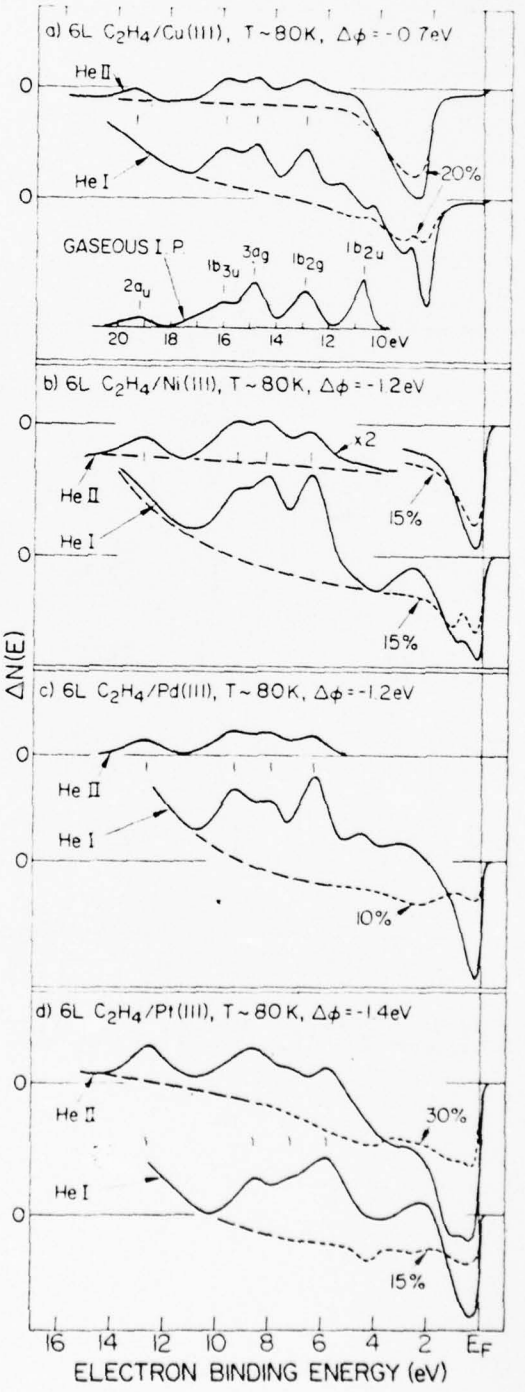
First, we can compare our detailed structural results for acetylene and ethylene on

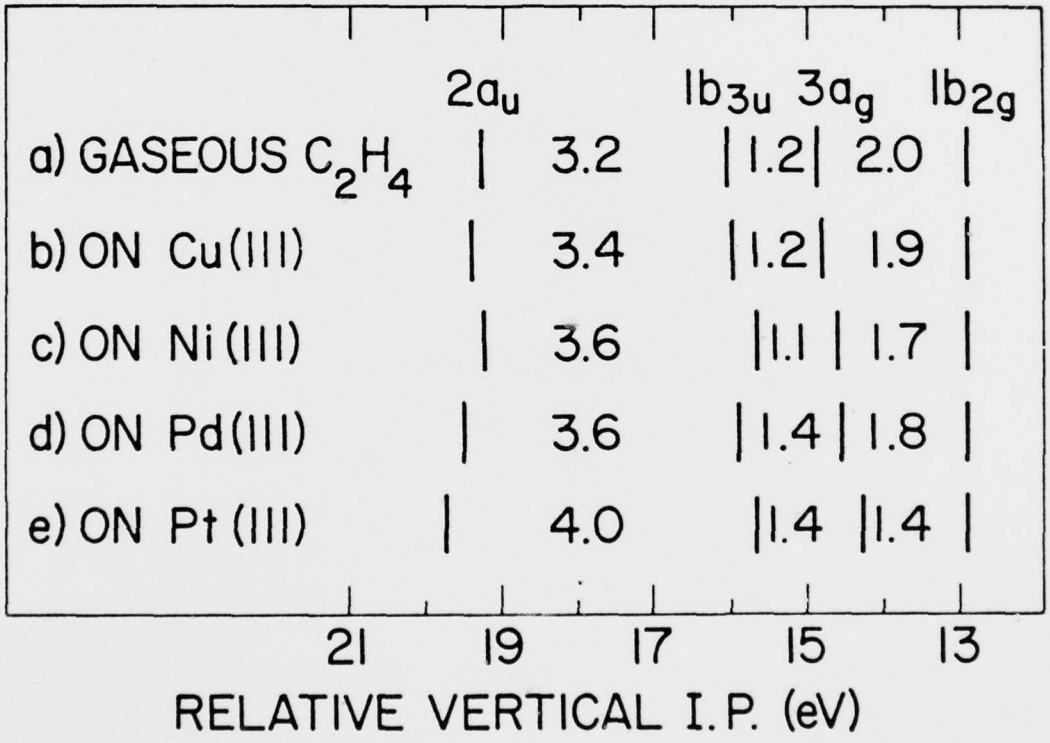
BEST AVAILABLE COPY



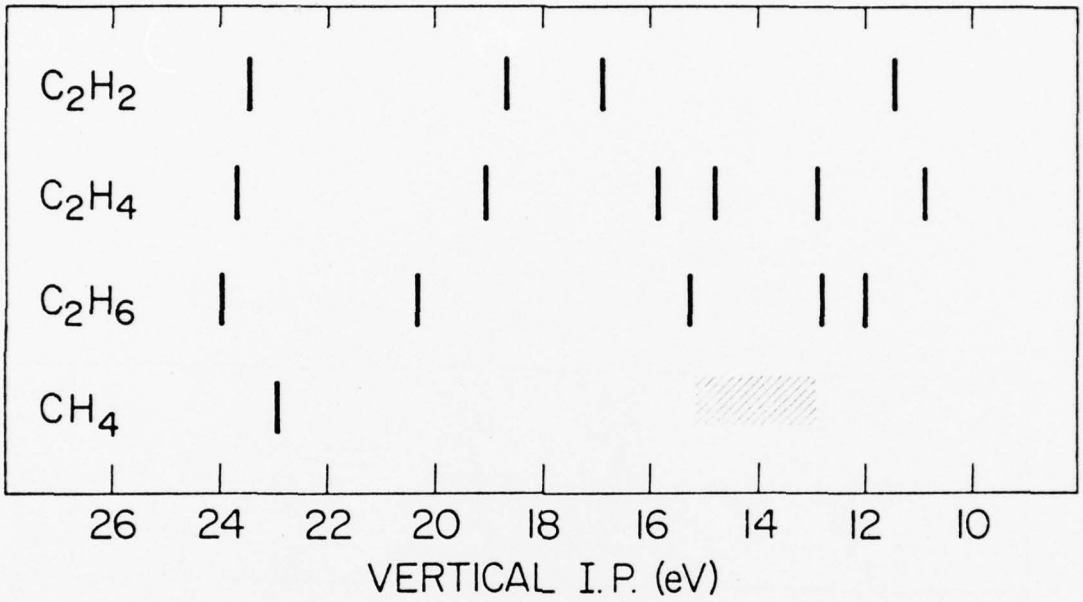

$2\sigma_g$
$2\sigma_u$
$3\sigma_g$
a) GASEOUS C_2H_2
4.5
2.1
b) ON Cu(100)
2.1
c) ON Ni(111)
2.2
d) ON Pd(111)
2.25
e) ON Pt(111)
2.3
25
23
21
19
17
RELATIVE VERTICAL I.P. (eV)

BEST AVAILABLE COPY

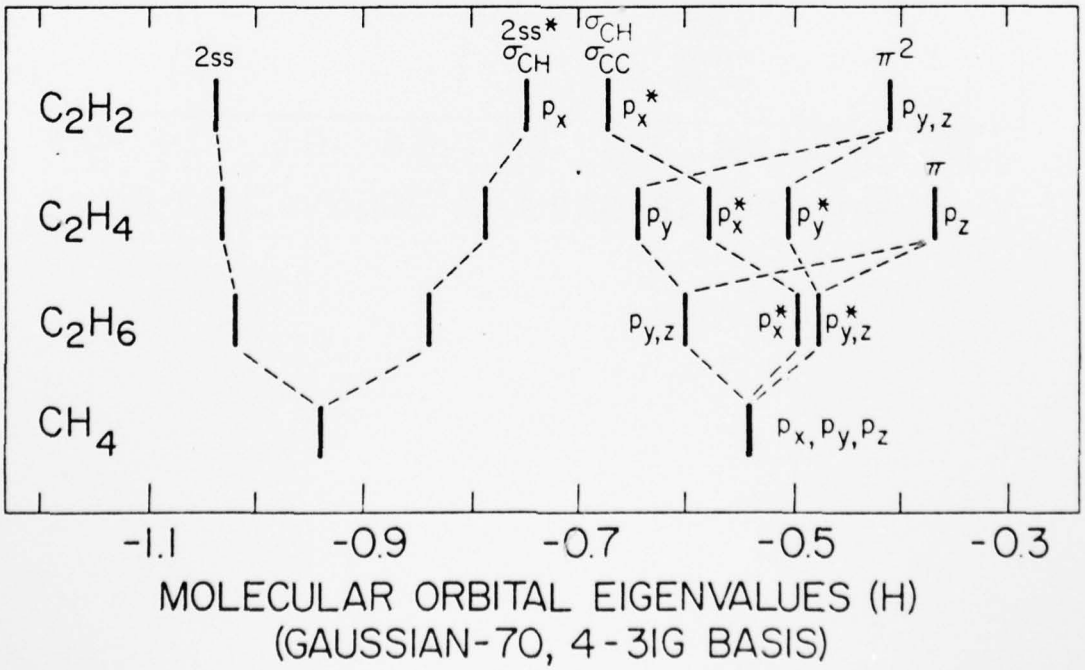


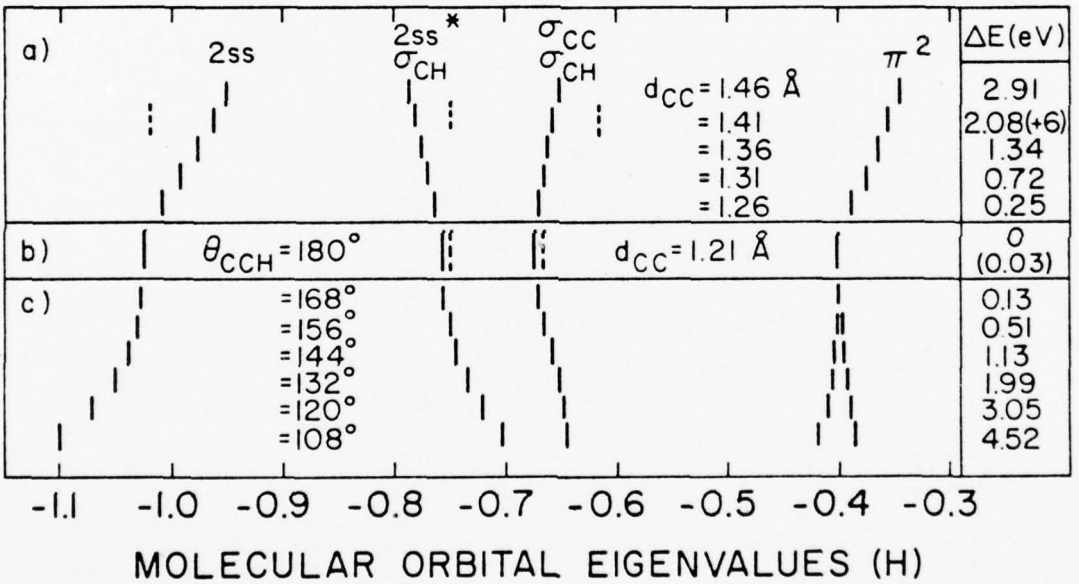

2a_u
1b_3u 3a_g 1b_2g
a) GASEOUS C_2H_4 | 3.2 | 1.2 | 2.0 |
b) ON Cu(111) | 3.4 | 1.2 | 1.9 |
c) ON Ni(111) | 3.6 | 1.1 | 1.7 |
d) ON Pd(111) | 3.6 | 1.4 | 1.8 |
e) ON Pt(111) | 4.0 | 1.4 | 1.4 |
21
19
17
15
13
RELATIVE VERTICAL I.P. (eV)

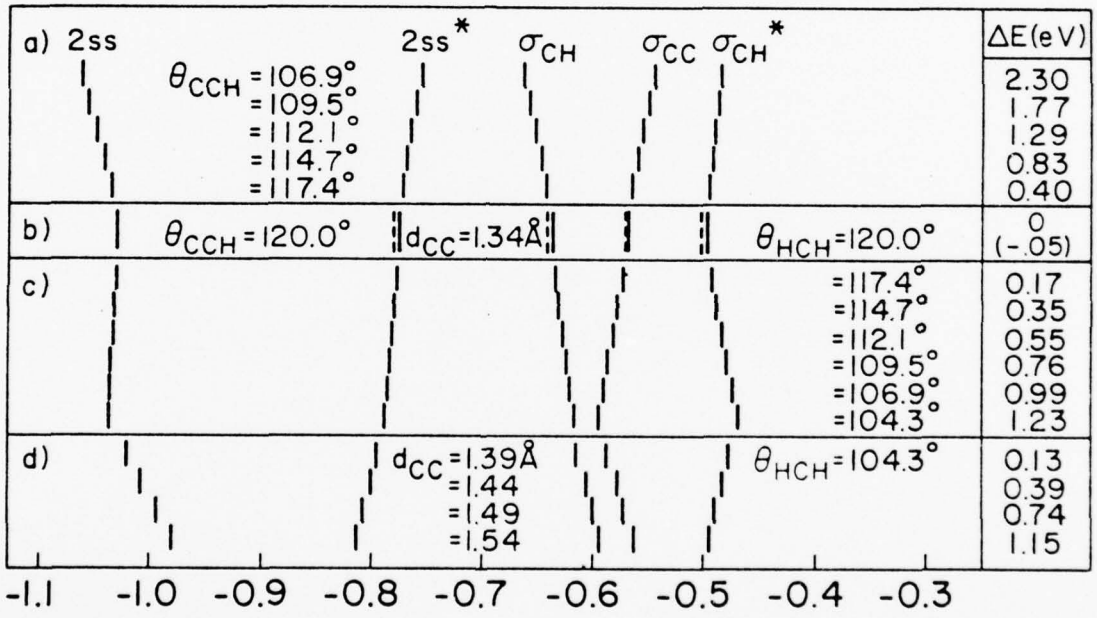
a) UPS



b) M.O. THEORY




a)
2ss
2ss*
σCH
σCC
σCH
π2
dCC = 1.46 Å
= 1.41
= 1.36
= 1.31
= 1.26
ΔE(eV)
2.91
2.08(+6)
1.34
0.72
0.25
b)
θCCH = 180°
dCC = 1.21 Å
0
(0.03)
c)
= 168°
= 156°
= 144°
= 132°
= 120°
= 108°
0.13
0.51
1.13
1.99
3.05
4.52
-1.1 -1.0 -0.9 -0.8 -0.7 -0.6 -0.5 -0.4 -0.3
MOLECULAR ORBITAL EIGENVALUES (H)


a) 2ss
2ss*
σCH
σCC
σCH*
θCCH = 106.9°
= 109.5°
= 112.1°
= 114.7°
= 117.4°
b)
θCCH = 120.0°
dCC = 1.34Å
θHCH = 120.0°
c)
= 117.4°
= 114.7°
= 112.1°
= 109.5°
= 106.9°
= 104.3°
d)
dCC = 1.39Å
= 1.44
= 1.49
= 1.54
θHCH = 104.3°
ΔE(eV)
2.30
1.77
1.29
0.83
0.40
0
(-.05)
0.17
0.35
0.55
0.76
0.99
1.23
0.13
0.39
0.74
1.15
-1.1 -1.0 -0.9 -0.8 -0.7 -0.6 -0.5 -0.4 -0.3
MOLECULAR ORBITAL EIGENVALUES (H)

APPENDIX

Item 4

SURFACE REFLECTANCE SPECTROSCOPY AND RELATED STUDIES OF SURFACE OPTICAL EXCITATIONS

G. W. Rubloff and J. L. Freeouf

IBM T. J. Watson Research Center

P.O. Box 218, Yorktown Heights, NY 10598

I. INTRODUCTION

The electronic structure of a surface involves (1) the density of occupied electron states (and wavefunctions), for which a valuable description is obtained from photoemission spectroscopy, and (2) the fundamental (optical) excitations of these occupied states. Initial experiments[1] have indicated that surface reflectance spectroscopy may provide a useful measure of surface optical excitations.

To better understand the characteristic electronic excitations of chemisorbed molecules on transition metal surfaces, we have carried out studies of such systems using surface reflectance spectroscopy (SRS) and also photoelectron yield and constant-initial-state (CIS) photoelectron spectroscopies. The purpose of this work has been to identify the fundamental intramolecular excitations of the chemisorbed molecule and possible charge transfer excitations between adsorbate and substrate and furthermore to assess the role and value of SRS as a source of information complementary to ultraviolet photoemission spectroscopy (UPS). We present here a preliminary discussion of some of these results.

II. EXPERIMENTAL TECHNIQUES

SRS measurements have been carried out in two overlapping spectral ranges using two different sets of experimental apparatus. In the photon energy range $1.5 < \hbar\omega < 10$ eV, measurements were made using a new system constructed at IBM expense and compatible with the ultrahigh vacuum surface analysis system at IBM, which includes facilities for uv photoemission, mass spectroscopy, electron energy loss, Auger, LEED, and flash desorption studies. This SRS optical system incorporates a high-stability double-beam/chopper technique for near-normal incidence reflectance measurements, various sources and detectors, and direct computer interfacing. It achieves a surface sensitivity comparable to previous work[1] but represents two very significant improvements: (1) SRS data are obtained in the vacuum ultraviolet (VUV) spectral region ($\hbar\omega > 6$ eV), where fundamental optical excitations of the adsorbed molecule are expected; and (2) by measuring the full reflectance spectrum for the clean and then the adsorbate-covered surface, the entire SRS spectrum is obtained quickly, giving a reduction in data acquisition/analysis time of ~ 10-100X compared to previous point-by-point (single wavelength) measurements[1].

SRS measurements with this system have been made for chemisorbed C_6H_6 on Ni(111), polycrystalline Pd, and polycrystalline Pt; for condensed C_6H_6 (formed at 77°K) on Ni(111); for chemisorbed CO on Ni(111); for hydrogen and oxygen chemisorbed on Ni(111); and for a thermally-grown oxide on Ni(111). The polycrystalline samples were evaporated films formed in situ by direct sublimation from a pure metal wire. Measurements were carried out in ultrahigh vacuum (operating pressures ~ 1×10^{-10} torr).

The inherent stability of the synchrotron radiation from an electron storage ring was utilized to extend SRS measurements to $\hbar\omega \sim 40$ eV with the sensitivity required for SRS. Radiation from the 240 MeV electron storage ring at the University of Wisconsin Synchrotron Radiation Center was used to measure chemisorption-induced changes in the optical excitations of the surface, using a simple monitor of the incident light to normalize the spectra as compen-

sation for the smooth decay of the electron beam current and corresponding synchrotron radiation intensity. SRS measurements for both s-and p-polarized light were carried out for chemisorbed CO and C_6H_6 on Ni(111). In a similar way, measurements of the relative change in total photoelectron yield were made for the same systems. Finally, the relative change in the $\hbar\omega$-dependent photoionization cross-section of CO orbitals and of various parts of the Ni d-band was measured for the CO/Ni(111) system.

In the following we present a summary of the data for CO and C_6H_6 on Ni(111) as examples of the SRS and related optical spectra. Since details of stray light and higher order corrections in the data have not yet been sorted out and analysis of the results is not complete, the possible physical conclusions suggested here should be considered preliminary.

III. CO/Ni(111)

A. SRS Results

Figure 1 shows the $\Delta R/R$ spectrum for CO/Ni(111) as measured at higher energies using synchrotron radiation. The spectrum for s-polarized light (dots), taken at near-normal incidence using the yield from a Au photodiode for detection, shows a peak near 9 eV. Further structure for s-polarized light includes a valley near 12 eV, a shoulder near 15 eV, and a broad peak near 24 eV. The spectrum for p-polarized light using the same kind of detector (triangles) in Fig. 1 displays similar features, except that the valley near 12 eV has filled in and the 15 eV shoulder has disappeared. These spectra have been terminated at ~ 8.5 eV since at lower $\hbar\omega$ higher-order contributions from the grating become important. We also measured the same p-polarized spectrum using a sodium salicylate fluorescence detector, for which higher-order corrections become important only below ~ 6 eV; this spectrum, shown by the squares in Fig. 2, displays a well-defined peak near 9 eV as indicated by the other spectra in Fig. 1.

A method to analyze the $\Delta R/R$ spectra is available from a generalization[1] of the dielectric model of McIntyre and Aspnes[2]. Feibelman[3] has shown that this classical dielectric model provides a useful and valid approximation to the complete nonlocal microscopic dielectric response at a surface for experiments using s-polarized light. He has also shown that the buildup of surface charge due to photon A-vector components normal to the surface renders the simple classical model invalid (at least in principle) for the case of p-polarized light, but quantitative estimates of the errors introduced by these complications are not presently available.

We have carried out a preliminary analysis of the s-polarized $\Delta R/R$ spectra for CO/Ni(111) using the classical dielectric model. We have arbitrarily assumed a surface layer thickness of 2Å (which enters as a simple scale factor) and have used the optical constants of bulk Ni from Vehse and Arakawa[4] for $3.5 < \hbar\omega < 22$ eV and those of Moravec, Rife, and Dexter[5] outside this range, multiplicatively scaled to smoothly join the Vehse and Arakawa data. The chemisorption-induced change in surface dielectric function $\Delta\hat{\epsilon}^s = \Delta\epsilon_1^s + i\Delta\epsilon_2^s$ was assumed to be a sum of several Lorentzian oscillators, parameters of which were adjusted to obtain a good fit of the calculated $\Delta R/R$ spectrum to the experimental data[1,6]. A preliminary fit to the $\Delta R/R$ ($\hbar\omega$) spectrum is shown in Fig. 2, together with the corresponding $\Delta\epsilon_2^s$ spectra. The peaks in $\Delta\epsilon_2^s$ indicate that CO chemisorption on Ni(111) produces new optical transitions in the surface region near 8 and 13 eV, with a broad band of additional excitations centered near 16 eV extending from ~ 13 eV to ~ 19 eV.

The two sharp structures in $\Delta\ _2^s$ are located at nearly the same energies as peaks in the electron energy loss spectra ($-\mathrm{Im}\ 1/\epsilon$) of Hinz[7] on vapor and solid phase CO, which are shown in Fig. 3. However, the loss spectra show no features corresponding to the large oscillator strength in the broad peak near 16 eV in $\Delta\epsilon_2^s$ (Fig. 2). An energy loss peak at 13 eV has also been observed for CO chemisorbed on Ni(110).[8] A final determination of the energy position and error for the optical structures deduced from the SRS $\Delta R/R$ data must

await completion of this analysis. The apparent correspondence of the sharp Δ_2^5 features to the vapor and solid phase CO energy loss data would be especially intriguing since the excitation near 8 eV in the energy loss and optical spectra of vapor and solid CO is a $X\ ^1\Sigma^+ \rightarrow A^1\pi$ valence excitation from the occupied 5σ orbital to the empty $2\pi^*$ orbital. UPS results indicate that the binding energy of the least tightly bound 5σ orbital of CO is increased considerably (1-3 eV) relative to the other occupied molecular orbitals upon chemisorption on transition metals.[9] The lowest empty states of the adsorbed molecule are expected to play as important a role in the energetics of chemisorption as that of the highest-lying filled states seen in UPS[10]. Thus the observation of the behavior of the empty states from optical excitations would be a significant step toward a complete understanding of chemisorption.

B. Total Yield Results

Chemisorption-induced changes in the total yield spectrum (total number of photoelectrons created versus photon energy) should also reveal optical excitations of the surface region here, although transitions to final states below the vacuum level can contribute only if they undergo significant nonradiative decay to produce other hot electrons above the vacuum level. The relative change in total photoelectron yield caused by chemisorption of CO on Ni(111) is shown in Fig. 4 for s-polarized light at near-normal incidence (dots) and for p-polarized light at 50° angle of incidence (triangles). The spectra shown have been terminated ~ 2 eV above the 6.0 eV photoelectric threshold for CO/Ni(111) to remove the range of low total yield where higher-order contributions from the grating are a problem. A peak at ~ 10 eV appears clearly for s-polarized incident light but is nearly absent for p-polarized light. Note that in this geometry the latter case (photon electric field in the plane of incidence) the photon produces electric field components both normal to and in the plane of the surface, whereas only in-plane components are present for the case of s-polarized light.

The yield spectra are dominated by a strong peak at ~ 15 eV which appears in both

polarizations. A shoulder near 23 eV is also present in both cases. The sharp increase in yield near 13 eV, which leads to the peak at 15 eV, probably represents the ionization threshold for the 5σ orbital of chemisorbed CO; this orbital lies at ~ 12.0 eV binding energy for CO/Ni(111), and the characteristic slow turn-on near threshold ($\sim(E-E_0)^{1/2}$) may shift the peak to somewhat higher energy.

C. Photoionization Cross-Section Results

We have also measured the chemisorption-induced change in the photoionization cross-section as a function of photon energy (i.e. constant-initial-state or CIS spectra) for various parts of the Ni(3d) band. In these measurements the electron energy analyzer (normally used for UPS) is operated such that it measures electrons having kinetic energies which are increased with the incident photon energy, so that the emission from a fixed initial (occupied) state is measured as a function of photon energy (or equivalently of photoelectron kinetic energy). Figures 5a and 5b show respectively the results for s- and s,p-polarized incident light for the top (dots), middle (triangles), and bottom (squares) of the d-bands, plotted as a function of photoelectron kinetic energy above a zero at the vacuum level (E_{VAC}) for the CO-covered surface.

When the CIS spectra are plotted as a function of photon energy, it becomes evident that the various parts of the d-band are not preferentially excited at common $\hbar\omega$ values. Rather, when plotted as a function of final state kinetic energy as in Fig. 5, it appears that the photoionization cross-section of the d-bands is enhanced for particular final state energies. Chemisorption-induced excitations to states ~ 5 eV above the vacuum level (E_{VAC}) are seen for all three parts of the d-band and for both polarization cases except perhaps that of s-polarized light exciting states at the top of the d-band. Enhanced emission is also observed at ~ 12 eV above E_{VAC} for the middle and bottom of the d-bands in both polarization cases and at ~ 2 eV above E_{VAC} in the s-polarized case for all three parts of the d-band. The latter

final state structure appears as an edge and is more dramatically illustrated in Fig. 7, which displays the polarization-dependence of the spectrum for each part of the d-band.

The CIS spectra in Figs. 5 and 6 clearly show that CO chemisorption causes preferential excitation of d-band electrons to particular final states, which may be either substrate- or adsorbate-derived orbitals. Furthermore, excitation to final states ~ 2 eV above E_{VAC} show a polarization dependence (see Fig. 6). One must keep in mind that these excitations could in principle result from direct non-radiative recombination of other photon-induced excitations rather than from direct photon absorption. Finally, differences in the spectral dependence of the CIS spectra in Fig. 5 show that CO chemisorption affects the top of the filled d-band in a different way than the middle or bottom regions of the band. This represents a new kind of demonstration of the qualitative difference between the behavior of the top of the filled d-band and the region below. In the past the preferentially stronger attenuation of the d-band top in conventional UPS spectra has often been cited as evidence for the difference; this effect is given simply by the relative magnitudes of the cross-section changes for the various parts of the d-band (Fig. 6) observed at a single $\hbar\omega$.

IV. C_6H_6/Ni(111)

A. SRS Results

The optical absorption/reflection and the electron energy loss spectra of vapor, liquid, and solid phase benzene (C_6H_6) have been the subject of considerable previous study. As an example, the absorption spectra of Shiho[12] are shown in Fig. 7. In the vapor phase significant singlet absorption begins near 6 eV with $^1A_{1g} \rightarrow {}^1E_{1u}$ transitions followed by a very strong absorption peak near 7 eV attributed to $^1A_{1g} \rightarrow {}^1B_{1u}$ excitations; both are $\pi \rightarrow \pi^*$ transitions. At energies above ~ 9 eV a complex absorption, not yet understood, is observed and likely includes $\sigma \rightarrow \pi^*$ and $\sigma \rightarrow \sigma^*$ valence excitations along with sharp Rydberg structure, as seen in Fig. 8 from Koch and Otto.[13] In the solid phase the $\pi \rightarrow \pi^*$ transitions are shifted toward lower energy but the overall shape of the spectra is maintained.

To make contact with the optical transitions characteristic of condensed phases of C_6H_6 and with previous UPS results[14], we measured the SRS spectra of C_6H_6 condensed on Ni(111) at 77K. The measured $\Delta R/R$ spectrum, seen in Fig. 9 (triangles), shows a sharp doublet valley near 6 eV and a drop near 8 eV (stray light problems are significant above ~ 9 eV). A preliminary lineshape analysis of the spectrum (for a surface layer thickness d=10. Å) yields a fit to $\Delta R/R$ (dots) and a corresponding $\Delta \epsilon_2^s$ spectrum (squares) consisting of a sharp peak at ~ 6.3 eV, a weaker shoulder on its low energy side at ~ 5.9 eV, and a broader, weaker peak near 8.5 eV. The 6.3 and 5.9 eV structures resemble very closely the $^1A_{1g} \rightarrow {}^1E_{1u}$ and $^1A_{1g} \rightarrow {}^1B_{1u}$ absorption bands of solid C_6H_6 observed at essentially the same energies[12,13].

The $\Delta R/R$ spectrum for a saturation coverage (~ 1 monolayer) of chemisorbed C_6H_6 on Ni(111) at 300K is shown in Fig. 10. This curve was constructed by shifting the spectrum for the H_2 lamp (above ~ 4.5 eV) vertically to match that from the Xe lamp source at lower $\hbar\omega$. No strong structure is evident below 8 eV, except perhaps for the change in slope near 3 eV.

The $\Delta R/R$ spectra for chemisorbed C_6H_6/Ni(111) at 300K measured using synchrotron radiation are shown in Fig. 11 for s-polarized light at near-normal incidence (dots) and for p-polarized light at ~ 50° angle of incidence using the Au diode (triangles) and sodium salicylate (squares) detectors. The gross features are similar to those for CO/Ni(111)-a valley near 13-15 eV and a broad peak near 25 eV, but the sharper structures which appeared near 10 and 15 eV for chemisorbed CO are not present. A rough lineshape analysis of the s-polarized case for surface layer thickness d=2 Å is shown in Fig. 12, where a fit to the overall shape of the $\Delta R/R$ spectrum yields a broad peak in $\Delta\epsilon_2^s$ centered near 15 eV. Because this feature is similar to the broad structure which dominates the CO/Ni(111) results, it could be associated with changes in the Ni optical response near the surface as induced by chemisorption in general.

B. Total Yield Results.

The relative change $\Delta Y/Y$ in total photoelectron yield caused by chemisorption of C_6H_6 on Ni(111) at 300K is shown in Fig. 13 for s-polarized light at near-normal incidence (dots) and for p-polarized light at ~ 50° angle of incidence (triangles). The spectra for both polarizations show a sharp shoulder at ~ 13 eV and broader features near 19 and 34 eV. The yield near 9-12 eV is strongly enhanced by chemisorption for s-polarized light but not for the p-polarized case. These spectra are totally different from the yield spectra observed for CO/Ni(111) and the structures seem to bear some correspondence to the ionization thresholds of the orbitals of adsorbed C_6H_6 seen in UPS.[14]

V. Conclusions

Although the analysis of the SRS and related yield and CIS data is still incomplete at present, several conclusions of physical significance seem to be suggested at this stage

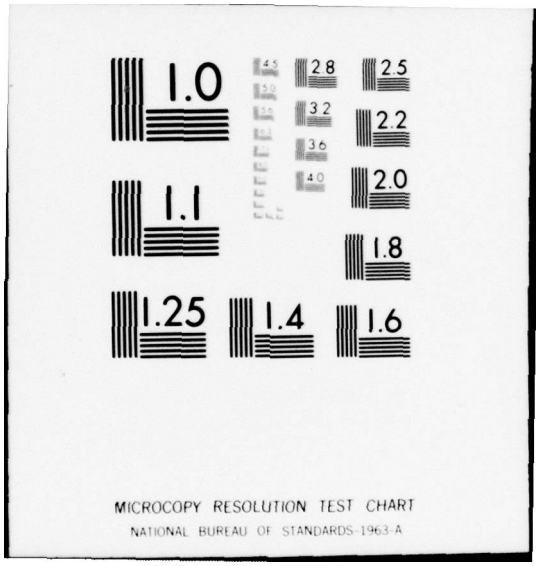
AD-A038 084 IBM THOMAS J WATSON RESEARCH CENTER YORKTOWN HEIGHTS N Y F/G 11/6
SPECTROSCOPIC STUDIES OF CHEMICAL ADSORPTION AND REACTIONS AT T--ETC(U)
MAR 77 J E DEMUTH, G W RUBLOFF N00014-75-C-0346

UNCLASSIFIED NL

2 OF 2
ADA038084



END
DATE FILMED
4-77


1.0
1.1
1.25
1.4
1.6
1.8
2.0
2.2
2.5
2.8
3.2
3.6
4.0
MICROCOPY RESOLUTION TEST CHART
NATIONAL BUREAU OF STANDARDS-1963-A

(1) The SRS spectra show some reasonably sharp features in the vacuum ultraviolet which may be related to the intramolecular excitations of the chemisorbed molecule, (e.g. the 8 and 13 eV transitions of CO).

(2) The SRS spectra show structures which are common to the two different adsorbates studied and may be related to chemisorption-induced changes in the surface optical response of the substrate.

(3) Correlations between SRS and yield spectra (e.g. CO SRS structure near 13-15 eV and yield peak at 15 eV) may indicate the importance of photoionizing transitions in the optical response of the chemisorbed molecules; the correlation of SRS features (e.g. the 13 eV CO peak) with corresponding gas or solid phase molecular spectra which involve Rydberg transitions may further suggest that some remnant of Rydberg-like excitations persists in the chemisorbed phase.

(4) The yield and CIS spectra display well-defined structures, some of which are polarization-dependent; the observed polarization-dependence may help identify the excitations by the approximate selection rules for dipole transitions of oriented chemisorbed molecules.

(5) Features in the d-band CIS spectra for CO/Ni(111) define particular final state energies above the vacuum level. These may be adsorbate affinity levels filled by charge-transfer excitations from the filled Ni d-bands, which would be the result of direct photoabsorption or of nonradiative decay of intramolecular excitations of the adsorbed molecule by direct recombination (configuration interaction).

(6) The spectral dependence of the d-band CIS results demonstrates that the top of the filled Ni d-band is affected differently by CO chemisorption than the rest of the filled band.

Even though it would be premature to make any final assessment of the value of SRS results, it is possible to note several clear conclusions about the possibilities and problems of the technique:

(1) Continuously-scanned SRS spectra with sufficient stability to observe surface optical transitions can be obtained rather quickly (~ 1/2-1 hour) either with the VUV optical system at IBM or with synchrotron radiation, a 10-100X increase in speed over previous techniques.

(2) Most structures observed to date in the SRS spectra lie in the VUV region above 9-10 eV, i.e. that accessible in practice only with synchrotron radiation.

(3) SRS suffers from the difficult problems of stray light and higher-order contributions which plague all broad-range optical spectroscopies in the vacuum ultraviolet.

(4) Total yield and CIS photoelectron spectroscopies may provide a very useful complement to SRS to aid interpretation and identification of the observed transitions.

REFERENCES

1. G. W. Rubloff, J. Anderson, M. A. Passler, and P. J. Stiles, Phys. Rev. B15 **10**, 2401 (1974).

2. J. D. E. Mc Intyre and D. E. Aspnes, Surf. Sci. **24**, 417 (1971).

3. P. J. Feibelman, Phys. Rev. B15 **14**, 762 (1976).

4. R. C. Vehse and E. T. Arakawa, Phys. Rev. **180**, 695 (1969).

5. T. J. Moravec, J. C. Rife, and R. N. Dexter, Phys. Rev. B15 **13**, 3297 (1976).

6. Results of this procedure and those obtained by Kramers-Kronig analysis have been found to be in reasonable agreement for H_2/W(100) data; see J. B. Restorff and H. D. Drew, APS Bulletin **21**, 305 (1976).

7. H. J. Hinz, in **Vacuum Ultraviolet Radiation Physics**, Proc. of the IV Int. Conf. on VUV Radiation Physics), ed. by E. E. Koch et. al. (N.Y., Pergamon, 1975), p. 176.

8. J. Küppers, J. Electron Spectros. **1**, 186 (1972).

9. T. Gustafsson, E. W. Plummer, D. E. Eastman, and J. L. Freeouf, Solid State Communications **17**, 391 (1975).

10. T. B. Grimley, in **Molecular Processes on Solid Surfaces**, ed. by E. Dranglis (N.Y., McGraw-Hill, 1969), p. 299.

11. J. W. Davenport, Phys. Rev. Letters **36**, 945 (1976); T. Gustafsson, E. W. Plummer, W. Gudat, and D. E. Eastman, to be published.

12. M. Shiho, Japan. J. Appl. Phys. **12**, 314 (1973).

13. E. E. Koch and A. Otto, Int. J. Radiat. Phys. Chem. 6, (1975).

14. J. E. Demuth and D. E. Eastman, Phys. Rev. Letters 32, 1123 (1974); D. E. Eastman and J. E. Demuth, Japan. J. Appl. Physics, Suppl. 2, Part 2, p. 827 (1974).

FIGURE CAPTIONS

Fig. 1. Relative reflectance change for CO/Ni(111) at 300K for s-polarized light at near-normal incidence (dots, Au diode detector); and p-polarized light at 50° angle of incidence for Au diode (triangles) and sodium salicylate (squares) detectors.

Fig. 2. Analysis of $\Delta R/R$ data for CO/Ni(111). Squares = experimental $\Delta R/R$ ($\hbar\omega$) spectrum for s-polarized light at near-normal incidence; dots = calculated $\Delta R/R$ spectrum obtained as a fit to experimental data; triangles = corresponding model $\Delta\epsilon_2^s$, the chemisorption-induced change in the imaginary part of surface dielectric function.

Fig. 3. Electron energy loss spectrum of solid and vapor phase CO from Ref. 7.

Fig. 4. Relative change in total yield due to chemisorption of CO on Ni(111) at 300K. Dots = s-polarized light at near-normal incidence; triangles = p-polarized light at 50° angle of incidence.

Fig. 5. Relative change in Ni 3d-band photoionization cross-section due to chemisorption of CO on Ni(111) at 300K, plotted as a function of electron final state kinetic energy above a zero at E_{VAC} for (a) s-polarized light and (b) a mixture of s- and p-polarized light; dots = top, triangles = middle, squares = bottom of d-band.

Fig. 6. Relative change in Ni 3d-band photoionization cross-section due to chemisorption of CO on Ni(111) at 300K, plotted as a function of electron final state kinetic energy above a zero at E_{VAC} for (a) top, (b) middle, and (c) bottom of d-bands; dots = s-polarized light; triangles = mixed s- and p-polarized light.

Fig. 7. Absorption spectra of solid, liquid, and vapor phase C_6H_6 from Ref. 12.

Fig. 8. Reflectance and absorption spectra of solid and vapor phase C_6H_6 from Ref. 13.

Fig. 9 SRS results for condensed C_6H_6 (170 Langmuirs) on Ni(111) at 77K. Triangles = experimental $\Delta R/R$ data; dots = calculated fit to $\Delta R/R$ spectrum; squares = corresponding model $\Delta\epsilon_2^s$, the change in the imaginary part of the surface dielectric function.

Fig. 10 SRS $\Delta R/R$ spectrum for chemisorbed C_6H_6 on Ni(111) at 300K, using s-polarized light at near-normal incidence. Spectra taken with different light source/detector combinations have been matched at ~ 4.5 eV.

Fig. 11 SRS $\Delta R/R$ spectra for chemisorbed C_6H_6 on Ni(111) at 300K for s-polarized light at near-normal incidence (dots) and p-polarized light at ~ 50° angle of incidence for Au diode (squares) and sodium salicylare (diamonds) detectors.

Fig. 12 Analysis of $\Delta R/R$ data for C_6H_6/Ni(111). Squares = experimental $\Delta R/R$ ($\hbar\omega$) spectrum; dots = calculated $\Delta R/R$ spectrum obtained as a fit to experimental data; triangles = corresponding model $\Delta\epsilon_2^s$, the chemisorption-induced change in the imaginary part of the surface dielectric function.

Fig. 13 Relative change $\Delta Y/Y$ in total yield caused by chemisorption of C_6H_6 on Ni(111) at 300K for s-polarized light at near-normal incidence (dots) and p-polarized light at ~ 50° angle of incidence (triangles).

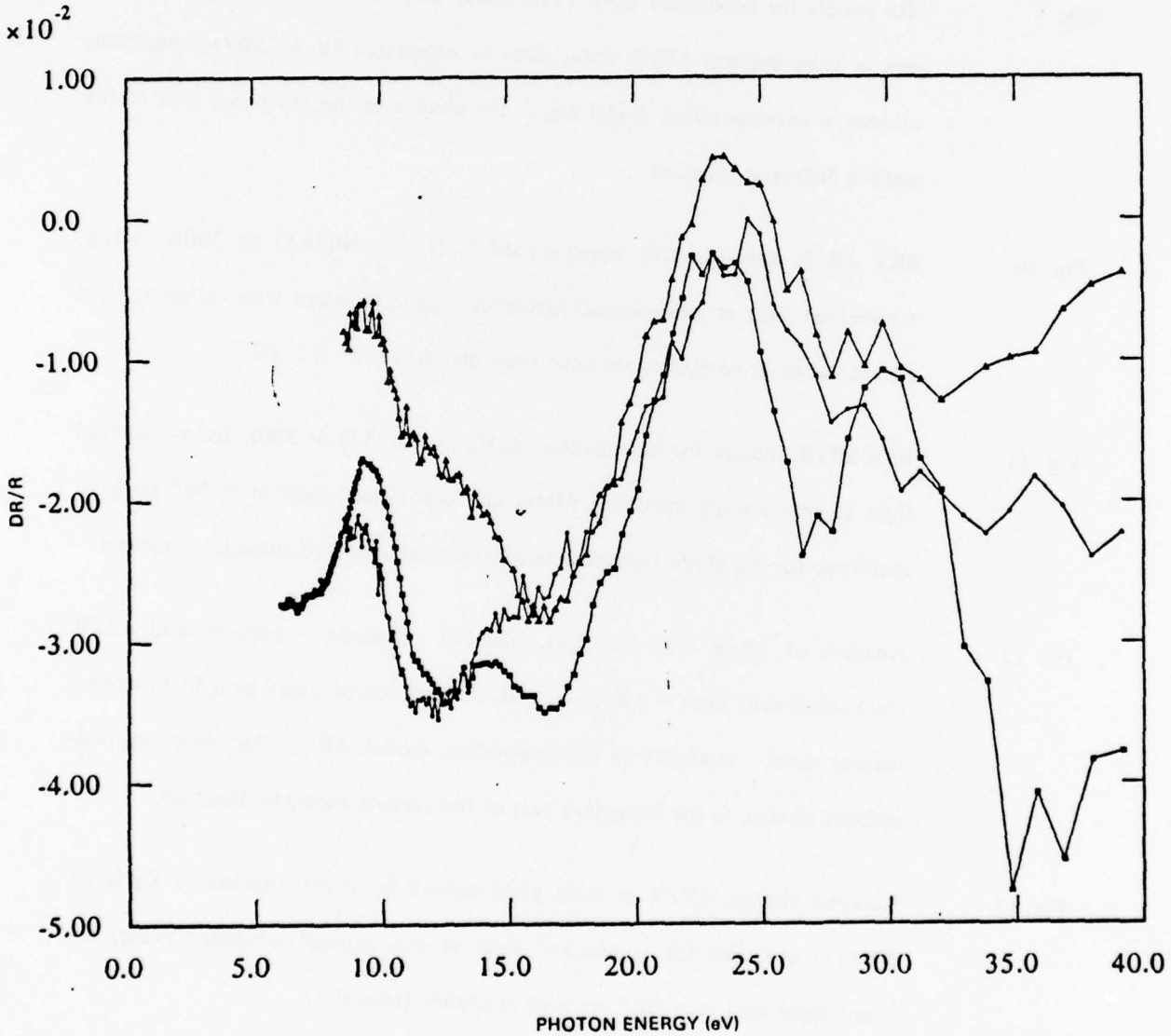

x10^-2
1.00
0.0
-1.00
-2.00
-3.00
-4.00
-5.00
DR/R
0.0
5.0
10.0
15.0
20.0
25.0
30.0
35.0
40.0
PHOTON ENERGY (eV)

FIG. 1

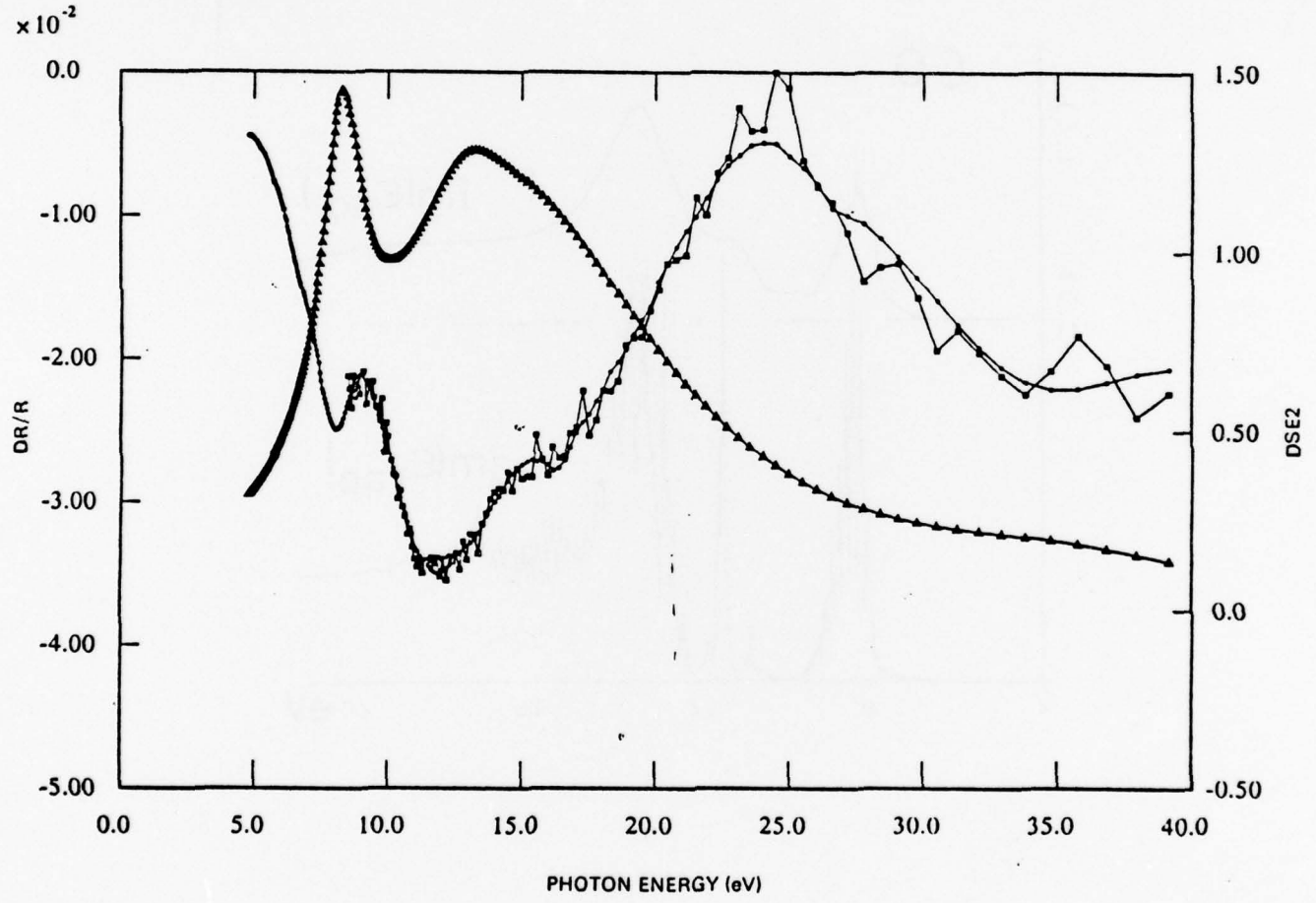

x 10^-2
0.0
-1.00
-2.00
-3.00
-4.00
-5.00
DR/R
1.50
1.00
0.50
0.0
-0.50
DSE2
0.0
5.0
10.0
15.0
20.0
25.0
30.0
35.0
40.0
PHOTON ENERGY (eV)

FIG. 2

BEST AVAILABLE COPY

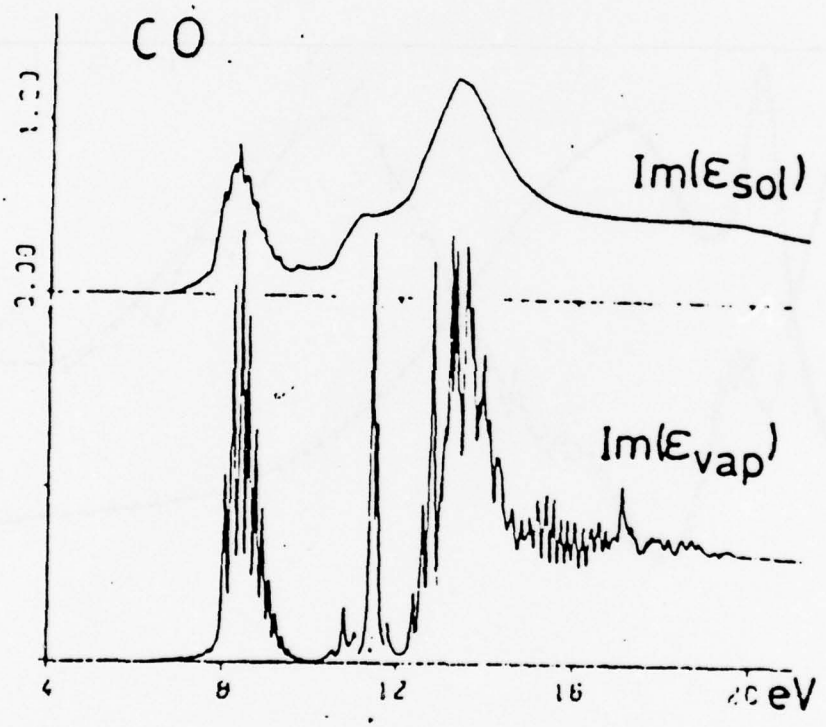


FIG. 3

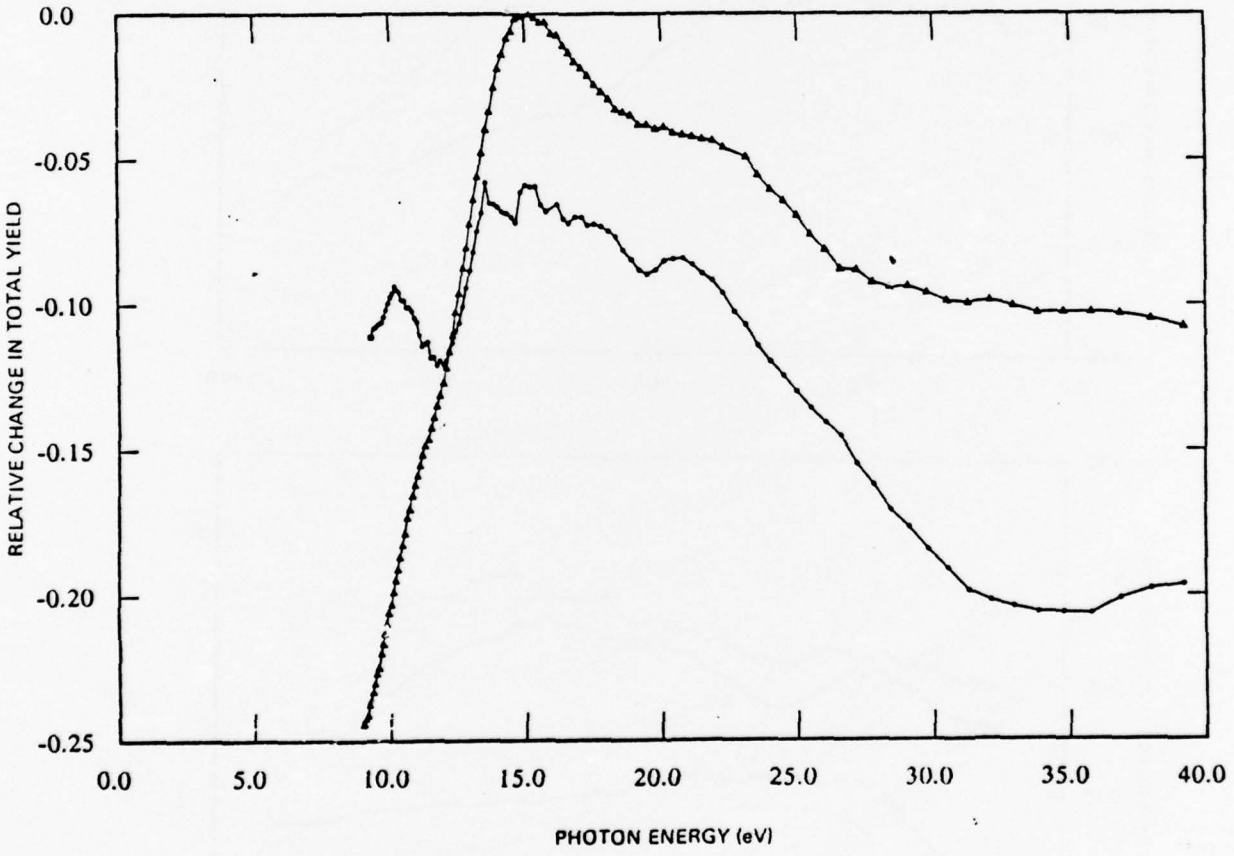

0.0
-0.05
-0.10
-0.15
-0.20
-0.25
RELATIVE CHANGE IN TOTAL YIELD
0.0
5.0
10.0
15.0
20.0
25.0
30.0
35.0
40.0
PHOTON ENERGY (eV)

FIG. 4

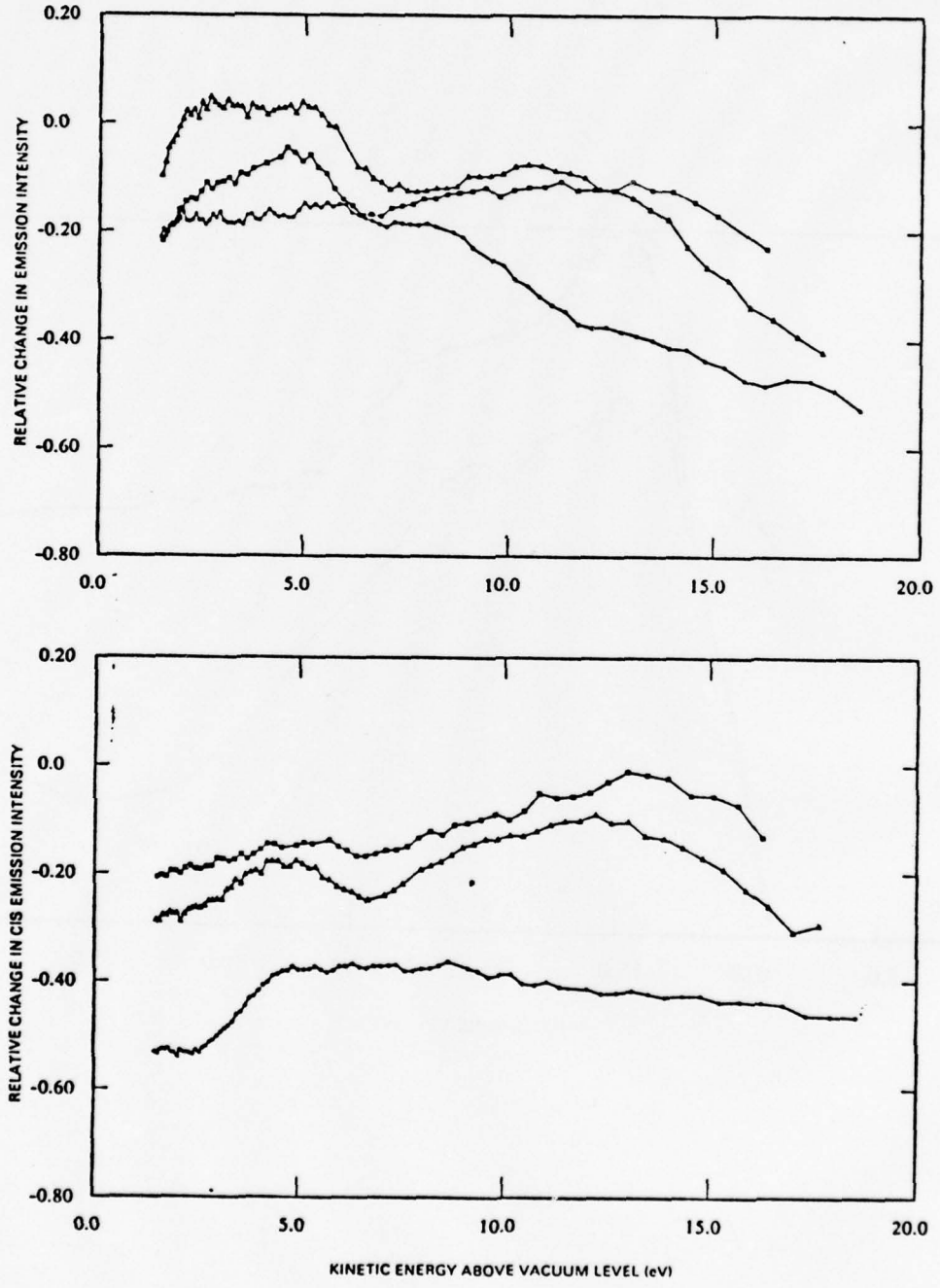

0.20
0.0
-0.20
-0.40
-0.60
-0.80
RELATIVE CHANGE IN EMISSION INTENSITY
0.0
5.0
10.0
15.0
20.0
0.20
0.0
-0.20
-0.40
-0.60
-0.80
RELATIVE CHANGE IN CIS EMISSION INTENSITY
0.0
5.0
10.0
15.0
20.0
KINETIC ENERGY ABOVE VACUUM LEVEL (eV)

FIG. 5

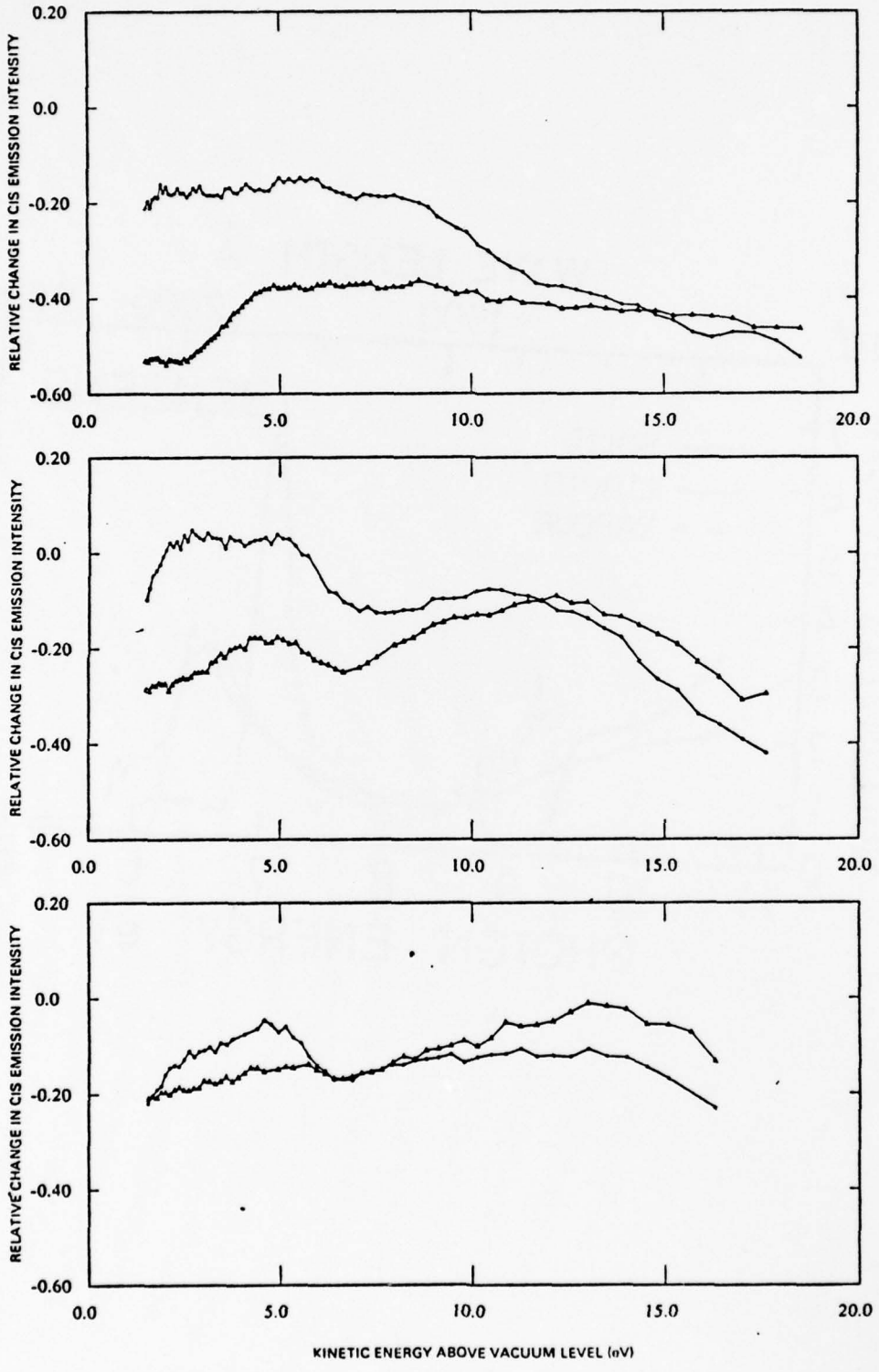

0.20
0.0
-0.20
-0.40
-0.60
RELATIVE CHANGE IN CIS EMISSION INTENSITY
0.0
5.0
10.0
15.0
20.0
KINETIC ENERGY ABOVE VACUUM LEVEL (eV)

FIG. 6

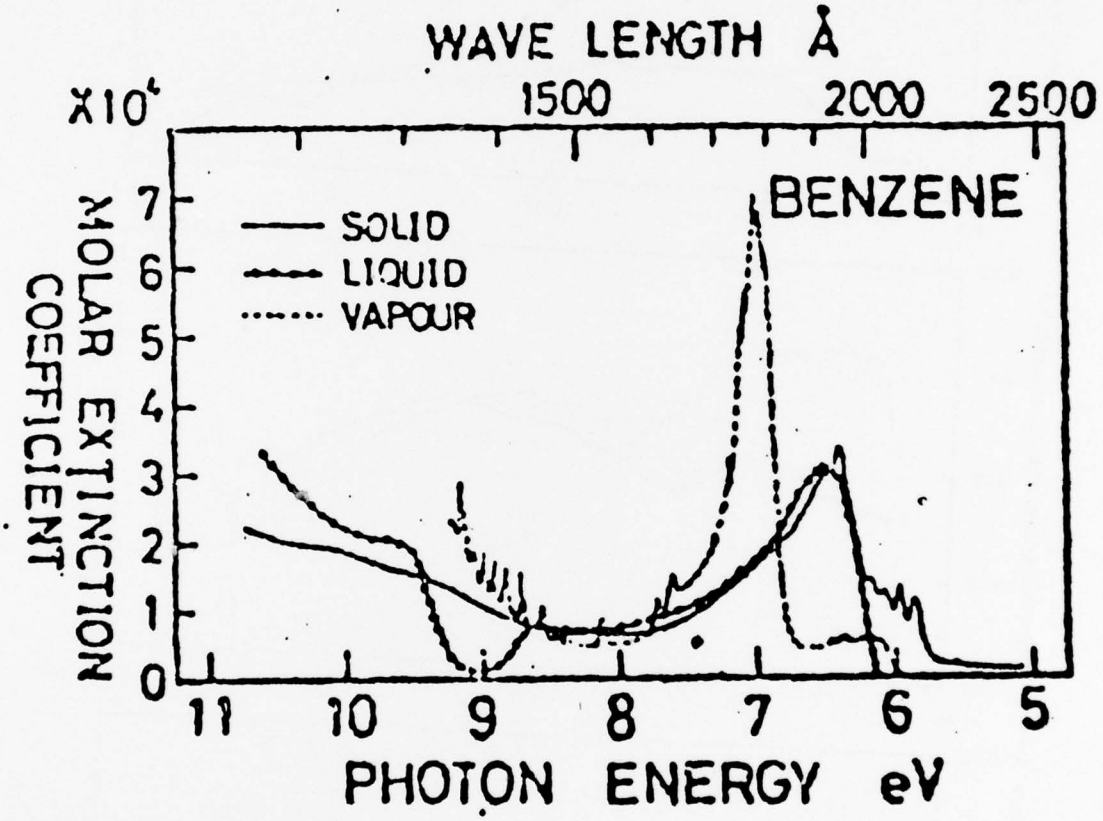

WAVE LENGTH Å
1500
2000
2500
X10⁴
BENZENE
SOLID
LIQUID
VAPOUR
MOLAR EXTINCTION COEFFICIENT
0
1
2
3
4
5
6
7
11
10
9
8
7
6
5
PHOTON ENERGY eV

FIG. 7

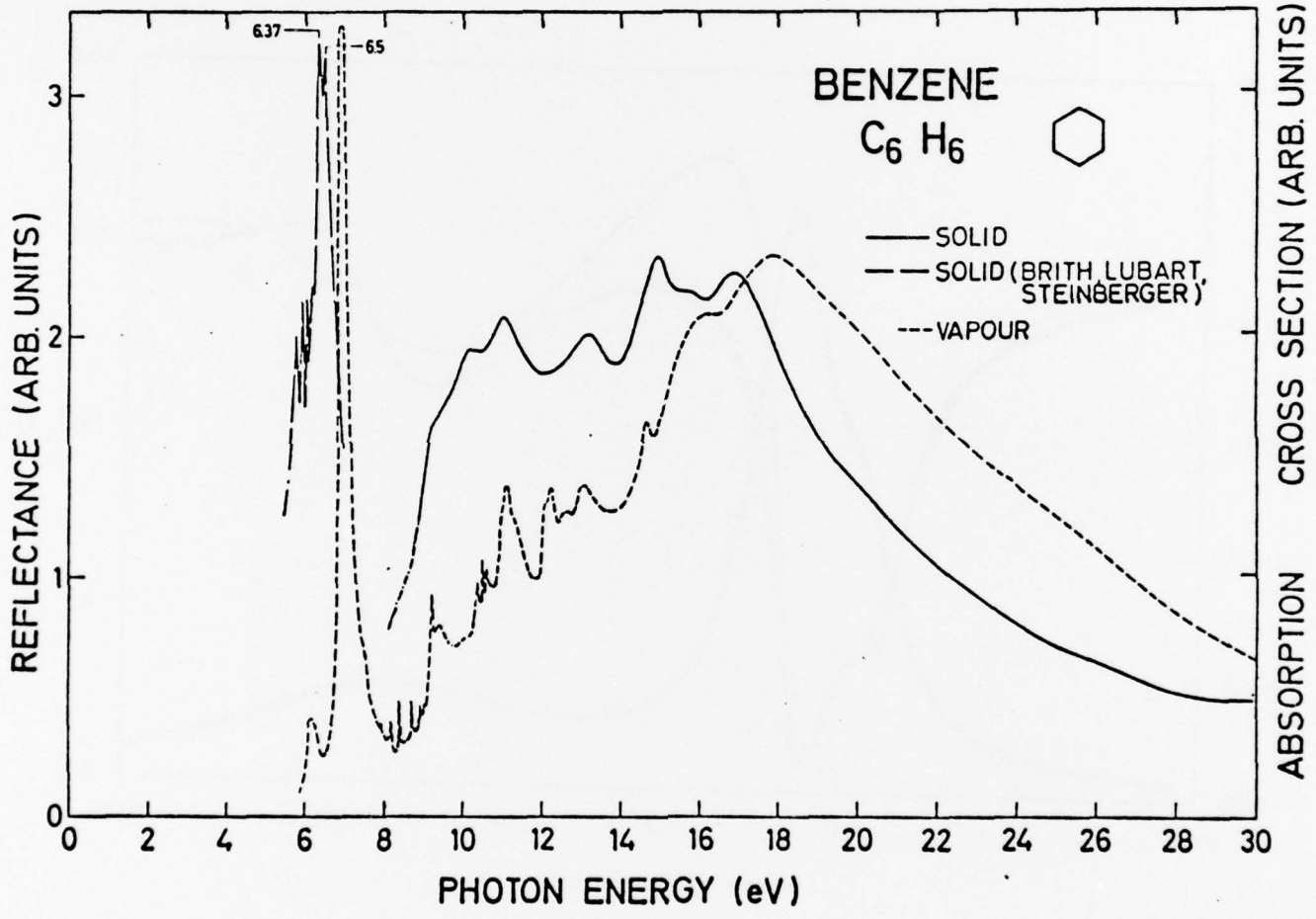

BENZENE
$C_6 H_6$
SOLID
SOLID (BRITH, LUBART, STEINBERGER)
VAPOUR
6.37
6.5
REFLECTANCE (ARB. UNITS)
ABSORPTION CROSS SECTION (ARB. UNITS)
PHOTON ENERGY (eV)
0
1
2
3
0
2
4
6
8
10
12
14
16
18
20
22
24
26
28
30

FIG. 8

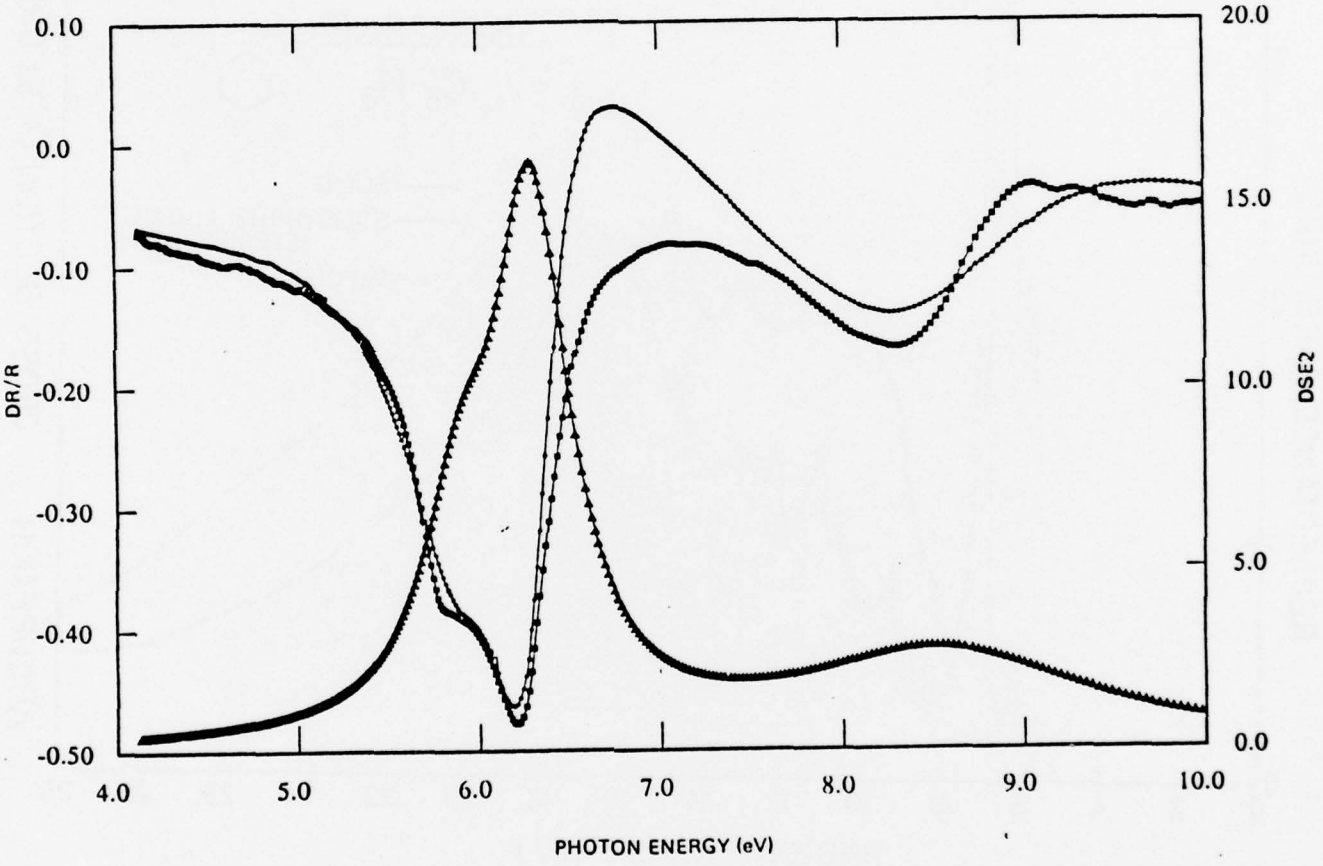

0.10
0.0
-0.10
-0.20
-0.30
-0.40
-0.50
DR/R
20.0
15.0
10.0
5.0
0.0
DSE2
4.0
5.0
6.0
7.0
8.0
9.0
10.0
PHOTON ENERGY (eV)

FIG. 9

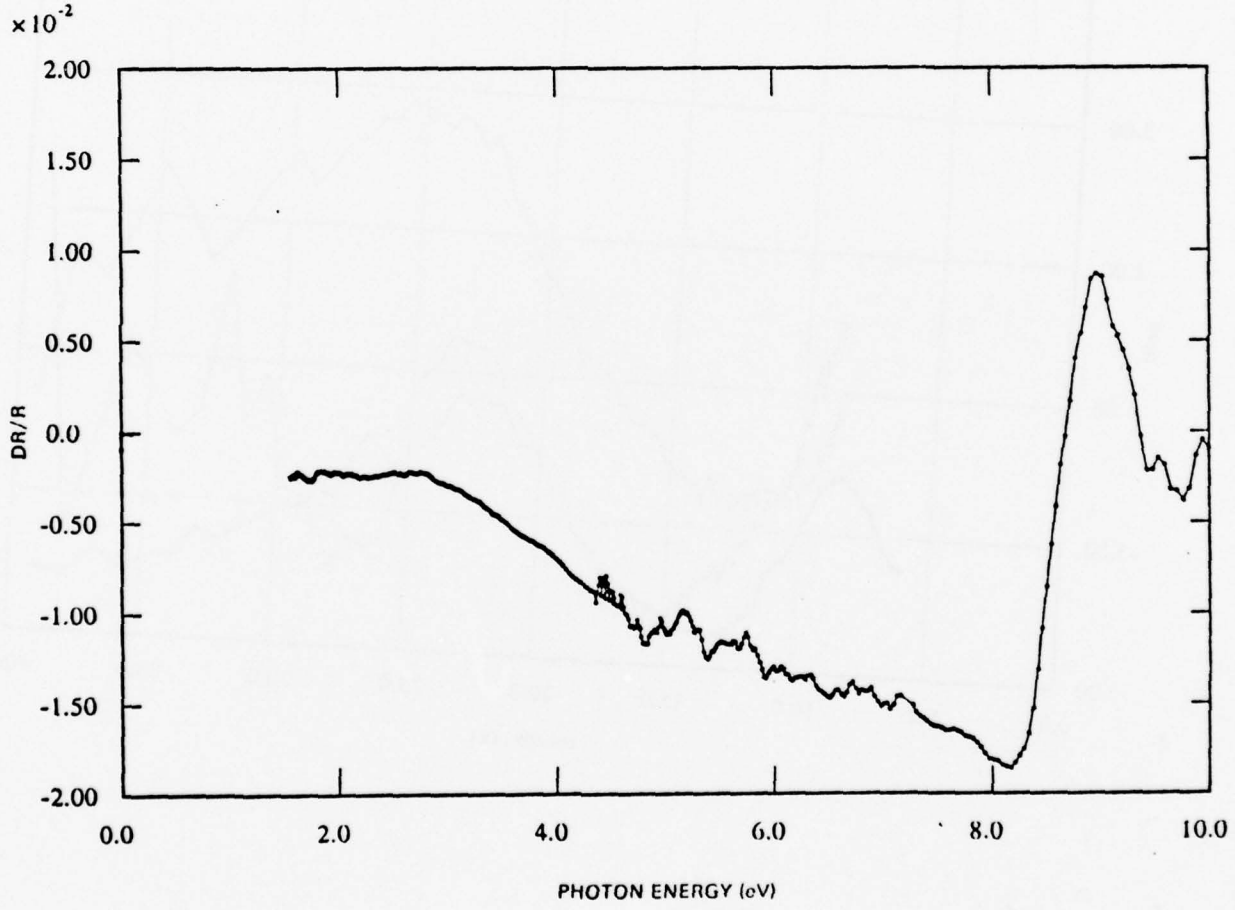

x 10^-2
2.00
1.50
1.00
0.50
0.0
-0.50
-1.00
-1.50
-2.00
DR/R
0.0
2.0
4.0
6.0
8.0
10.0
PHOTON ENERGY (eV)

FIG. 10

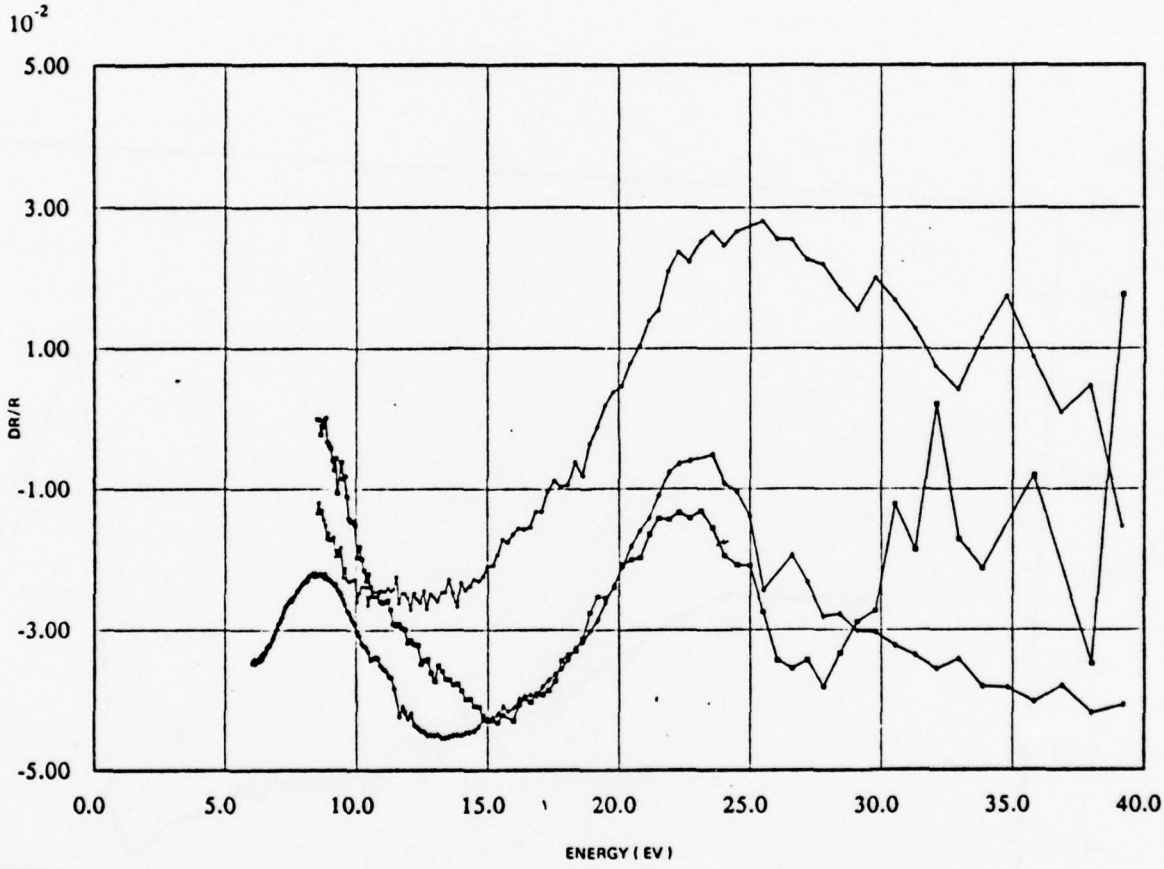

10^{-2}
5.00
3.00
1.00
-1.00
-3.00
-5.00
DR/R
0.0
5.0
10.0
15.0
20.0
25.0
30.0
35.0
40.0
ENERGY (EV)

FIG. 11

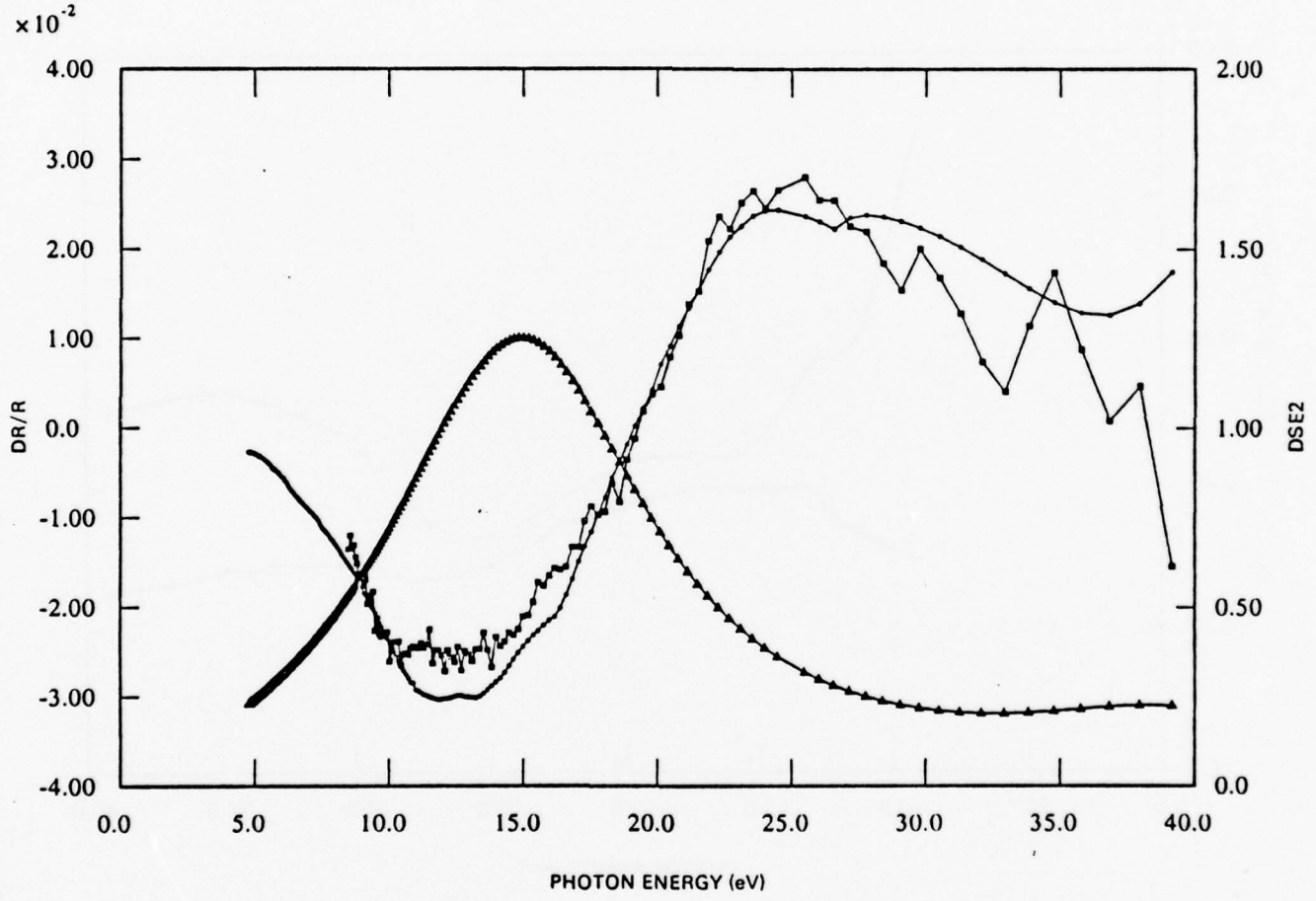

x10^-2
4.00
3.00
2.00
1.00
0.0
-1.00
-2.00
-3.00
-4.00
DR/R
2.00
1.50
1.00
0.50
0.0
DSE2
0.0
5.0
10.0
15.0
20.0
25.0
30.0
35.0
40.0
PHOTON ENERGY (eV)

FIG. 12

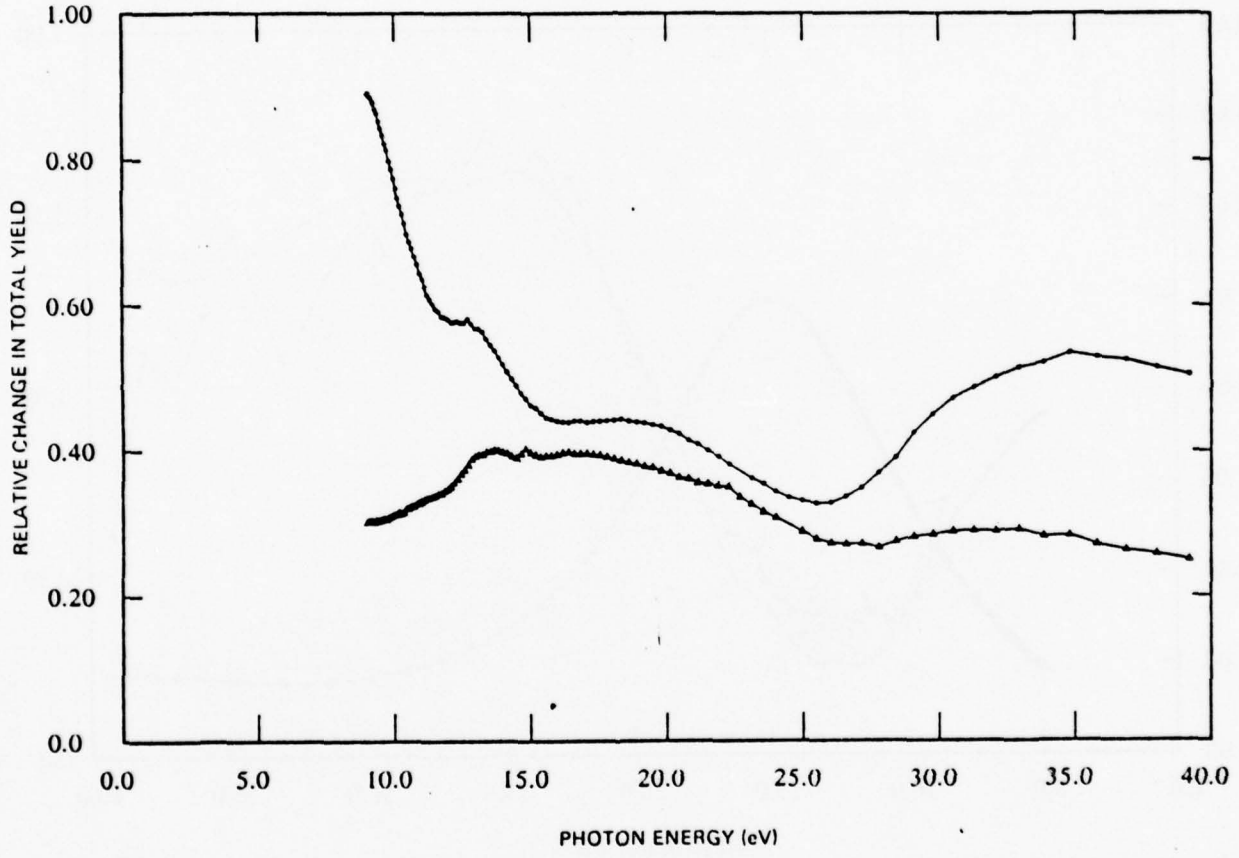

1.00
0.80
0.60
0.40
0.20
0.0
RELATIVE CHANGE IN TOTAL YIELD
0.0
5.0
10.0
15.0
20.0
25.0
30.0
35.0
40.0
PHOTON ENERGY (eV)

FIG. 13

APPENDIX

Item 5

THE INTERACTION OF ACETYLENE WITH Ni(111), CHEMISORBED OXYGEN ON Ni(111), AND NiO(111): THE FORMATION OF CH SPECIES ON CHEMICALLY MODIFIED Ni(111) SURFACES *

J.E. Demuth

IBM Thomas J. Watson Research Center

Yorktown Heights, New York 10588

ABSTRACT: Ultraviolet photoelectron spectroscopy, temperature programmed thermal desorption and low-energy electron diffraction have been used to study the interaction of acetylene with a clean Ni(111) surface, with a Ni(111) surface having co-adsorbed oxygen and with an epitaxially grown NiO(111) surface produced by room temperature oxidation of Ni(111). The adsorption of a (2x2) overlayer of π-bonded acetylene or oxygen on the Ni(111) surface markedly alters the subsequent interaction and reaction of the surface with incident acetylene. We find that in the presence of either a (2x2) overlayer of oxygen or π-bonded acetylene, a new more strongly bound acetylene-derived phase forms at room temperature. We identify this new phase from its ionization levels as a CH radical, and for saturation coverages we find approximately twice as many of these radicals as the number of π-bonded acetylene molecules in the (2x2) structure. Preadsorption of oxygen limits the adsorption of π-bonded acetylene but does not affect the formation of this CH species. Exposure of acetylene to NiO at room temperature produces only CH species. Based upon these results we propose models for the bonding geometry of π-bonded acetylene and CH

---

* Work partially supported by ONR contract NOOO14-75-C-0346.

species on the Ni(111) surface. The conditions for the formation of CH species and the significance of CH species to surface reactions on Ni are also discussed.

The manner by which hydrocarbon molecules bond to surfaces and react with the surface to form new species or reaction products is of importance in understanding catalytic processes on surfaces. Here we investigate the interaction of acetylene with various types of chemically modified Ni(111) surfaces using several techniques - ultraviolet photoemission spectroscopy (UPS), temperature programmed thermal desorption (TPTD) and low-energy electron diffraction (LEED). Of particular relevance to this study is our previous UPS study on the adsorption of small unsaturated hydrocarbons on a clean Ni(111) surface, which showed that acetylene is π-bonded to the surface[1] and that little if any rehybridization of acetylene occurs in bonding[2]. It was also found that π-bonded acetylene starts to decompose upon warming to T ~ 400K into carbon and hydrogen - the latter being released to the gas phase. In contrast to the behavior of acetylene on Ni, we have found that acetylene on Pd(111) and Pt(111) at room temperature forms a di-σ like olefinic surface complex[3]. This latter rehybridized specie has a higher activation barrier to decomposition than in the case of π-bonded acetylene on Ni(111) and starts to decompose to carbon and hydrogen at T ~ 460K. Other work with hydrocarbons on Cu[4], Fe[4-5], Ir(100)[6] and W(110)[7] and W(100)[8] has also shown interesting differences in bonding from that on Ni. Such variations in the chemical state of acetylene at room temperature or as a function of temperature on different surfaces reflect differences in chemical bonding and/or activation barriers that allow certain distortions or reactions to proceed on one surface but not on another.

Here we present new results which show that the adsorption and reaction of acetylene on a Ni(111) surface is dramatically modified by the presence of other species. Namely, we find that chemical modification of the Ni(111) surface by the presence of a (2x2) overlayer of either π-bonded acetylene or oxygen changes the reaction path from that of the clean surface so as to allow the room temperature formation of a new species not observed on the clean surface. We identify this new species from its ionization levels and conclude that it is a CH species. We also find that only CH species form at room temperature on a NiO surface.

Based upon these results we propose structural models for the locations of π-bonded acetylene on the clean surface and of the CH species on the chemically modified surfaces.

Experimental procedure: The present studies were performed in a turbomolecular pumped UHV system whose base pressure is less than $1x10^{-10}$ Torr. The system is equipped with a d.c. resonance lamp whose operation introduces an additional He partial pressure of $1x10^{-10}$ Torr and a double pass cylindrical mirror (CMA) electron energy analyser. The system also contains low energy electron diffraction (LEED) facilities, a UTI quadrupole mass spectrometer and an auxiliary electron gun for Auger electron spectroscopy. The single crystal sample was prepared by conventional techniques[9] and mounted on a multiple sample holder which permitted the sample to be liquid nitrogen cooled to T ~ 78K or resistively heated to T ~ 1600K as measured with a Chromel-Alumel thermocouple spot welded to the back of the crystal. All studies presented here were performed at room temperature or above. The sample was cleaned by mild oxidation treatments, argon ion sputter-etching and subsequent annealing[9]. Surface characterization was performed by LEED, Auger and photoemission analyses. Separate gas manifolds and leak valves were used for oxygen and acetylene. Purified Matheson acetylene (> 99.6%) was used and examined for other impurities mass spectroscopically. In particular, the acetylene extraction procedures used in loading the gas manifold provided essentially acetone free acetylene. The ratio of mass 43 to mass 26, the principal mass numbers for acetone and acetylene, respectively, was 1/750 for ionizer voltages which produce 70V electrons and 15V ions. Temperature programmed thermal desorption (TPTD) was performed with the mass spectrometer in line of sight to the sample, the latter being located ~ 3" away from the ionizer grids. The pressures and exposures cited here are based on uncorrected ion gauge readings. The actual pressure at the sample may have been slightly lower since the sample was located in another part of the system inside a magnetic shield for the CMA.

Energy analysis of the photoemitted electrons was performed with a double pass cylindrical mirror analyzer (CMA) operated in a fixed pass mode so as to have a resolution of ~ .15 eV for He I and ~ .25 eV for He II UPS work. These two photon energies provide wider energy windows than NeI or II radiation and therefore were used almost exclusively. The sample could be rotated with its normal direction in the plane defined by the axis of the CMA and the photon beam. The photon beam lies 73° off the axis and the CMA, and we arbitrarily chose the sample normal to be 20° from the axis of the CMA into the photon beam. Work functions and their changes were measured using the low-energy cutoffs of the photoemission energy distributions.

Experimental Results

Our photoemission electron energy distributions N(E) with $h\nu$ = 40.8 eV for clean Ni(111) and after $3x10^{-6}$ and $6x10^{-6}$ Torr-seconds (3 and 6 Langmuirs, L) exposures to acetylene are shown in Fig. 1a. In Fig. 1b we show the difference spectrum $\Delta N(E)$ between the clean and chemisorbed N(E) spectra for the 3L acetylene exposure. For direct comparison we also show the gas phase ionization spectrum for acetylene obtained in a gas phase spectrometer[10] of similar resolution and geometry as used in our measurements and shifted so as to align the lower lying $2\sigma_u$ and $3\sigma_g$ levels. This difference spectrum corresponds to that discussed previously as π-bonded acetylene[1]. The level we observe at ~15.8 eV below E_F has not been observed before. Although this level lies near the onset of emission from the 23.7 eV resonance line of Helium, we have observed it in several spectra taken on different occasions when the intensity of this 23.7 eV photon excited emission has varied relative to that at 40.8 eV. We correlate this level to the $2\sigma_g$ level of gaseous acetylene.

An additional 3L exposure to acetylene produces new emission which we show by the difference curves between the N(E) spectra for the 3L and 6L exposure in Fig. 2c. Here, we observe a broad level ~ 2 eV wide centered at 8 eV as well as a ~ 1 eV wide level at 15.2 eV

which we associate with a second acetylene-derived phase. We note that the combination of a peak of unestablished origin near 6 eV in clean Ni, which is also observed in X-ray photoelectron spectroscopy[11], as well as the low signal intensity at $h\nu$ = 40.8 eV for adsorbate derived levels, cast some uncertainty in precisely determining the adsorbate-induced peak position near 8 eV. We also find stronger preferential d-band attenuation near E_F for this second acetylene-derived phase than that for π-bonded acetylene.

For photon energies of $h\nu$ = 21.2 eV the adsorbate derived levels are more intense relative to the d-band and secondary background. Thus, in Fig. 2a we show the $\Delta N(E)$ spectra at $h\nu$ = 21.2 eV for a 1.5 L exposure to acetylene as well as the corresponding gaseous ionization spectra for acetylene[10] again taken under similar experimental conditions. The comparison shown in Fig. 2a is similar to our initial work at $h\nu$ = 21.2 eV in a retarding field analyser system[1]; however, we note a slightly smaller bonding shift of ~ 1.2 eV of the π-orbitals than the 1.5 eV shift observed earlier. Such differences likely arise from uncertainties in separating the π-orbital derived ionization feature from other chemisorption-induced changes in both the d-band and the forementioned Ni structure between 4-8 eV.

With an additional acetylene exposure of 1.5L we find an increase in the amount of chemisorbed acetylene as shown in Fig. 2b by the $\Delta N(E)$ spectra taken between 1.5 and 3L exposures. This difference spectra almost replicates the emission pattern shown in Fig. 1a but has slightly greater emission between ~ 6-8 eV below E_F. Further exposure to 3L of acetylene shows no additional π-bonded acetylene and instead a broad level centered about 7.3 eV below E_F similar to the level observed for $h\nu$ = 40.8 eV characteristic of the second acetylene-derived phase. Although the 7.3 eV value for the center of this peak might be considered more reliable than that determined with $h\nu$ = 40.8 eV, the possibility of two frequency dependent components in this broad peak should not be overlooked and we shall denote the position for the center of this peak as 7.3-8 eV to reflect this possibility.

Heating the sample which contains only π-bonded acetylene to 450K decomposes this species on the surface and leaves chemisorbed carbon as characterized by the $\Delta N(E)$ spectra in Fig. 2d. Clearly, the second acetylene-derived phase can be readily distinguished from chemisorbed carbon.

In examining LEED patterns, we find that for a 3L acetylene exposure a (2x2) pattern occurs which has diffuse spots. Upon higher exposures of ~ 5L these spots tend to streak and we also observe a weak 1/2 order diffraction ring. As previously noted[1] the electron beam quickly modifies these patterns thereby severly limiting LEED observations and making detailed observations difficult. Decomposition to carbon by heating to 450K gives rise to a very complex diffraction pattern whose spots sharpen up with subsequent heating to 650K.

We have examined the desorption products formed by heating the sample, i.e., temperature programmed thermal desorption (TPTD), and find that H_2 is the only significant product. We can readily distinguish hydrogen desorption from the two acetylene-derived phases which we see in UPS. For acetylene exposures below 3L one desorption feature is observed with a "peak" at ~ 413K as shown in Fig. 3a. For exposures above 3L we observe additional desorption features between 440K to 670K which have "peaks" near 500K and 620K. Warming the sample which has both acetylene-derived phases to only 450K leaves some chemisorbed carbon and the second phase which is observed in UPS to be the combination of Fig. 2d and 2c. (The work function change relative to the clean surface after a saturation exposure and such a treatment is $\Delta \phi = -0.7$ eV). Upon additional heating to 690K further hydrogen desorption occurs leaving more carbon. Clearly, the second acetylene-derived phase is more stable than π-bonded acetylene.

The occurrence of a broad desorption feature for this second phase with perhaps two components rather than one well defined desorption feature may be the result of interactions of this second phase with the carbon formed from the initial decomposition of π-bonded

acetylene. This carbon may reorganize or coalesce as the temperature is increased to produce the second hydrogen desorption structure above ~ 550K. Although the possibility exists that polymerization of some of this second acetylene-derived phase could occur with increased temperature to form a small number of new species which then decompose at higher temperatures, we do not observe any new phases with UPS after heating to 500K. For saturation exposures of ~ 12L the ratios of areas under the hydrogen desorption peaks indicate ~ 15% more hydrogen derived from the second phase than from the π-bonded phase of acetylene. Thus, knowledge of the chemical formulae for this second acetylene-derived phase will allow us to determine its coverage relative to that for π-bonded acetylene.

In coadsorption studies with oxygen on Ni(111) we observe both acetylene phases but find a striking reduction in the amount of π-bonded acetylene that can form after preadsorption of oxygen. This is evident in both our TPTD and UPS results. In Fig. 3b we show the flash desorption results for a 6L exposure of C_2H_2 to a Ni(111) surface predosed with oxygen to give $\Delta\phi$ ~ 0.3 eV. The hydrogen desorption structure characteristic of π-bonded acetylene is shifted up by 15K to 428K and has markedly less hydrogen than would occur for an equivalent exposure to the clean surface. The desorption characteristic of the second acetylene-derived phase now occurs over a wide temperature range with a single maximum at ~ 520K and contains approximately the same amount of hydrogen as on the clean surface. The principal desorption product upon decomposition is mass 28, CO, which shows not only a maximum desorption at 600K but enhanced CO desorption at lower temperatures which coincides with the formation of carbon on the surface from the decomposition of the two acetylene-derived phases.

The dependence of the coverages of these two acetylene phases upon preadsorption of oxygen has been obtained using UPS and is shown in Fig. 4. Here we show the trend in the intensity of the ionization feature derived from the $3\sigma_g$ orbital of π-bonded acetylene

(indicated by the triangles) as a function of the work function change $\Delta\phi$ of chemisorbed oxygen. We have not calibrated the oxygen coverages but we know that the (2x2) oxygen overlayer with the sharpest diffraction spots and the largest work function change ($\Delta\phi$ = 0.8 eV) corresponds to a 1/4 monolayer coverage. Although chemisorbed oxygen reduces the amount of the π-bonded phase of acetylene that forms, we find that the amount of the second acetylene-derived phase (indicated by the circles in Fig. 4) which forms is independent of oxygen coverage. For the (2x2) oxygen overlayer little π-bonded acetylene forms. (The work function change observed upon the formation of the second acetylene-derived phase on the (2x2) oxygen structure is $\Delta\phi$ = -.6 eV).

The interaction of acetylene with the oxidized Ni(111) surface produces a result similar to that which we observe on the Ni(111) surface having a (2x2) oxygen overlayer. Namely, the room temperature exposure of acetylene to the Ni(111) surface oxidized either at room temperature or at ~ 400K produces a chemisorbed phase that appears to be similar to the second acetylene-derived phase. We note that from previous oxidation studies on Ni(111)[12-13] it has been established that the room temperature oxidation of Ni(111) allows the epitaxial growth of NiO islands having the (111) surface exposed and the same orientation as the substrate. In Fig. 5a we show the photoemission spectra N(E) with $h\nu$ = 40.8 eV for the oxide (solid line) and after a 3L exposure to acetylene (dashed line). Correcting for 0.3 eV band bending, we observe new ionization levels at 10.1 and 16.2 eV below E_F of the clean oxide as shown in the ΔN(E) spectra in Fig. 5b and c. These levels are of similar width and relative intensity to those observed for the second acetylene-derived phase on Ni(111) but shifted 2.1 and 1.0 eV, respectively, from the former toward larger binding energies. A shift in the levels of this phase to larger binding energies on the oxide relative to the metal is expected on the basis of differences in the screening and relaxation effects observed for other absorbed species on oxides[14]. For example, we observe that the σ-levels of acetylene adsorbed on oxidized Ni at T ~ 100K are shifted 1.7 eV below those found on clean Ni.

From these similarities we believe that the acetylene-derived species formed on the oxide is chemically similar to the second acetylene-derived phase which occurs on the chemically modified Ni(111) surfaces. We note that in the valence band region of the oxide, the peak at ~ 1.5 eV below E_F, which is attributed to emission from $Ni^{+2}(d^8)$ like states of the oxide[15], is most strongly attenuated upon adsorption while smaller changes occur in the oxide p-band region 4-8 eV below E_F. Finally, although one would like to relate relative photoemission level intensities of this phase on the oxide to that on the metal surface to establish relative coverages, we cannot do so since the optical response of oxide and metal surfaces are markedly different and will likely modify optical matrix elements for photoionization.

The Chemical Nature of the Second Acetylene-Derived Phase

It is clear that in addition to the formation of π-bonded acetylene on Ni(111), a second acetylene-derived phase forms on Ni(111) after the completion of a (2x2) acetylene overlayer. This same phase appears to form directly on either a (2x2) oxygen overlayer on Ni(111) or on a NiO(111) surface. In each case this second acetylene-derived phase decreases the work function of the surface indicative of a polarization of the adsorbate electrons toward the surface, i.e., charge transfer to the surface atoms. Based upon our photoemission observations and a consideration of the energy levels of chemisorbed hydrocarbons and those expected for a variety of possible radicals derived from acetylene, we can conclude that the second acetylene-derived phase is a CH species.

This identification is as follows and largely depends on our ability to observe the lower lying ionization levels derived from atomic C 2s orbitals with $h\nu = 40.8$ eV. Here the ~ 7.5 eV separation between the two principle levels observed for this new phase on Ni(111), as well as the fact that the lowest level lies well below the σ_{CC} - σ_{CH} valence orbitals of chemisorbed C_2 hydrocarbons on Ni, precludes any assignment of these levels in terms of species having two or more carbon atoms. This arises since the bonding-antibonding combination of

C 2s atomic orbitals have splitting of ~ 3-5 eV in C_2 hydrocarbons[16-17]. For open chain alkanes the corresponding splitting would be larger but would also contain non-bonding or other bonding-antibonding combinations of pairs of C 2s atomic orbitals.[17] Further, the lowest lying ionization feature at 15.2 eV on Ni(111) (or at 16.2 eV on NiO) is too low relative to the next higher lying ionization feature to correlate to an ionization from an antibonding combination of C 2s orbitals even considering possible differences in screening/relaxation shifts for a chemisorbed specie. Thus, such considerations suggest that this molecular species likely has only one carbon atom and that the weak level at 15.2 eV on the metal (16.2 eV on the oxide) is derived from a single C 2s atomic orbital.

In considering the nature of this second phase on Ni(111), we find it significant that the locations of the 15.2 and 7.3-8 eV levels for this second acetylene derived phase are similar to the relative levels observed for gaseous methane. The gas phase ionization levels for methane and acetylene are shown in Fig. 6a while in Fig. 6b we show the corresponding ground state molecular orbital energies calculated with an ab-initio SCF LCAO method [18] using a 4-31G basis set. The similarities in the trend in relative locations of ionization levels and eigenvalues shown in Fig. 6 is typical of the trends we have observed for a large variety of small molecules. We also indicate in Fig. 6a by the dashed lines the location of the ionization levels of gaseous acetylene and, thus, to the second acetylene-derived species relative to chemisorbed acetylene since the σ-levels of chemisorbed acetylene are nearly uniformly shifted upon chemisorption. In Fig. 6b we similarly compare the energy levels of CH species on Ni(111) calculated by Anderson[21] which we shall discuss in more detail later. We note a close similarity between the relative I.P.'s of methane and our new phase; however, the similarity in the width of the 7.3-8 eV level of the observed width or shape of the highest lying ionization level in methane may be largely fortuitous as the latter is believed to be a result of Jahn-Teller distortions in the ion.[19-20]

We have used molecular orbital calculations to examine the energy levels of likely free radicals and, in particular, how methane's energy levels are modified upon ligand substitutions - i.e., to stimulate a surface compound. For X_3CH or X_2CH_2 species where X = H, Li or Be, we find that the triply degenerate $3\sigma_g$ orbital of methane splits into three non-degenerate levels for X_2CH_2 or two non-degenerate levels for X_3CH species. The magnitude of this splitting appears to be related to the ligand's electronegativity and the location of energy levels of the ligand relative to those of hydrogen and carbon. For either X_3CH or X_2CH_2 species the location of the C 2s orbital relative to the lower of the orbitals derived from the $3\sigma_g$ orbital of methane remains similar to that in methane. Thus, the energy levels of a CH_2 or CH radical coordinated to two or three Ni atoms, respectively, are consistent with our experimental results. Our UPS results show no free carbon when the second acetylene-derived phase forms and suggests that only CH species exist.

As previously mentioned, Anderson has calculated the eigenvalues and total energies for CH fragments bonded to a cluster of Ni atoms representing a (111) surface with an extended Hückel approach[21]. He finds the three-fold hollow bonding sites to be preferred for these species. In comparing Anderson's calculated eigenvalues for this species on Ni to our experimentally observed levels, we examine the locations of Anderson's calculated molecular orbitals for CH radicals on Ni relative to those calculated for chemisorbed acetylene on Ni. Such relative level positions are of more significance than absolute level positions due to, for example, uncertainties and approximations within the calculation as well as the neglect of relaxation effects, etc. In Anderson's calculations the C 2s orbital of the CH species lies ~ 2 eV above the $2\sigma_u$ orbital of chemisorbed acetylene while two higher lying states are ~ 1.5 and ~ 3.5 eV above the $3\sigma_g$ orbital of chemisorbed acetylene - the latter tending to form a band when several CH radicals occur on the surface[21]. For convenience, we have shown these predicted levels in Fig. 6b relative to our own molecular orbital calculations for acetylene and methane. In view of the uncertainties in these calculations and comparisons (such as, for

example, the neglect of possible differences in screening and relaxation effects), the similarity of the relative ionization levels of acetylene and the new phase with the eigenvalues for acetylene and a CH surface species are notable and confirm our previous expectations.

Another acetylene species has been suggested from infrared work on Ni oxide [22] which we have also examined more carefully in our molecular orbital calculations and briefly mention here. These are CCH alkyne species which can be related to complexes of the type: X-C ≡ C-H and X_3-C ≡ C-H where X=H, Li or Be. For these complexes our calculations show that the bonding-antibonding splitting of the C 2s derived molecular orbitals is similar to that found for acetylene. Also, the separation between the antibonding C 2s molecular orbitals and the next highest lying σ-orbital, although larger than in the case of acetylene, is not larger enough to account for that observed in our second acetylene-derived phase. We also find little correspondence between the relative eigenvalues of other radicals species such as CC or CCH_2 and the ionization levels observed for the second acetylene-derived phase. Thus, we conclude that the observed ionization levels for the second acetylene-derived phase on Ni(111) can be only well accounted for by the presence of a CH surface species.

The Surface Geometry of Acetylene and CH Radicals on Ni(111)

On the basis of the LEED patterns for acetylene adsorption on Ni(111), our TPTD results, the sequential formation of acetylene phases on both Ni(111) and the (2x2) oxygen overlayer on Ni(111), as well as the known bonding site for chemisorbed oxygen on Ni(111), we propose an idealized structural model for the arrangement and bonding of acetylene and CH radicals to Ni. Since chemisorbed oxygen occupies the three-fold hollow site on Ni(111)[23] and blocks the formation of π-bonded acetylene, the bonding of acetylene likely involves the three-fold hollow site. Such a site is consistent with a recent LEED intensity

analysis for the (2x2) acetylene structure on Pt(111)[24] which favors two bonding orientations - both involving the three-fold hollow sites. The first location which is of higher symmetry places acetylene straddled across both threefold hollow sites. In the second location the molecule resides over a single three-fold hollow site and is rotated 90° in the plane of the surface from the first orientation. A recent extended-Hückel calculation by Anderson[25] for one acetylene molecule on 4,5 and 13 Ni atom clusters suggests the second location preferred over yet another location, the di-σ (bridging) location, but the first bonding location was not considered.

On the basis of simple steric considerations for a (2x2) acetylene overlayer on Ni we can discriminate between the various proposed bonding geometries of acetylene on Ni(111). First, the Van der Waals radii for gaseous acetylene constructed in an analogous fashion as by Gland[26] for other hydrocarbons, indicates that due to the anistropy of the unit cell of the Ni(111) surface only the first bonding orientation is allowed as the second and the di-σ orientation would produce an 0.8 Å overlap in the Van der Waals radii at the hydrogen ends of the molecule. Since little rehybridization occurs in acetylene bonding to Ni[2], we doubt that the second orientation or di-σ orientation could occur. Also, although the π-levels for chemisorbed unsaturated hydrocarbons are broad[1], we see no evidence of a splitting in the π^2 orbitals of acetylene likely to be more characteristic of a lower symmetry bonding location. Thus, such arguments favor the first, high symmetry location of acetylene straddling the two three fold hollow sites as shown in Fig. 7 by the horizontal lines. We note that the steric arguments used for selecting the geometry of acetylene on Ni(111) cannot be used a priori to preclude any of the three proposed bond sites for acetylene on Pd(111) or Pt(111) since at room temperature acetylene is strongly rehybridized on these surfaces.[3]

In considering the formation of CH fragments on Ni(111) from acetylene, we must consider the possible role of surface defects since it has been shown by Blakely and

Somorjai[27] that C-C bond scission in cyclic organic molecules occurs on kink sites of stepped Pt surfaces. (We have found that acetylene chemisorbed on Ni(110) at T ~ 80K undergoes C-C bond breaking to form CH species upon warming to T > 200K[28]. Such a behavior is not unexpected as the atoms along the <100> rows of the (110) surface are geometrically similar to the atoms at step edges and kinks that exist on the vicinal (755) or (976) surfaces.) However, LEED patterns of clean Ni(111) show no indication of periodic step or strong diffuse elastic background which would be characteristic of a large numbers of surface defects. Further, since significant amounts (~ 1/2 monolayer) of CH species form after the π-bonded phase at room temperature and low exposures, we do not believe that the majority of C-C bond breaking found here occurs at surface defects. We thus consider a different mechanism for C-C bond breaking.

We believe that the presence of adsorbed species on the surface is responsible for C-C bond breaking: these adsorbed species have likely changed an activation barrier to C-C bond scission so as to allow formation of CH species from additional acetylene. The interaction of additional acetylene with π-bonded acetylene alone would not likely provide the energy required for C-C bond scission. We thus postulate that after acetylene initially forms a (2x2) overlayer, additional impinging acetylene molecules fragment upon access to regions of the chemically modified substrate adjacent to π-bonded acetylene but not covered by π-bonded acetylene. The center of each (2x2) cell of π-bonded acetylene marked by xX in Fig. 7 provides such an accessible region of exposed Ni atoms for an impinging acetylene molecule which would also appear to be favorable for interacting with Ni substrate atoms since it is similar to the bonding site for π-bonded acetylene. Here the incident molecule might fragment into CH species which then bond to three Ni atoms in each of the three-fold hollow sites (x,X) - the same bonding site as suggested by Anderson[21]. This gives rise to twice as many CH species per (2x2) cell as π-bonded acetylenes - consistent with our hydrogen TPTD measurements. Additional CH fragments likely form not only at crystalline defects but also at the

terminal edges and imperfections of the (2x2) π-bonded acetylene structure. Other locations at the sides of the (2x2) π-bonded acetylene cell (indicated by •) would be sterically inaccessible to impinging acetylene but may become available if π-bonded acetylene molecules can disorder during their interaction with impinging molecules. In fact, the disorder in the LEED pattern upon formation of CH species supports this latter possibility.

The determination of the bonding sites for CH species on the (2x2) oxygen covered surface is less certain due to a lack of insight as to the interaction of oxygen with acetylene. Also, we might expect differences in the mechanism of C-C bonds breaking associated with the chemical differences of chemisorbed oxygen versus π-bonded acetylene. Due to a lack of other knowledge, we use the same assumptions as used previously for the case of (2x2) acetylene on Ni(111) and find these consistent with our results. Again, impinging acetylene molecules could most easily access three regions of the (2x2) oxygen on Ni(111) cell, one being the same as previously (x,X) and the other two being near the sides of this (2x2) cell. These latter sites correspond to positions marked by (X,•) in Fig. 7. Access of acetylene to any one of these sites and decomposition to CH fragments, which then bond to the three neighboring Ni atoms as before, may preclude access to the other two sites. In this manner the same amount of CH species would form on the (2x2) oxygen covered surface as on the (2x2) π-bonded acetylene covered surface. Irregularities in the (2x2) oxygen structure likely permit π-bonding of some impinging acetylene.

The bonding geometry of CH species to the NiO surface is unclear due to several questions regarding the surface geometry and perfection of our epitaxially grown NiO(111) surface. Nickel oxide consists of two interpenetrating F.C.C. lattices to give the rocksalt structure with each lattice expanded by 18.4% from Ni[29]. Along the <111> direction NiO consists of alternating hexagonal layers of Ni or O - the surface terminating in either O or Ni. It is not known whether our NiO(111) surface consists of islands of terminal O or Ni layers, a

single terminal oxygen layer, a lower density layer of chemisorbed oxygen, or a single layer of Ni metal atoms. For all these surface oxide terminations but that having a complete oxygen layer, Ni atoms would be present in an arragement similar to the (111) surface to allow a similar bonding geometry of CH radicals as on the oxygen or acetylene covered Ni(111) surfaces. It is further possible that the epitaxial oxide formed may contain numerous defects which may also influence the fragmentation of acetylene.

Adsorbate-Induced Alterations in Surface Reaction Paths

A notable feature of our results is the ability of the chemically modified Ni(111) surface to permit C-C bond breaking which did not occur on the clean Ni(111) surface. This may arise for the same reasons as proposed for C-C bond breaking on stepped surfaces,[27] and we briefly mention these here. Recent calculations of the electronic structure of stepped surfaces indicate a local potential at the step that is sizeably different from that on the flat surface. This potential can cause strong field gradients and may affect d-wavefunctions, at those steps[30,31]. Although theoretical calculations[32-34] show promise to understand changes in d-wavefunctions at steps no rigorous self-consistent calculations have been done for real surfaces and, more importantly, how such wavefunction changes might affect C-C bond breaking. It has also been suggested that the strong field gradients at steps could help polarize valence bonds within the molecule to help break C-C or C-H bonds.[35]

In considering the chemically modified surface it becomes clear from the observed magnitudes of the work function changes that preadsorbed oxygen or π-bonded acetylene produce strong field gradients and variations in the local potential on the surface. Further, due to the interaction of these adsorbates with the surface atoms, modifications are also likely to occur in d-wavefunctions of adjacent Ni surface atoms. Thus, similar conditions may occur on the chemically modified surface as on the stepped surface. Unfortunately, we cannot discriminate which of these two physical factors is primarily responsible for C-C bond breaking on

these chemically modified surfaces. Again, for acetylene on NiO, C-C bond scission may occur also as a result of either local field gradients or the Ni^{+2} (d^8) d-wavefunctions of the oxide.

Summary and Implications:

Acetylene exposure to a clean Ni(111) surface produces a second acetylene-derived phase after an initial (2x2) overlayer of π-bonded acetylene forms. The ionization levels found for this new phase are consistant with the orbital energies for CH species on Ni. From calibration of the amount of hydrogen desorbed from the CH species relative to that for (2x2) π-bonded acetylene, we determine that approximately twice the number of CH species exist relative to the π-bonded acetylene species both at saturation coverages. The amount of π-bonded acetylene formed is also inversely proportional to the amount of preadsorbed oxygen on Ni(111) where the (2x2) oxygen overlayer nearly completely inhibits chemisorption of π-bonded acetylene. On the other hand, the presence of preadsorbed oxygen does not affect the number of CH species which can form. Based on these facts we postulate an idealized geometric model for the arrangement of π-bonded acetylene and CH fragments on these surfaces. We also find that exposure of a NiO(111) surface to acetylene at room temperature forms only CH species. Such a specie has not been observed in previous IR studies on NiO[27] - possibly due to differences in adsorption and surface conditions.

The result that we observe and can identify surface stabilized CH radicals may be of significance for understanding catalytic reactions on Ni and their oxides. In particular, this radical may be important in several catalytic processes; for example, for chain growth in polymers or in Fischer-Tropsch synthesis, as an intermediate in hydrogenolysis and methanation reactions, or in the oxidation of hydrocarbons. For the latter case it is believed that surface hydrocarbon radicals can interact with adsorbed oxygen to form an intermediate surface complex which decomposes to the oxidation products[36].

These results are also interesting in that a different reaction path occurs for acetylene incident on the Ni(111) surface covered with a (2x2) overlayer of oxygen or π-bonded acetylene than on the clean surface. That is, fragmentation of acetylene to CH does not occur on the clean (111) surface at room temperature or after heating but does occur on the chemically modified surface. This ability of the chemically modified surface to break the triple C-C bond of acetylene at room temperature prior to the C-H bond is surprising since double or triple C-C bond energies are larger than C-H bond energies.[37] Thus, as shown here the initially chemisorbed species can modify reaction barriers and decomposition paths to allow access to a surface reaction which requires more energy than other possible reactions and does not occur readily on the clean surface. It has been recognized that adsorbates can passivate the surface but to our knowledge such an adsorbate-induced enhancement of a reaction which requires more energy has not been identified. Finally, it is interesting to consider the possibility that some of the so called "active sites" for surface reactions on metals may arise because of the presence, arrangement and/or the nature of the adsorbed species on regions of the surface which allow the formation of new species as observed here.

ACKNOWLEDGEMENT

The author is grateful to D. E. Eastman and G. W. Rubloff for simulating discussions and for their careful reading of the manuscript prior to publication.

REFERENCES

1. J.E. Demuth and D.E. Eastman, Phys. Rev. Letters 32, 1123 (1974); D.E. Eastman and J.E. Demuth, Jap. Journal of Applied Phys., Suppl. 2, 827 (1974).
2. J.E. Demuth and D.E. Eastman, Phys. Rev. B 13, 1523 (1976).
3. J.E. Demuth, Chem. Phys. Letters 45, 12 (1977).
4. K.Y. Yu, W.E. Spicer, I. Lindau, P. Pianetta and S.F. Lin, Surface Sci. 57 157 (1976).
5. C. Brucker and T.N. Rhodin, Jour. of Catalysis, to be published.
6. G. Broden and T.N. Rhodin, Chem. Phys. Letters 40, 247 (1976).
7. E.W. Plummer, B.J. Waclawski and T.V. Vorburger, Chem. Phys. Letters, 28 510 (1974).
8. T.V. Vorburger, B.J. Waclawski, E.W. Plummer, Chem. Phys. Letters, to be published.
9. J.E. Demuth and T.N. Rhodin, Surface Science 42, 261 (1974).
10. W.D. Grobman, Private Communication.
11. S. Hufner, G.K. Wertheim and J.H. Wernick, Phys. Rev. B8, 4511 (1974).
12. R.L. Park and H.E. Farnsworth, Applied Phys. Letters 3 167 (1963).
13. J. Holloway and J.B. Hudson, Surface Science 42, xxx (1974).
14. G.W. Rubloff, H. Lüth, and W.D. Grobman, Chem Phys. Letters 39 493 (1976).
15. D.E. Eastman and J.K. Cashion Phys. Rev. Lett., 27, 1520 (1971).
16. J.N. Murrell and W. Schmidt, J. Chem. Soc. Faraday Trans. II 68 1709 (1972).
17. D.G. Streets and A.W. Potts J. Chem. Soc. Faraday Trans. II 70, 1505 (1975).
18. R. Ditchfield, W.J. Hehre and J.A. Pople, J. Chem. Phys. 54, 724 (1971).
19. D.W. Turner, Molecular Photoelectron Spectroscopy (J. Wiley, Interscience, 1970) p. 164.
20. A.W. Potts and W.C. Price, Proc. Roy. Sco. A 326, 165 (1972).
21. A.B. Anderson, J. Chem. Phys. 65, 1729 (1976).

22. L.H. Little, Infrared Spectra of Adsorbed Species (Academic Press, New York, 1966) p. 142.

23. P.M. Marcus, J.E. Demuth and D.W. Jepsen, Surface Sci., 53, 501 (1975).

24. L.L. Kesmodel, P.C. Stair, R.C. Bastzold and G.A. Somorjai, Phys. Rev. Letters, 36, 1316 (1976).

25. A.B. Anderson, to be published.

26. J.L. Gland, Ph.D. thesis, University of California at Berkley, September 1973. (LBL report number 1816).

27. D.W. Blakely and G.A. Somorjai, J. of Catalysis 42 181 (1976).

28. J.E. Demuth, to be published.

29. E.I. Alessandrini and J.F. Freedman, Acta. Cryst. 16, 54 (1973).

30. L.L. Kesmodel and L.M. Falicov, Solid State Comm., 16, 1201 (1975).

31. Y.W. Tsang and L.M. Falicov, Phys. Dev., B 12, 2441 (1975).

32. R.O. Jones, P.J. Jennings and G.S. Painter, Surface Sci., 53 409 (1975).

33. M.C. Desjonquères and F. Cyrot-Lackman, Surface Sci., 53, 429 (1975).

34. R.P. Messmer, S.K. Knudson, K.H. Johnson, J.B. Diamond and C.Y. Yang, Phys. Rev. B 13 1396 (1976).

35. G. A. Somorjai, J. of Colloid and Interface Sci. 58 XXX (1977).

36. J.M. Thomas and W.J. Thomas, Introduction to the Principles of Heterogeneous Catalysis, (Academic Press, New York, 1967) p. 383.

37. L. Pauling, The Nature of The Chemical Bond, (Cornell Univ. Press, Ithaca, New York, 1948) p. 131.

FIGURE CAPTIONS:

Figure 1. Photoemission energy distribution N(E) for $h\nu$ = 40.8 eV of the Ni(111) surface (solid line), and after a 3 x 10^{-6} Torr sec (3L) exposure to acetylene (dotted line) or a 6 x 10^{-6} Torr sec (6L) exposure to acetylene (dashed line) all at room temperature. The difference in emission $\Delta N(E)$ from the clean surface for the 3L exposure is shown in (b) while Δ N(E) between 3L and 6L exposures is shown in (c). Included in panel (b) is the gas phase spectra of acetylene taken in a gas phase spectrometer with similar resolution and geometry (Ref. 10) where the molecular orbitals are indicated. The short dashed lines shown in (b) is the expected attenuation if a 10% attenuation of the Ni d-band occurred while the longer dashed lines indicate the estimated change in the secondary electron background.

Figure 2. Photoemission difference spectra $\Delta N(E)$ for $h\nu$ = 21.2 eV between (a) 1.5 x 10^{-6} Torr sec (1.5L) acetylene exposure and clean Ni, (b) 1.5L and 3L exposures to acetylene (c) 3L and 6L exposures to acetylene all with the sample at room temperature. The $\Delta N(E)$ spectra after a 2L acetylene exposure and heating to 440K is shown. All work function changes indicated are relative to the clean surface. Indicated in panel (a) is the estimated change in secondary electron background (long dashed lines), the expected d-band attenuation if a uniform 10% attenuation occurred (short dashed lines) and a gas phase ionization spectra for acetylene taken in a gas phase spectrometer of similar geometry and resolution (Ref. 10).

Figure 3. Temperature programmed thermal desorption spectra of (a) H_2 from exposure of clean Ni(111) to 2x10^{-6} Torr-sec (2L) of H_2 and 1.5L to 12L of C_2H_2 and

(b) H_2 and mass 28 evolved after a 6L acetylene exposure to a Ni(111) surface pre-exposed to oxygen to give $\Delta\phi = +.3$ eV. The heating rate was 10K/sec.

Figure 4. Relative concentrations of π-bonded acetylene (triangles) and the second acetylene-derived phase (circles) after saturation exposures to acetylene as a function of the amount of preadsorbed oxygen. Oxygen coverages are indicated by its work function change $\Delta\phi$ where $\Delta\phi = 0.8$ eV corresponds to a saturation coverage of chemisorbed oxygen in a (2x2) structure. Relative concentrations of π-bonded acetylene and the second acetylene-derived phase were obtained from the intensity of the $3\sigma_g$ derived ionization level and the intensity of the peak at ~ 7.3 eV, respectively. Both concentrations are normalized to the same value for $\Delta\phi = 0$. We note that preadsorbed oxygen shifts the ionization levels of acetylene 0.2 eV closer to E_F consistent with the increased work function after oxygen adsorption.

Figure 5. Photoemission distribution curve N(E) at $h\nu = 40.8$ eV for a $3x10^{-6}$ Torr-sec (3L) exposure of acetylene to a thermally oxidized Ni(111) sample with $\phi = 5.0$ eV. $\Delta N(E)$ is shown in (b) for $h\nu = 40.8$ and (c) for $h\nu = 21.2$ eV where a 0.3 eV band bending of the oxide is accounted for and all energies are referred to the E_F of the underlying clean Ni(111) surface. Also, note that the metallic emission onset at 23.7 eV was accounted for in obtaining $\Delta N(E)$ for the peak at ~ 16.2 eV as shown in (c).

Figure 6. Experimental vertical ionization potentials (I.P.) for gaseous acetylene (Ref. 10) and methane (Refs. 19-20) and the ionization levels of the new, second acetylene-derived phase (dashed lines) relative to gaseous or chemisorbed acetylene (panel a). For comparison panel b shows the ground state molecular orbital eigenvalues for gaseous acetylene and methane

which we have calculated with an ab-initio SCF LCAO molecular orbital calculation (Ref. 18) using a 4-31G basis set. Also shown relative to our eigenvalues of gaseous acetylene are the relative eigenvalues of a CH specie on Ni (dashed lines) as found in calculations by Anderson (Ref. 21).

Figure 7. Idealized model for the arrangement and geometric location of π-bonded acetylene (———), oxygen (O) and CH species (x, X or •) on the Ni(111) surface as discussed in the text. Both the unit cell of the clean surface and the (2x2) cell for π-bonded acetylene or oxygen on Ni(111) are indicated. The location of oxygen on the Ni(111) surface has been established previously from LEED intensity analysis (Ref. 23).

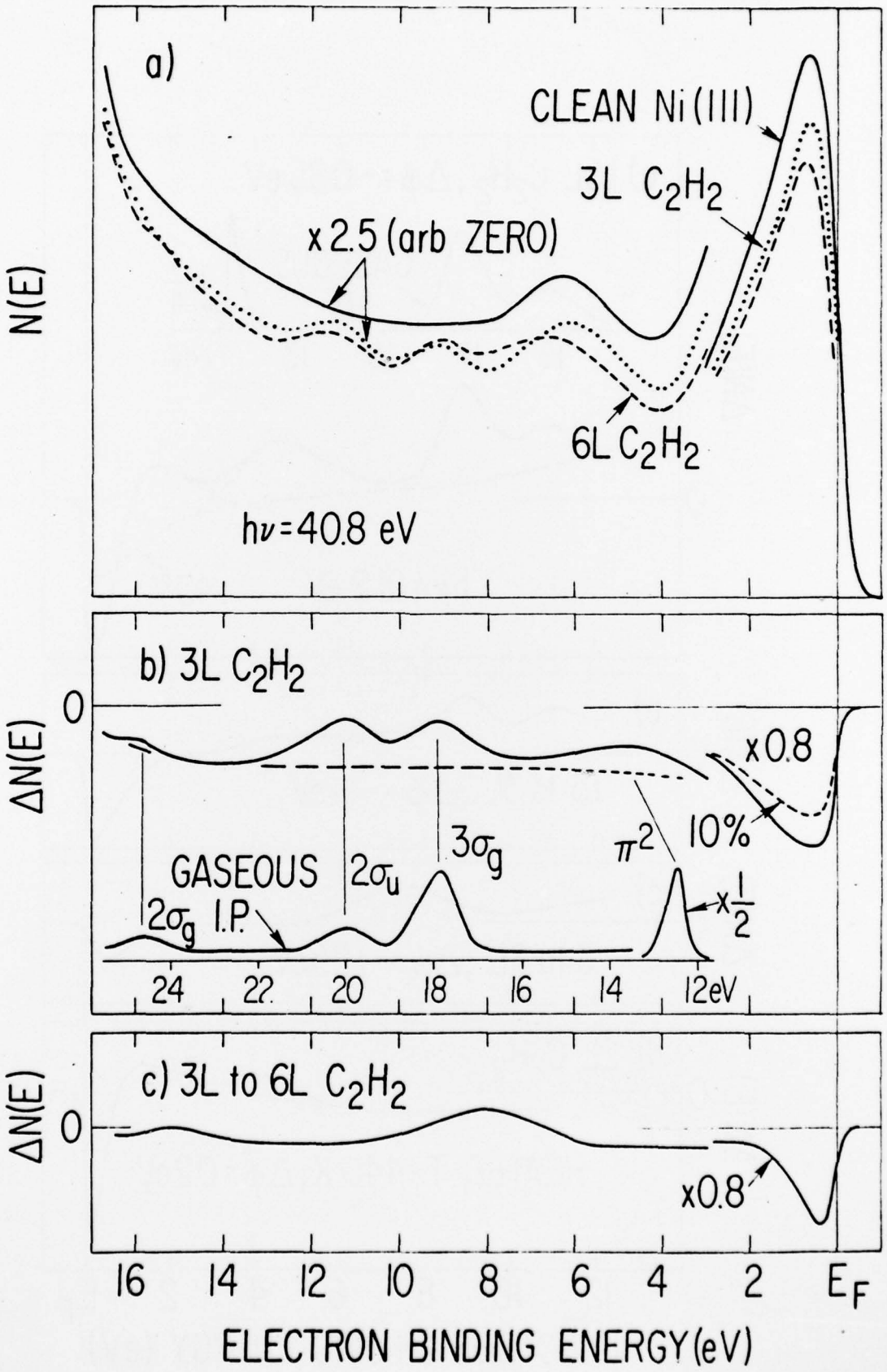

a)
CLEAN Ni(111)
3L C_2H_2
x 2.5 (arb ZERO)
6L C_2H_2
$h\nu$=40.8 eV
N(E)
b) 3L C_2H_2
0
ΔN(E)
x0.8
π^2
10%
GASEOUS
$2\sigma_g$ I.P.
$2\sigma_u$
$3\sigma_g$
x$\frac{1}{2}$
24
22
20
18
16
14
12eV
c) 3L to 6L C_2H_2
0
ΔN(E)
x0.8
16
14
12
10
8
6
4
2
E_F
ELECTRON BINDING ENERGY(eV)

FIG 1
DEMUTH

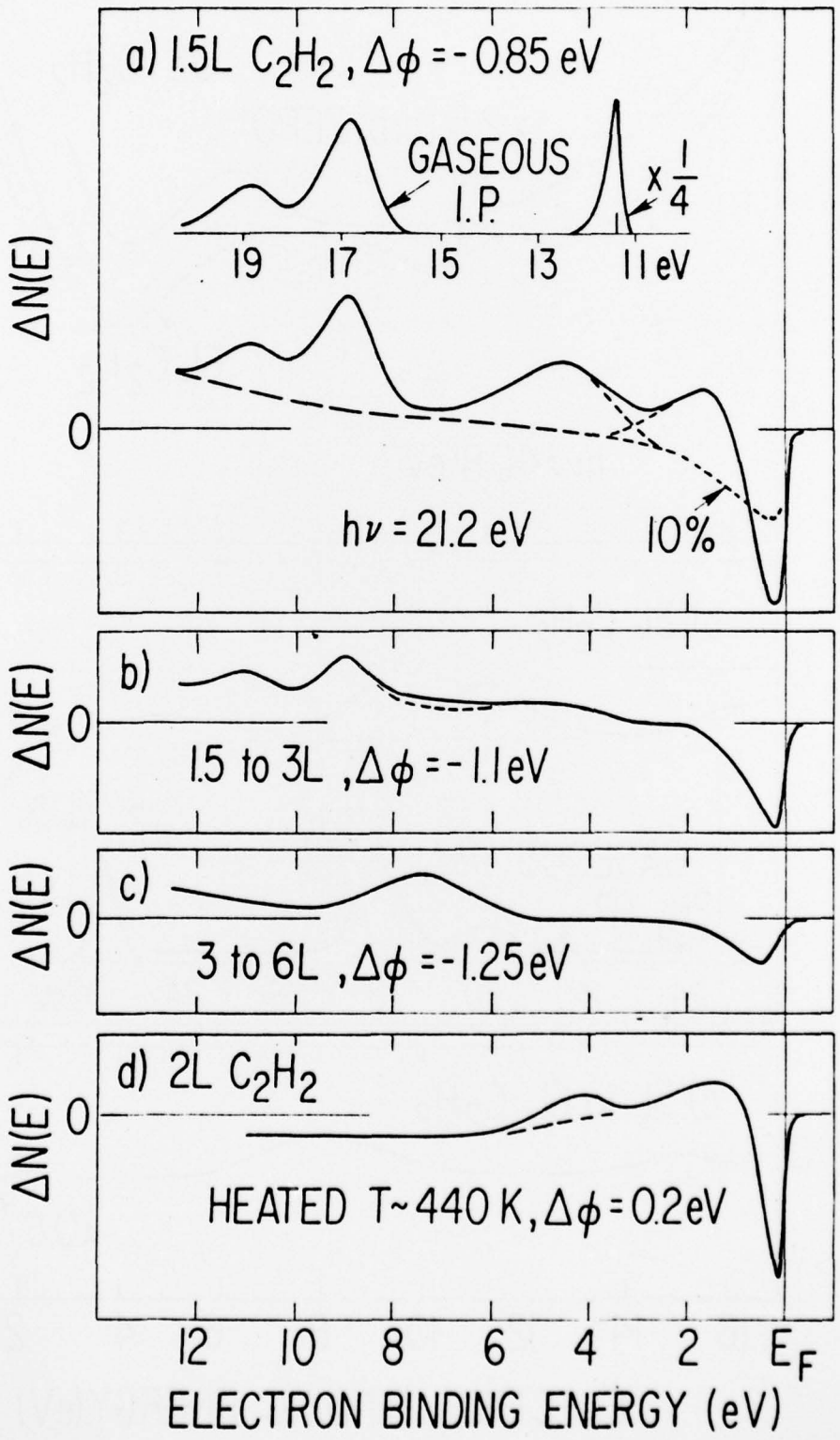

a) 1.5L C_2H_2, $\Delta\phi$ = - 0.85 eV
GASEOUS I.P.
x 1/4
19
17
15
13
11 eV
ΔN(E)
0
hν = 21.2 eV
10%
b)
1.5 to 3L, $\Delta\phi$ = - 1.1 eV
c)
3 to 6L, $\Delta\phi$ = - 1.25 eV
d) 2L C_2H_2
HEATED T~440 K, $\Delta\phi$ = 0.2 eV
12
10
8
6
4
2
E_F
ELECTRON BINDING ENERGY (eV)

FIG 2
DEMUTH

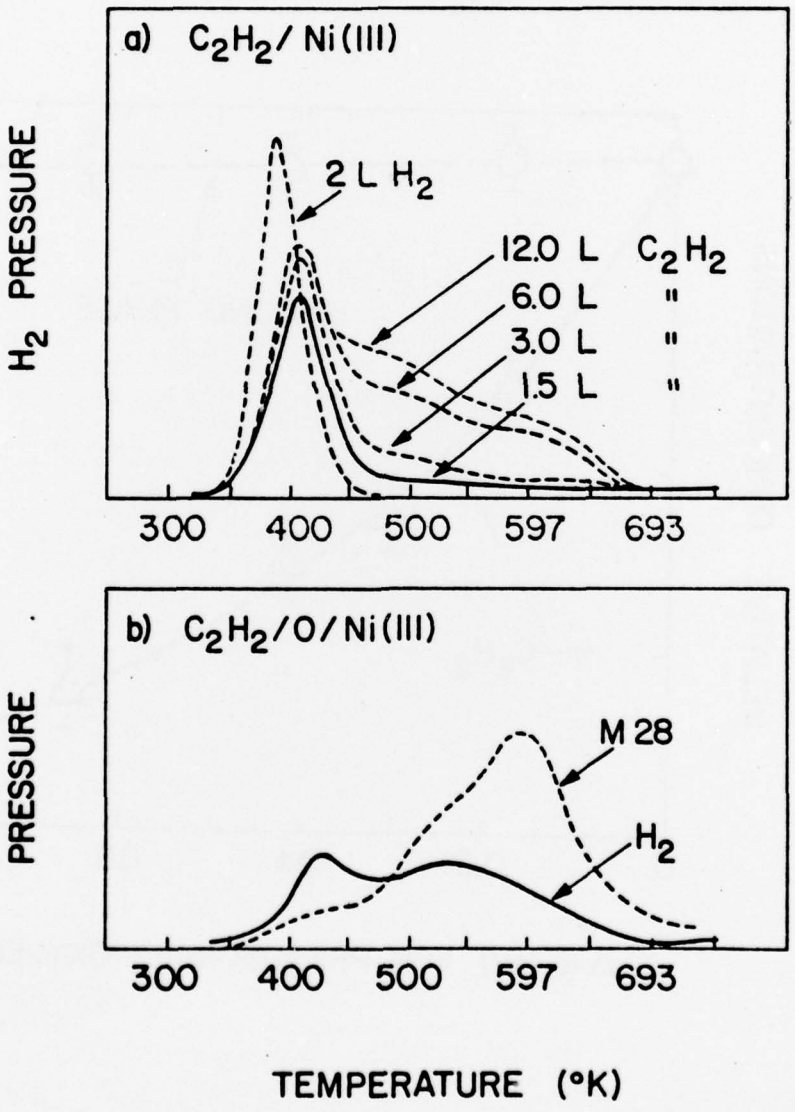

a) C_2H_2/ Ni(111)
2 L H_2
12.0 L C_2H_2
6.0 L "
3.0 L "
1.5 L "
H_2 PRESSURE
300
400
500
597
693
b) C_2H_2/O/ Ni(111)
M 28
H_2
PRESSURE
300
400
500
597
693
TEMPERATURE (°K)

FIG 3

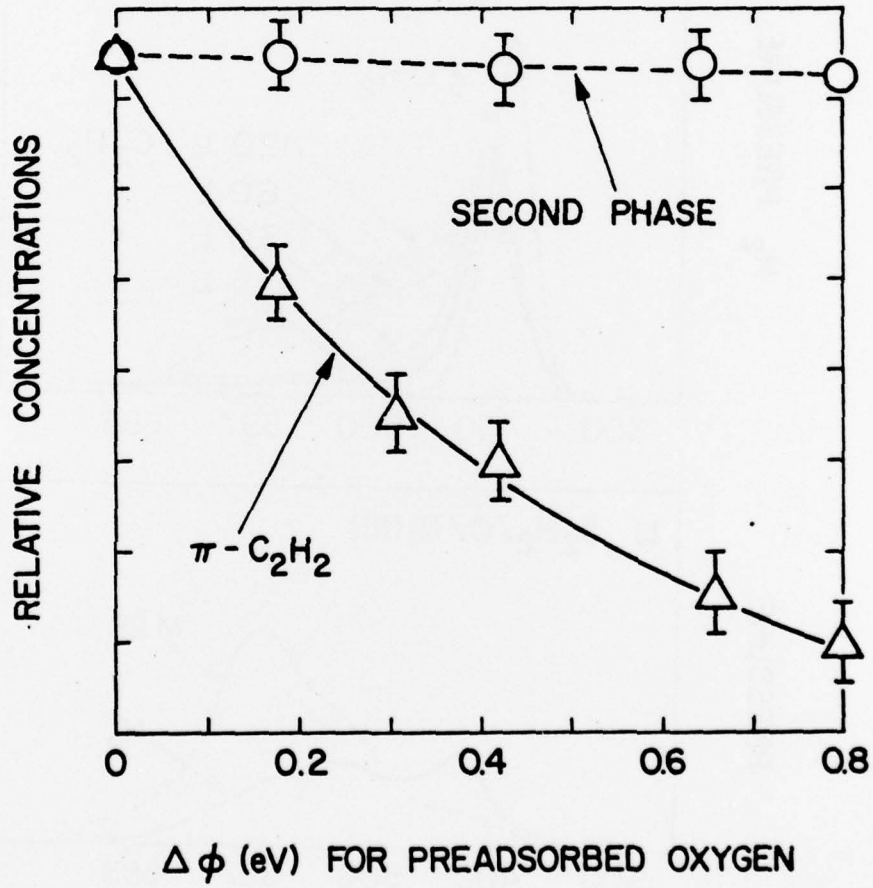

RELATIVE CONCENTRATIONS
SECOND PHASE
π - C2H2
0
0.2
0.4
0.6
0.8
Δφ (eV) FOR PREADSORBED OXYGEN

FIG 4
DEMUTH

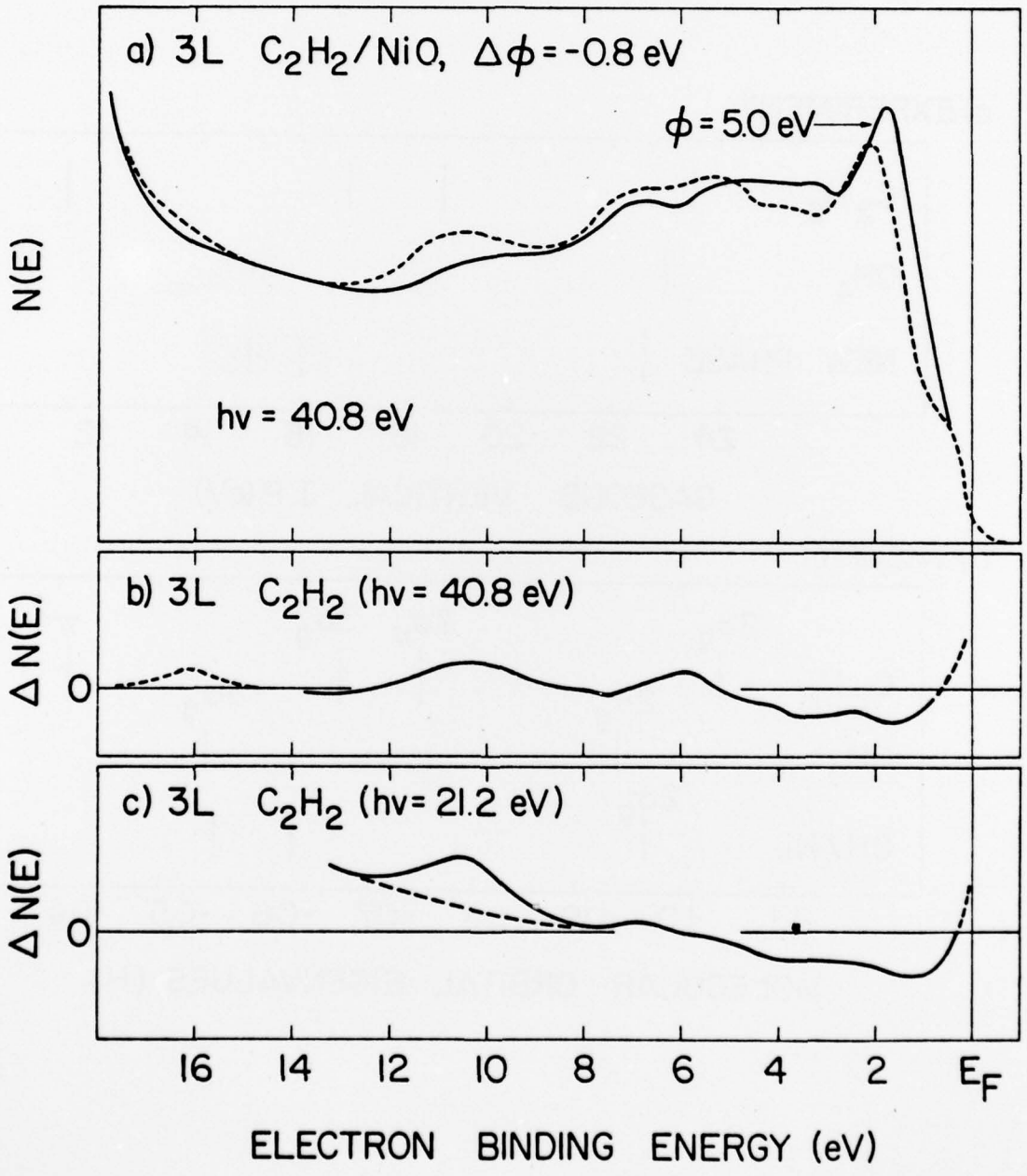
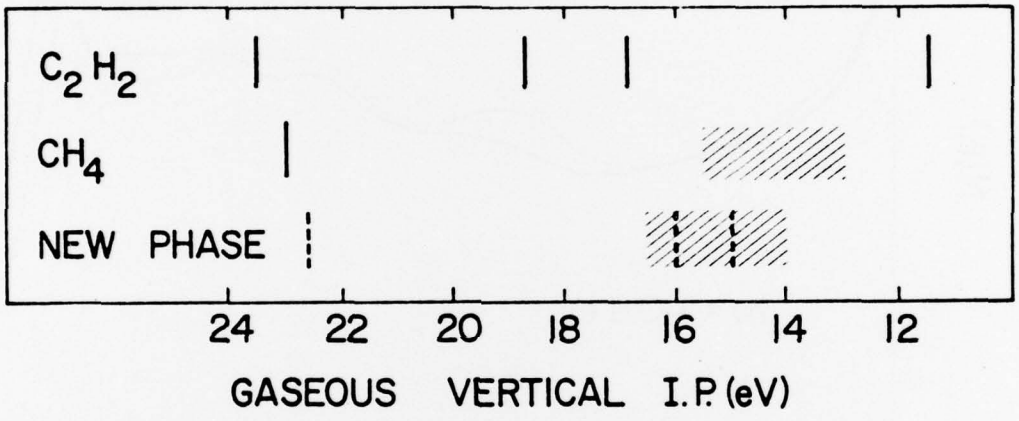

a) 3L C_2H_2/NiO, $\Delta\phi$ = -0.8 eV
ϕ = 5.0 eV
hv = 40.8 eV
N(E)
b) 3L C_2H_2 (hv = 40.8 eV)
Δ N(E)
0
c) 3L C_2H_2 (hv = 21.2 eV)
Δ N(E)
0
16
14
12
10
8
6
4
2
E_F
ELECTRON BINDING ENERGY (eV)

FIG 5

a) EXPERIMENT



b) THEORY

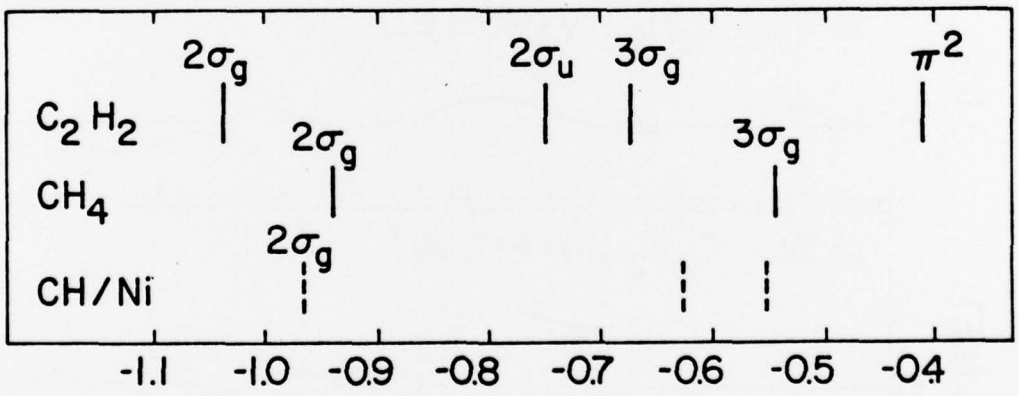


FIG 6
DEMUTH

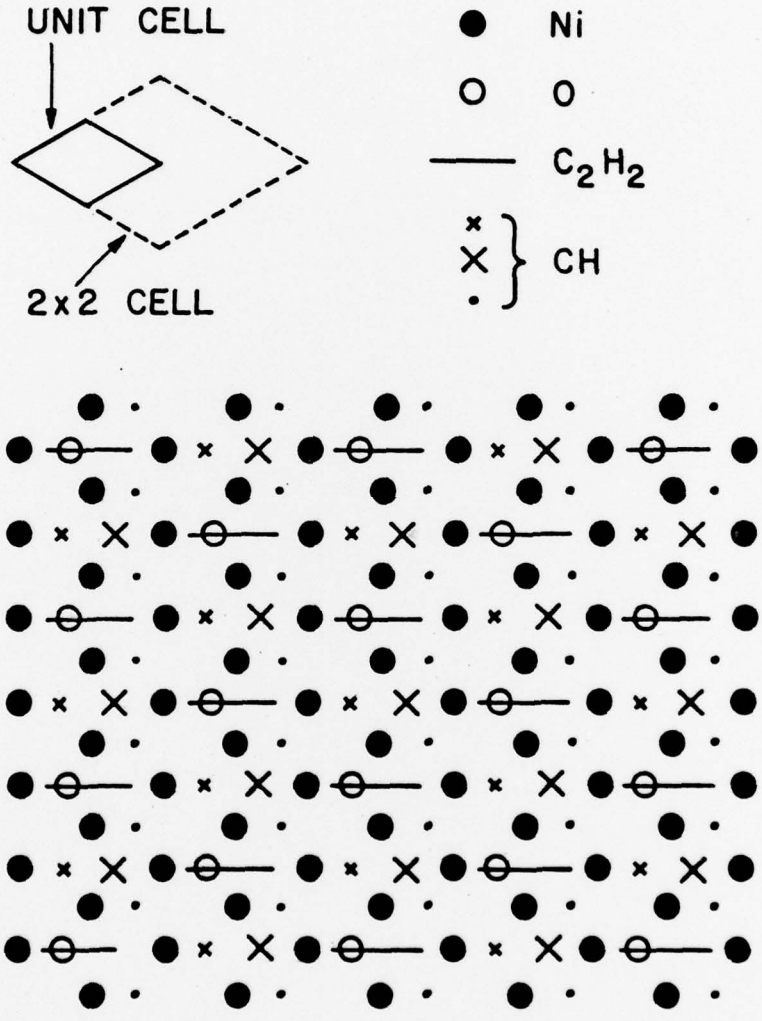
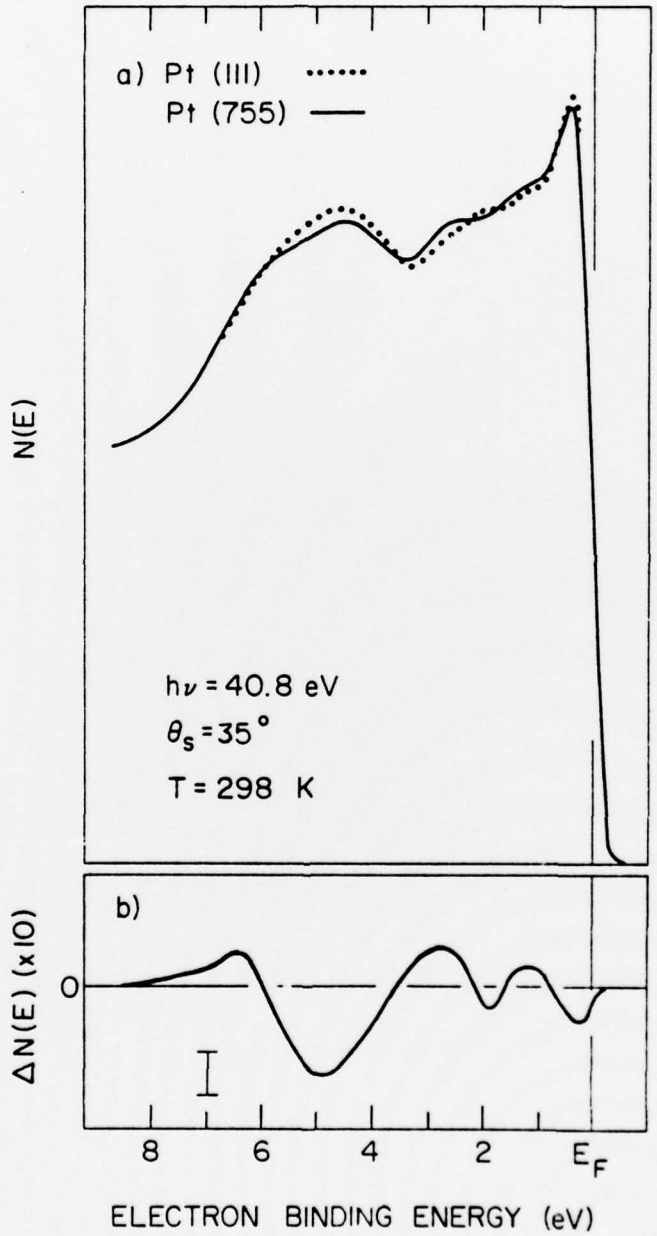


FIG 7
DEMUTH

APPENDIX

Item 6


a) Pt (111)
Pt (755)
N(E)
hν = 40.8 eV
θs = 35°
T = 298 K
b)
ΔN(E) (x10)
0
8
6
4
2
EF
ELECTRON BINDING ENERGY (eV)